Mechanistic Analysis and Quantification of Clofazimine

by

Jennifer Diaz-Espinosa

A dissertation submitted in partial fulfillment
of the requirements for the degree of
Doctor of Philosophy
(Pharmaceutical Sciences)
in the University of Michigan
2023

Doctoral Committee:

Professor Kathleen A. Stringer, Co-Chair
Associate Professor Haojie Zhu, Co-Chair
Assistant Professor Ashlee D. Brunaugh
Professor James J. Moon
Professor Gus R. Rosania

Jennifer Diaz-Espinosa

jendiaz@umich.edu

ORCID iD: 0000-0002-2463-7298

Acknowledgements

As I conclude this work, I would like to express my sincere gratitude to the many who have supported me throughout my research endeavor. First, I would like to extend my heartfelt appreciation to Prof. Kathleen A. Stringer and Prof. Gus R. Rosania for their exceptional leadership and guidance throughout my graduate education and research, as well as the scientific and philosophical training they provided. Additionally, I would like to thank Prof. Haojie Zhu, Prof. Ashlee D. Brunaugh, and Prof. James J. Moon, for their invaluable contributions and insights throughout the completion of this project.

I would like to express my appreciation to Andrew Willmer, Winnie Wen, Laura McLellan, Steve Dunne, Dr. Larisa Yeomans, Marian Fu, and Jae Hyun Kim for their friendship and unwavering scientific support. Their encouragement and feedback were important to me throughout my research journey. In addition, I am grateful for the mentorship of Drs. Vernon LaLone, Mikhail Murashov, and Phil Rzeczycki. Their guidance and expertise were vital to my growth as a researcher.

Last but not least, I would like to thank my friends and family for their support. I could not have accomplished this without their love and backing.

Table of Contents

List of Tables

List of Figures

List of Equations

Abstract

In drug therapy, knowledge of the mechanism of drug distribution is important because it can inform the origins of adverse drug reactions (ADRs) that can result from high concentrations of drug in specific tissues. To this end, we conducted a study of the Food and Drug Administration (FDA) approved drug, clofazimine (CFZ), a weakly basic, highly lipophilic drug that is known to bioaccumulate in macrophages of both humans and mice. By analyzing age-related, CFZ-induced changes in tissue composition, metabolic function, drug sequestration ability, and immune response, we can better understand the processes and risk factors that contribute to ADRs.

We focused our studies on the assessment of CFZ accumulation in a macrophage-rich tissues (spleen and bone marrow), and skeletal muscle. Since ADRs are more prevalent in older individuals and skeletal muscle mass and function decline with age, we also investigated the impact of age on drug accumulation in the skeletal muscle. We used young (4-weeks-old) and old (61-weeks old) C57BL6 male mice, and after prolonged CFZ exposure, we isolated and weighed tissues to quantify the amount of drug and used microscopy techniques to detect drug within cells. Since CFZ targets macrophages, we conducted cytokine arrays to determine the cytokine signals associated with macrophage differentiation. We also modeled changes in muscle mass of mice treated with CFZ throughout its lifespan (birth to 3-years-old) and performed functional tests to understand tissue structure ADRs over time. Additionally, since CFZ is known to disrupt mitochondrial function, we tested the utility of blood levels of the mitochondrial metabolites, L-carnitine and acetylcarnitine, to detect CFZ-induced ADRs.

Our results showed that CFZ accumulation in the bone led to decreased marrow density, increased cargo capacity of bone cells with treatment duration, and a cytokine array signature that was indicative of macrophage differentiation. Spleen mass from CFZ-treated mice increased but its cargo capacity was maintained between young and old mice. However, the amount of CFZ and cargo capacity of skeletal muscle macrophages increased in old mice compared to young mice, even though muscle mass was lost with treatment. The cytokine signals of skeletal muscle from old CFZ-treated mice was consistent with that of diseased muscle, which was not evident in young mice. Mitochondrial metabolism, determined by the ratio of acetylcarnitine to L-carnitine was altered in old skeletal muscle but not in the blood.

In conclusion, our study highlights the impact of prolonged drug treatment and age on drug bioaccumulation in macrophage-rich tissues like the spleen and skeletal muscle. These findings emphasize the importance of understanding how drug distribution could potentially contribute to ADRs. Specifically, we found that the accumulation of CFZ led to altered cell differentiation in the bone marrow, an increase in spleen mass suggests a potential role in drug sequestration, and age-related changes in the muscle increase drug accumulation. These findings provide important insights that could direct future research to mitigate ADRs.

Chapter 1 Introduction

1.1 Background and Significance

1.1.1 Age-Related Drug Distribution and Adverse Drug Reactions

In the USA, adverse drug reactions (ADRs) are a significant concern, accounting for a leading cause of death and health cost of 30 billion dollars per year [1]. Despite efforts to correct dose for patient variabilities, such as renal function, age, and body weight and perform clinical trials that assess drug safety, ADRs continue to occur across medications for various indications (**Table 1-1**) [2].

As the population ages, there is an increasing concern about age-related changes in drug distribution, which can affect drug efficacy and safety. One of the primary factors contributing to age-related changes in drug distribution is an alteration in tissue structure that leads to decreased drug clearance; thus increasing drug exposure [3]. This includes changes in body composition, such as decreased muscle mass and increased fat, both of which can affect drug absorption, distribution, metabolism, and excretion (**Table 1-2**) [4]. These changes can impact medication disposition in 90% of older adults that regularly take at least one prescription drug (**Figure 1-1**) [5].

Polypharmacy, the use of multiple medications, is also more common in older adults, which can further increase the risk of ADRs due to drug-to-drug interactions [6]. This is concerning because many medications have not been adequately tested in the elderly, where drug trials often

exclude this population [7]. Additionally, the elderly population is often placed on long-term medication for chronic illnesses, making them more susceptible to ADRs over time [8].

1.1.2 Bioaccumulation via Macrophages

Macrophages play a crucial role in seizing and digesting foreign material, cellular debris, and initiating immune responses [9]. Although macrophages can phagocytose components, including bacteria, and environmental particles, lipophilic drugs have been found to permeate macrophages and accumulate intracellularly, contributing significantly to the bioaccumulation of drugs [10].

Macrophages serve as "garbage collectors," and their lysosome is a vital compartment for their function. As a result, macrophages have a highly active lysosomal digestive compartment that contains a membrane proton transporter, H+-ATPase, to maintain an acidic pH (4.5-5) [11]. This low pH environment is key for the capturing material [12]. Macrophages can uptake compounds continuously, leading to expansion and densification [13]. As the accumulation of material increases, cellular compartments undergo alterations that result in changes in cellular metabolism at both molecular and systemic levels [14].

In aging, macrophage display an alteration in cytokines, polarization, and tissue regeneration [15]. These age-related changes may result in a greater extent of intracellular accumulation of lipophilic drugs in older individuals, leading to an increase of ADRs [16].

1.1.3 The Lysosome as a Storage Compartment

Drugs that accumulate in lysosomes share specific physicochemical properties that allow them to be taken up and stored. These properties include high lipophilicity (logP>3), which helps the drug permeate through membranes, and weakly basic characteristics (pKa>8), which are

present in 75% of approved drugs, allowing them to become trapped in an acidic environment [17, 18]. When a weakly basic drug, such as clofazimine (CFZ), amiodarone, chloroquine, or azithromycin, enters the lysosome, it becomes protonated, resulting in ion trapping [19-21]. The positive charge on the amine group prevents the molecule from leaving and becoming trapped intracellularly, leading to drug accumulation (**Figure 1-2**) [22]. By tracking the distribution of accumulated drugs in the body, we can determine the significance of lysosomal accumulation on cellular response and how it changes throughout aging and dosing. Among these drugs, CFZ is a notable example due to its ability to continuously accumulate with dosing in the lysosome, resulting an extended half-life and potential for adverse effects [23].

Lysosomes undergo age-related changes such as an increase in size, and number [24, 25]. Variations in lysosomal pH and an increase of lysosomal gene expression are also seen with age [26, 27]. These changes can affect ion-trapping of weakly basic drugs that dependent on an acidified lysosomal compartment.

1.1.4 Age-Related Drug Distribution in Vital and Non-Vital Organs

Understanding how age affects the body and its relationship with drug distribution is important for optimizing drug therapies and improving health outcomes in the elderly population. To do so, studying drug distribution in tissues such as the bone, spleen, and skeletal muscle is important, as they play different physiologic roles in the aging process. Although these tissues have their own distinct functions, they are interconnected through physiological processes, thus effecting the entire body [28].

The bone, a vital tissue, provides structural support and protection for organs and plays a crucial role in the immune system by serving as a site of immune cell generation; bone remodeling and maintenance are important for a sustained macrophage population [29, 30]. With increasing

age, bone mass, strength, and density decrease, making bones more prone to fractures and other injuries (**Figure 1-5**) [31]. With the structural and immune system changes that occur throughout aging, the bone maybe become more prone to deviations in drug distribution.

The spleen filters blood, is a reservoir for immune cells, and is a known drug sequestering organ. However, it also undergoes changes in structure and function throughout aging, leading to alterations in its role in immune and drug sequestering ability [32-34]. As individuals age, the cellularity of the spleen decreases, leading to a decline in immune function and increased susceptibility to infection (**Figure 1-6**) [35]. Therefore, the spleen's drug-sequestering function may have significant implications for drug efficacy and safety.

Skeletal muscle is the largest tissue in the human body, accounting for 40% of body weight, and is responsible for generating movement, supporting the body's posture and structure, and regulating metabolic processes, such as glucose uptake and utilization [36, 37]. Age-related changes in skeletal muscle include a loss of muscle mass, strength, and performance, leading to sarcopenia (**Figure 7**), which can lead to mobility difficulties, and falls [38, 39]. Sarcopenia can be classified as primary, resulting solely from aging, or secondary, when additional factors such as disease, activity, nutrition, and obesity accelerate its development [40]. Age-related changes in skeletal muscle can also affect the immune system, including macrophage function, increasing the risk of muscle injury [41]. Understanding drug distribution mechanisms in muscle is crucial, especially since weakly basic and commonly used drugs such as omeprazole, amiodarone, and doxorubicin have been reported to cause adverse effects on muscle [42-44].

1.1.5 Clofazimine as a Model Bioaccumulating Drug

Clofazimine (CFZ) is an FDA-approved antibiotic with a half-life of 70 days and a large volume of distribution (**Figure 1-3**) [45, 46]. It has been widely used in the treatment of leprosy

and other infectious diseases [47]. The drug has physicochemical properties that enable it to become trapped inside lysosomes and bind with lysosomal chloride, which leads to extensive intracellular accumulation that results in the formation of crystal-like drugs inclusions (CLDIs, **Figure 1-4**) [48].

The ability of CFZ to accumulate in the lysosome provides a potential avenue for understanding molecule accumulation during aging. CFZ's fluorescent properties make it possible to quantify and investigate the mechanisms and localization of CFZ distribution [49]. This could lead to determining the cellular and biochemical mechanisms of drug accumulation and its relationship to the accompanying changes in structure and function during aging and long-term dosing.

1.2 Innovation

The current drug approval pipeline involves pre-clinical and clinical trials to assess safety of candidate drug molecules, but these trials are limited by short-term animal and human research that often exclude the older population, resulting in under reporting of ADRs in this population [7, 50]. Post-market analysis relies on patient reports, which may not accurately identify ADRs. The proposed research represents a departure from this status quo by using in-lab microscopy techniques to establish response patterns to long-term drug accumulation and age throughout the lifespan. This new approach permits examination of age-related drug accumulation in various compartments, the pinpointing of drug localization, and identification of mechanisms of drug accumulation. The findings from the work have the potential to lead to more accurate drug dosing and the prevention of ADRs in elderly patients.

1.3 Rationale

The aim of this project was to further the understanding between drug exposure and cellular cargo loading during the aging process, in order to identify appropriate drug doses that reduce the risk of ADRs. C57BL/6 male mice are widely used aging models, as they exhibit age-related changes, including sarcopenia, caused by similar underlying mechanisms as observed in humans [51]. Since prolonged drug exposure may disrupt the maintenance of homeostasis by accumulating in organelles faster than it can be cleared, the accumulated drug may cause intracellular disruptions. Thus, mice received CFZ-treatment for up to 65 weeks in accordance with ULAM guidelines. Using available mouse models that mimic human aging, and the FDA-approved drug CFZ, which is known to bioaccumulate in both humans and mice, the objective of this project was to comprehend the effects of prolonged drug dosing on health span [13]. By studying the constant presence of foreign molecules, such as bioaccumulating drugs, I aimed to enhance our understanding of the relationship between drug exposure, cellular cargo load, and the body's sensitivity to drug toxicity during the aging process.

1.4 Central Hypothesis and Specific Aims

1.4.1 Central Hypothesis

Age-related changes in organ structure and function alters drug distribution in the organism with consequent downstream changes in off-target side effects.

1.4.2 Specific Aim 1: Quantitatively Measure CFZ Distribution in Young and Old Mice to Determine Drug Localization Sites

Adverse drug reactions (ADRs) are frequently caused by drug accumulation in tissues. The aim of this objective was to identify the tissues that displayed the largest differences in drug content

between young (4-weeks-old) and old (6-weeks-old) mice. To achieve this goal, we tested the working hypothesis that drug accumulation is more likely to occur in tissues that undergo extensive age-related changes. We measured drug accumulation in mice treated with CFZ for 8 weeks in mice, starting at 4-weeks and 61-weeks of age. The rationale for this objective was that its successful completion would enhance our understanding of the behavior of weakly basic drugs, which is critical to improving pharmacokinetic (PK) models.

1.4.3 Specific Aim 2: Determine the Mechanism of CFZ Accumulation in the Skeletal Muscle

Skeletal muscle is highly impacted by age and can sequester drugs, yet the mechanism of drug accumulation within the muscle remains to be fully understood. The objective of this aim was to investigate candidate mechanisms of CFZ accumulation within the skeletal muscle. To achieve this objective, we tested the working hypothesis that drug accumulation results from the entrapment of drug within myocytes (e.g., macrophages). Our approach measured the form of CFZ that accumulated in the muscle, whether it was in a soluble-free base or an insoluble form, such as free base aggregates or protonated crystalline structures, since CFZ undergoes different phase changes depending on its location of accumulation. The rationale for this aim was to gain insight into the ability of skeletal muscle to accumulate CFZ and to identify drug and skeletal muscle properties that promote CFZ accumulation. This is essential for understanding the body's ability to retain high amounts of drug and to design new drug with longer or shorter half-life properties depending on the desired drug concentration goal. Upon completion of aim #2, we expected to determine the mechanism of CFZ accumulation in the skeletal muscle and identify key features that contribute to drug accumulation in the muscle. These findings would be significant for drug developers, providing insights into drug design.

1.4.4 Specific Aim 3: Compare the Accumulation of CFZ in Relation to Exposure Times and Associated Differences in the Structure of the Muscle

The skeletal muscle undergoes dynamic changes throughout the aging process, including an alteration in cell composition and fiber diameter. The objective of this aim was to investigate the impact of long-term CFZ accumulation in mice and how age-related changes in muscle structure alter the progression of CFZ bioaccumulation. To achieve this objective, we tested our working hypothesis that old mice experience decreased drug clearance which can lead to more severe ADRs. Our approach was to use mice treated for 8 to 65 weeks and monitor their muscle strength, function, metabolism, and muscle mass kinetics throughout treatment. The rationale for this aim was that it will enable us to determine how drug accumulation influences muscle function and structure. This knowledge is crucial for understanding the effects of age and drug accumulation on skeletal muscle. We expect to identify differences in muscle strength, composition, metabolism, cytokine levels, and mass during aging. Additionally, we anticipated showing that age is a significant factor in drug accumulation within the skeletal muscle. These findings are essential for accurate medication dosing in older adults.

With an increasing number of patients taking multiple drugs for longer periods, there is a need to understand the distribution patterns of drugs within the compartments of the skeletal muscle and the mechanisms of accumulation of CFZ. This study aimed to investigate age-related drug accumulation in the skeletal muscle using different exposure times to assess potential benefits and risks.

1.5 Future Directions

This research aimed to investigate the accumulation mechanism and effects of long-term drug regimens during the aging process to evaluate potential toxicities over time and the mechanisms behind ADRs in the skeletal muscle. The ultimate goal of the work was to identify candidate biomarkers that can detect potential ADRs before they become severe or fatal, which could improve the quality of life for older individuals. By gaining a better understanding of the risks and benefits of drug accumulation in the muscle, we can develop more accurate dosing guidelines for the elderly population. This research can improve the safety of drug therapies for older individuals.

1.6 Figures

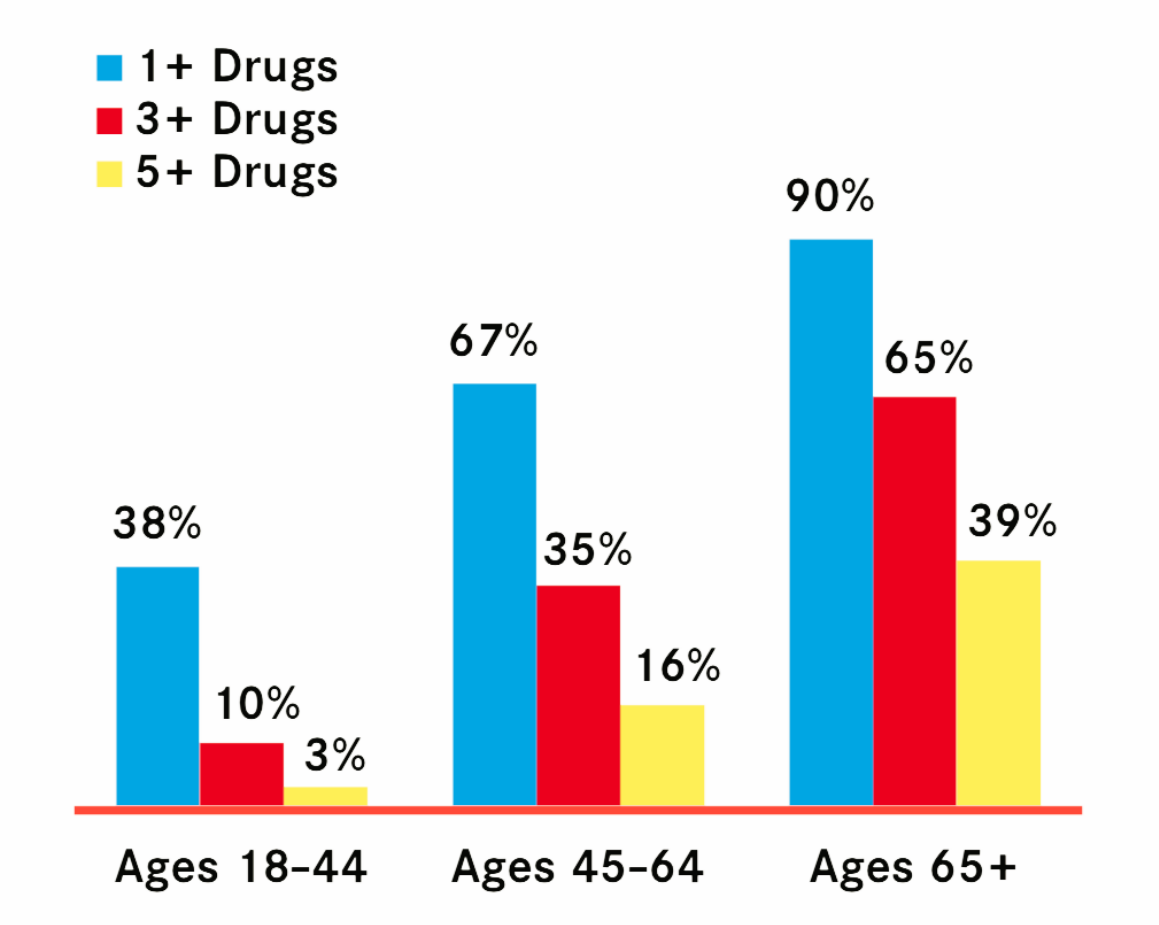

Adapted From National Center for Health Statistics (US). *Health, United States, 2015.*

Figure 1-1 Prescription Drug Usage Across Age Groups

According to data collected between 2009 and 2012, there is a correlation between age and the number of prescription drugs taken in the past 30 days. Patients aged 65 and above have the highest number of individuals taking at least one prescription drug, while the group between 18-44 has a smaller number of individuals on medication.

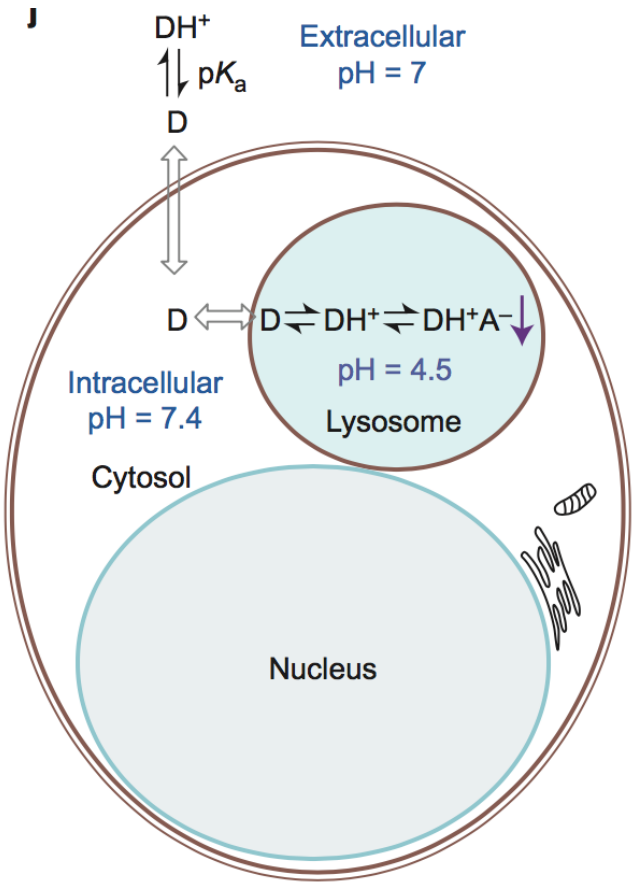

Adapted From Fu, D., et al. *Nature chemistry*, 2014.

Figure 1-2 Diagrammatic Representation of Ion Trapping and Drug Precipitation in the Lysosome

A thermodynamic equilibrium model of lysosomotropism, incorporating solubility equilibrium: The drug within the lysosome primarily exists in its protonated form, resulting from the low pH, and loses its membrane-permeability. Once the concentration of the protonated drug surpasses its solubility, it precipitates within the lysosome, along with the counter ion A−.

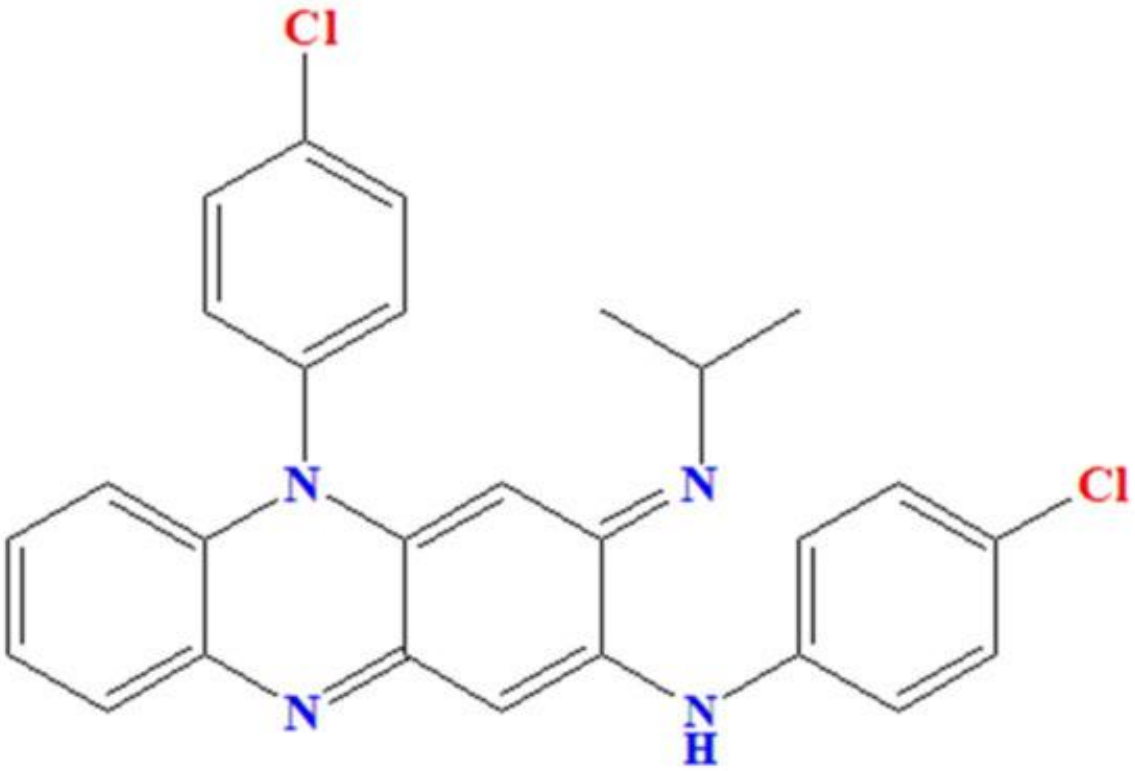

Retrieved From Nugraha, R., et al. Scientia Pharmaceutica, 2021.

Figure 1-3 Molecular Structure of Clofazimine Freebase (CFZ-FB)

Clofazimine, a lipophilic riminophenazine, was first synthesized in 1957. Its primary structure consists of a phenazine nucleus along with phenyl substituents and an R-imino group.

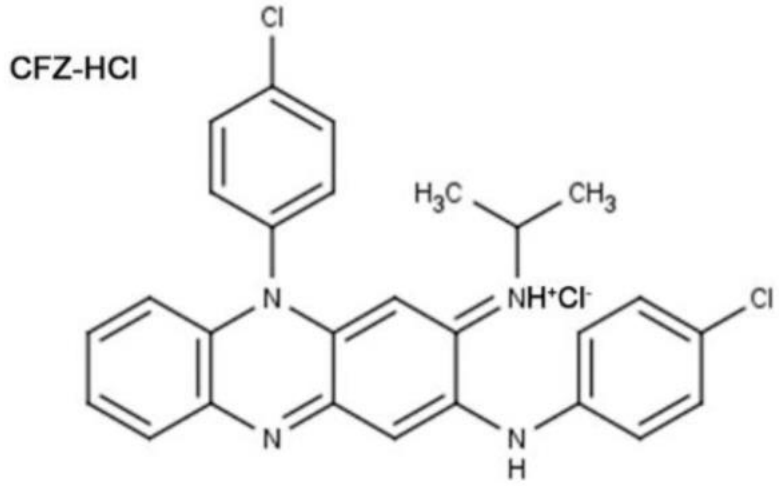

Adapted From Murashov, M., et al. Pharmaceutics, 2018.

Figure 1-4 Molecular Structure of Clofazimine Hydrochloride (CFZ-HCL)

Crystal-like drug inclusions (CLDIs) are hydrochloride salt forms of clofazimine that form intracellularly in the lysosome of macrophages.

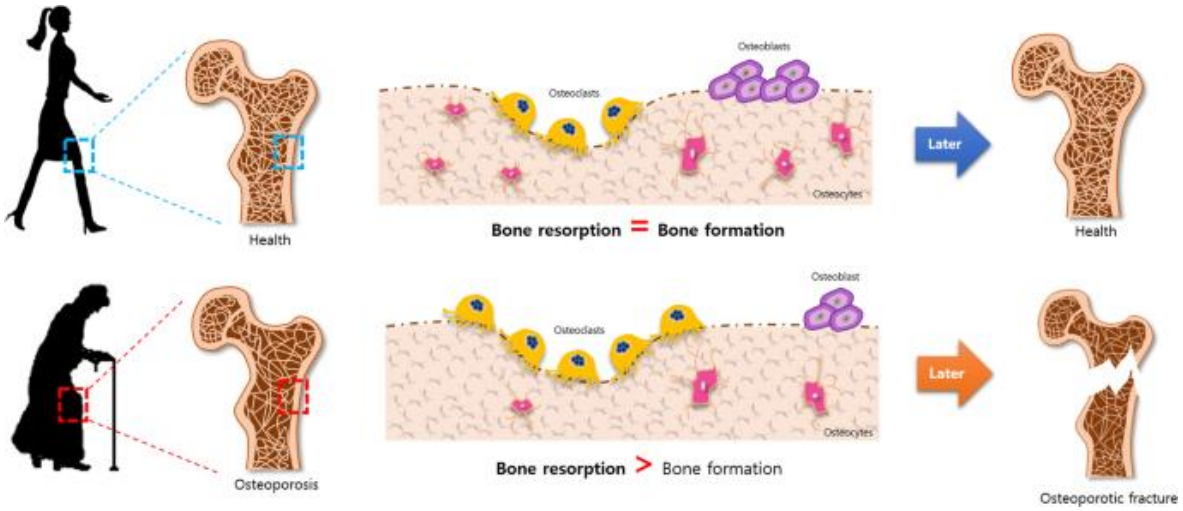

Retrieved From Chang, Y., et al. Experimental & Molecular Medicine, 2019.

Figure 1-5 Comparison of Bone Restructuring in Young and Old Individuals

As individuals age, there is a shift in the composition of the bone cell population. This results in a greater amount of bone resorption than bone formation, thereby disrupting the balance between the two, resulting in loss of bone density.

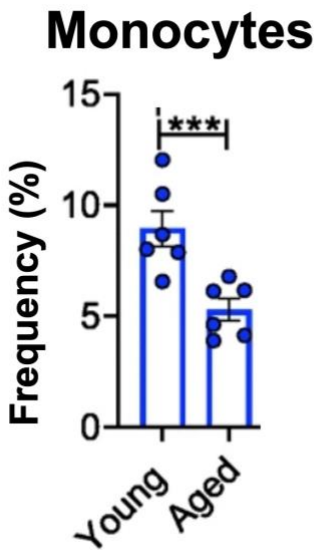

Adapted From Menees, B., et al. Immunity & Ageing, 2021.

Figure 1-6 Age Changes in the Profile of Monocytes in the spleen in C57BL/6J

Splenic monocytes composition is altered in an age-dependent manner (mean ± SEM). The plots represent the frequency of B cells, monocytes (includes macrophages), neutrophils, NK cells, CD4 + T cells, and CD8 + T cells in young (2-3 months) and aged (21-22 months) male mice. Old male mice show a decrease in monocyte frequency compared to young mice.

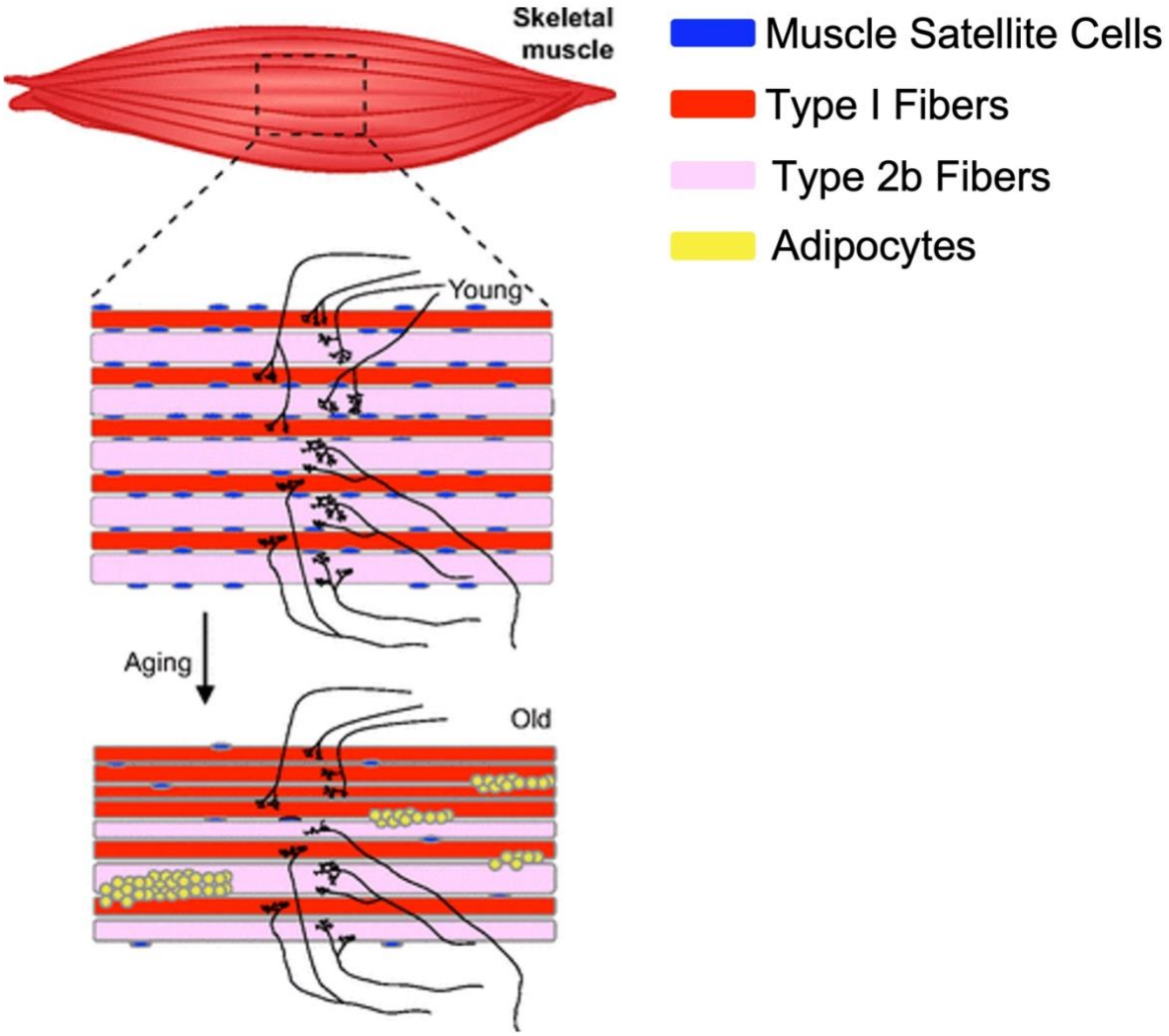

Adapted From Demontis, F., *et al. Disease models & mechanisms*, 2013.

Figure 1-7 Morphological Alterations in Muscles with Aging

During muscle aging in mammals, there is a decline in regenerative capacity due to a reduction in the number and function of muscle satellite cells (shown in blue). Additionally, there is a decrease in overall muscle strength and mass caused by a reduction in the number and size of type IIb fibers (pink) and, to a lesser extent, type I fibers (red). There is also an age-related accumulation of interstitial adipocytes (yellow).

1.7 Figures

Table 1-1 Increase of ADRs between 1999 and 2008

In 2008, the majority of ADRs were classified as mild (n=48, 90.6%). Whereas, in 1999, 54.3% (n=25) of ADRs were categorized as mild. These findings suggest an increase in the number of ADRs associated with FDA-approved drugs.

Drug groups (ATC)	ADR causative drugs (n)/total drugs in group (n) (%)[#]		Examples of ADRs (causative drug)	
	1999 Cohort, Total n = 710	2008 Cohort, Total n = 1343	1999 Cohort	2008 Cohort
analgesics* (N02)	N = 0/23 (0.0%), 95%CI NA	N = 2/225 (0.9%), 95%CI (0.1–3.2)	-	thrombocytopenia (metamizol), sedation aggravated (tramadol)
antibacterials for systemic use* (J01/J02)	N = 24/201 (11.9%), 95%CI (7.8–17.2)	N = 20/291 (6.9%), 95%CI (4.2–10.4)	diarrhea (amoxicillin, imipenem), exanthema (amoxicillin, vancomycin), eosinophilia (cefaclor, cefotiam)	eosinophilia (vancomycin, cefotaxim, tobramycin), exanthema (amoxicillin, benzylpenicillin), neutropenia (cefotaxim)
antiepileptics* (N03)	N = 1/22 (4.5%), 95%CI (0.1–2.3)	N = 8/53 (15.1%), 95%CI (6.7–27.6)	elevated liver enzymes (phenobarbital)	thrombocytopenia (valproic acid), leucopenia (valproic acid, topiramate)
anti-inflammatory and antirheumatic products (M01)	N = 3/12 (25%), 95%CI (5.5–5.7)	N = 0/119 (0.0%), 95%CI NA	nausea & vomiting (indometacin), GI-bleeding (ibuprofen)	-
immuno-suppressive agents* (L04)	N = 3/15 (20%), 95%CI (4.3–4.8)	N = 8/36 (22.2%), 95%CI (10.1–39.2)	diarrhea & hypertrichosis (ciclosporin), herpes zoster (azathioprine)	hyponatriaemia & hyperkaliaemia (tacrolimus), hypertrichosis (ciclosporin)
corticosteroid for systemic use* (H02)	N = 9/27 (33.3%), 95%CI (16.5–54.0)	N = 15/54 (27.8%), 95%CI (16.5–41.6)	hypokaliaemia (methylprednisolone), leucocytosis (methylprednisolone)	hyperglycaemia, hypertension, Cushing's syndrome (prednisone), leucocytosis (prednisolone),
drugs for obstructive airway diseases (R03)	N = 2/77 (2.6%), 95%CI (0.3–9.1)	N = 0/60 (0.0%), 95%CI NA[††]	eosinophilia (theophylline), tachycardia (epinephrine)	-

Drugs marked with (*) are high risk drugs;
[#]percentage of total prescriptions in this group causing an ADR.
[†]most often prescribed drugs (n>25),
[††]NA = not applicable as it is one-sided, 97.5% CI.
doi:10.1371/journal.pone.0044349.t004

Retrieved From Oehme, A., et al. PLos One, 2012

Table 1-2 Age-Related Physiological Changes Affecting Drug Pharmacokinetics and Clinical Implications

The absorption, distribution, metabolism, and excretion of drugs can be altered due to physiological changes that occur during aging. In addition to increasing age, multiple drug regimens, and environmental changes may also impact pharmacokinetic processes. Changes in body composition can also affect drug distribution and pharmacologic response. Lipophilic drugs have increased volumes of distribution and half-lives in the elderly population.

Pharmacokinetic Process	Physiologic Change	Clinical Significance
Absorption	Altered gastrointestinal motility Decreased absorptive surface Decreased gastric emptying rate Decreased splanchnic blood flow Increased gastric pH	Little change in absorption with increasing age
Distribution	Altered protein binding Decreased serum albumin Increased α-acid glycoprotein	Increased or decreased unbound concentration of drugs in plasma
	Decreased lean body mass Decreased total body weight Increased adipose tissue	Higher concentration of drugs that distribute into body fluids; altered volume of distribution of some drugs often leads to a prolonged elimination half-life
Metabolism	Decreased phase I metabolism No change in phase II metabolism Decreased hepatic blood flow Decreased hepatic mass	Decreased hepatic clearance of drugs and metabolites with increased plasma concentrations
Elimination	Reduced glomerular filtration rate Reduced renal blood flow Decreased tubular secretion function	Decreased renal clearance of drugs and metabolites with increased plasma concentrations

Adapted from References 28, 29, and 34.

Retrieved From Cooke, S., et al. Journal of Pharmacy Practice, 2001.

1.8 References

1. Sultana, J., P. Cutroneo, and G. Trifiro, *Clinical and economic burden of adverse drug reactions.* J Pharmacol Pharmacother, 2013. **4**(Suppl 1): p. S73-7.

2. Oehme, A.K., et al., *Adverse drug reactions in hospitalised children in Germany are decreasing: results of a nine year cohort-based comparison.* PLoS One, 2012. **7**(9): p. e44349.

3. Mangoni, A.A. and S.H. Jackson, *Age-related changes in pharmacokinetics and pharmacodynamics: basic principles and practical applications.* Br J Clin Pharmacol, 2004. **57**(1): p. 6-14.

4. Cooke, S.C. and M.L. Tucker, *Geriatric Depression.* Journal of Pharmacy Practice, 2001. **14**(6): p. 498-510.

5. Dean, O., *Prescription Drug Abuse amoung Older Adults*, in *Public Policy Institute*. 2017, AARP: www.aarp.org/ppi.

6. Dagli, R.J. and A. Sharma, *Polypharmacy: a global risk factor for elderly people.* J Int Oral Health, 2014. **6**(6): p. i-ii.

7. van Marum, R.J., *Underrepresentation of the elderly in clinical trials, time for action.* Br J Clin Pharmacol, 2020. **86**(10): p. 2014-2016.

8. Ritz, P. and B. Vellas, *Pharmacokinetics and drug toxicity in elderly patients: a case for geriatric core data in clinical trials.* J Nutr Health Aging, 2007. **11**(3): p. 261-4.

9. Hirayama, D., T. Iida, and H. Nakase, *The Phagocytic Function of Macrophage-Enforcing Innate Immunity and Tissue Homeostasis.* Int J Mol Sci, 2017. **19**(1).

10. Lemaire, S., P.M. Tulkens, and F. Van Bambeke, *Cellular pharmacokinetics of the novel biaryloxazolidinone radezolid in phagocytic cells: studies with macrophages and polymorphonuclear neutrophils.* Antimicrob Agents Chemother, 2010. **54**(6): p. 2540-8.

11. Wang, S.P., et al., *Regulation of enhanced vacuolar H+-ATPase expression in macrophages.* J Biol Chem, 2002. **277**(11): p. 8827-34.

12. Westman, J. and S. Grinstein, *Determinants of Phagosomal pH During Host-Pathogen Interactions.* Frontiers in Cell and Developmental Biology, 2021. **8**.

13. Willmer, A.R., et al., *Molecular design of a pathogen activated, self-assembling mechanopharmaceutical device.* J Control Release, 2022. **347**: p. 620-631.

14. Trexel, J., et al., *Macrophage-Mediated Clofazimine Sequestration Is Accompanied by a Shift in Host Energy Metabolism.* J Pharm Sci, 2017. **106**(4): p. 1162-1174.

15. Linehan, E. and D.C. Fitzgerald, *Ageing and the immune system: focus on macrophages.* Eur J Microbiol Immunol (Bp), 2015. **5**(1): p. 14-24.

16. Vida, C., et al., *Role of macrophages in age-related oxidative stress and lipofuscin accumulation in mice.* Redox Biol, 2017. **12**: p. 423-437.

17. Logan, R., A.C. Kong, and J.P. Krise, *Time-dependent effects of hydrophobic amine-containing drugs on lysosome structure and biogenesis in cultured human fibroblasts.* J Pharm Sci, 2014. **103**(10): p. 3287-96.

18. Kaur, N., A. Narang, and A.K. Bansal, *Use of biorelevant dissolution and PBPK modeling to predict oral drug absorption.* Eur J Pharm Biopharm, 2018. **129**: p. 222-246.

19. Yoon, G.S., et al., *Clofazimine Biocrystal Accumulation in Macrophages Upregulates Interleukin 1 Receptor Antagonist Production To Induce a Systemic Anti-Inflammatory State.* Antimicrob Agents Chemother, 2016. **60**(6): p. 3470-9.

20. Morissette, G., et al., *Intracellular sequestration of amiodarone: role of vacuolar ATPase and macroautophagic transition of the resulting vacuolar cytopathology.* Br J Pharmacol, 2009. **157**(8): p. 1531-40.

21. Derendorf, H., *Excessive lysosomal ion-trapping of hydroxychloroquine and azithromycin.* Int J Antimicrob Agents, 2020. **55**(6): p. 106007.

22. Fu, D., et al., *Imaging the intracellular distribution of tyrosine kinase inhibitors in living cells with quantitative hyperspectral stimulated Raman scattering.* Nat Chem, 2014. **6**(7): p. 614-22.

23. Holdiness, M.R., *Clinical pharmacokinetics of clofazimine. A review.* Clin Pharmacokinet, 1989. **16**(2): p. 74-85.

24. Truschel, S.T., et al., *Age-related endolysosome dysfunction in the rat urothelium.* PLoS One, 2018. **13**(6): p. e0198817.

25. Yang, C. and X. Wang, *Lysosome biogenesis: Regulation and functions.* J Cell Biol, 2021. **220**(6).

26. Shi, D., et al., *Lysosomal polarity increases with aging as revealed by a lysosome-targetable near-infrared fluorescent probe.* Sensors and Actuators B: Chemical, 2020. **319**: p. 128302.

27. de Magalhaes, J.P., J. Curado, and G.M. Church, *Meta-analysis of age-related gene expression profiles identifies common signatures of aging.* Bioinformatics, 2009. **25**(7): p. 875-81.

28. Tarantino, G., et al., *Spleen: A new role for an old player?* World J Gastroenterol, 2011. **17**(33): p. 3776-84.

29. Lorenzo, J., M. Horowitz, and Y. Choi, *Osteoimmunology: interactions of the bone and immune system.* Endocr Rev, 2008. **29**(4): p. 403-40.

30. Cho, S.W., *Role of osteal macrophages in bone metabolism.* J Pathol Transl Med, 2015. **49**(2): p. 102-4.

31. Chang, Y., et al., *Direct conversion of fibroblasts to osteoblasts as a novel strategy for bone regeneration in elderly individuals.* Exp Mol Med, 2019. **51**(5): p. 1-8.

32. Lewis, S.M., A. Williams, and S.C. Eisenbarth, *Structure and function of the immune system in the spleen.* Sci Immunol, 2019. **4**(33).

33. Willmer, A.R., et al., *An Adaptive Biosystems Engineering Approach towards Modeling the Soluble-to-Insoluble Phase Transition of Clofazimine.* Pharmaceutics, 2021. **14**(1).

34. Turner, V.M. and N.A. Mabbott, *Influence of ageing on the microarchitecture of the spleen and lymph nodes.* Biogerontology, 2017. **18**(5): p. 723-738.

35. Menees, K.B., et al., *Sex- and age-dependent alterations of splenic immune cell profile and NK cell phenotypes and function in C57BL/6J mice.* Immun Ageing, 2021. **18**(1): p. 3.

36. Kim, K.M., H.C. Jang, and S. Lim, *Differences among skeletal muscle mass indices derived from height-, weight-, and body mass index-adjusted models in assessing sarcopenia.* Korean J Intern Med, 2016. **31**(4): p. 643-50.

37. Wang, J., et al., *Engineered skeletal muscles for disease modeling and drug discovery.* Biomaterials, 2019. **221**: p. 119416.

38. McCormick, R. and A. Vasilaki, *Age-related changes in skeletal muscle: changes to life-style as a therapy.* Biogerontology, 2018. **19**(6): p. 519-536.

39. Demontis, F., et al., *Mechanisms of skeletal muscle aging: insights from Drosophila and mammalian models.* Dis Model Mech, 2013. **6**(6): p. 1339-52.

40. Therakomen, V., A. Petchlorlian, and N. Lakananurak, *Prevalence and risk factors of primary sarcopenia in community-dwelling outpatient elderly: a cross-sectional study.* Sci Rep, 2020. **10**(1): p. 19551.

41. Peake, J., P. Della Gatta, and D. Cameron-Smith, *Aging and its effects on inflammation in skeletal muscle at rest and following exercise-induced muscle injury.* Am J Physiol Regul Integr Comp Physiol, 2010. **298**(6): p. R1485-95.

42. Jakubowski, J.K., R. Patel, and V. Buddharaju, *Polymyositis Presenting as Rhabdomyolysis After the Initiation of Omeprazole.* Cureus, 2020. **12**(5): p. e8125.

43. Roten, L., et al., *Rhabdomyolysis in association with simvastatin and amiodarone.* Ann Pharmacother, 2004. **38**(6): p. 978-81.

44. Tarpey, M.D., et al., *Doxorubicin causes lesions in the electron transport system of skeletal muscle mitochondria that are associated with a loss of contractile function.* J Biol Chem, 2019. **294**(51): p. 19709-19722.

45. Love, M.S., et al., *A high-throughput phenotypic screen identifies clofazimine as a potential treatment for cryptosporidiosis.* PLoS Negl Trop Dis, 2017. **11**(2): p. e0005373.

46. Nugraha, R.V., et al., *Clofazimine as a Treatment for Multidrug-Resistant Tuberculosis: A Review.* Scientia Pharmaceutica, 2021. **89**(2): p. 19.

47. Arbiser, J.L. and S.L. Moschella, *Clofazimine: a review of its medical uses and mechanisms of action.* J Am Acad Dermatol, 1995. **32**(2 Pt 1): p. 241-7.

48. Murashov, M.D., et al., *Synthesis and Characterization of a Biomimetic Formulation of Clofazimine Hydrochloride Microcrystals for Parenteral Administration.* Pharmaceutics, 2018. **10**(4).

49. Baik, J. and G.R. Rosania, *Molecular imaging of intracellular drug-membrane aggregate formation.* Mol Pharm, 2011. **8**(5): p. 1742-9.

50. Van Norman, G.A., *Limitations of Animal Studies for Predicting Toxicity in Clinical Trials: Part 2: Potential Alternatives to the Use of Animals in Preclinical Trials.* JACC Basic Transl Sci, 2020. **5**(4): p. 387-397.

51. van Dijk, M., et al., *Sarcopenia in older mice is characterized by a decreased anabolic response to a protein meal.* Arch Gerontol Geriatr, 2017. **69**: p. 134-143.

Chapter 2 Distribution Patterns of Clofazimine in Bone and Spleen

2.1 Relevance to Thesis

This chapter focuses on the investigation of the mechanism of clofazimine (CFZ) accumulation in young (4-weeks-old) and old (61-weeks-old) mice, particularly in relation to drug exposure times. For this work, I utilized the bone, responsible for the origin and storage of macrophages, and the spleen, a reservoir for macrophages. I used imaging technique that I previously described in [1], to create brightfield and fluorescence profiles for CFZ freebase (CFZ-FB) and CFZ hydrochloride (CFZ-HCL) to distinguish the mechanism of accumulation. In this analysis, crystal-like drug inclusions (CLDIs) formed by CFZ-HCL are associated with macrophages, while CFZ-FB is associated with lipids.

The study presented in this chapter also identified cytokines involved in differentiating cells into a drug-sequestering population and showed that CLDIs rely on macrophage viability to remain stable. Most importantly, bone marrow cells are programmed to accumulate xenobiotics at their origin. It also demonstrated that the mechanism of CFZ accumulation is tissue dependent.

These results have important implications for detecting accumulation mechanisms and adverse drug reactions (ADRs). Overall, this chapter successfully addressed the major goals of specific aims 1, 2, and 3.

2.2 Abstract

Clofazimine (CFZ), is an antimycobacterial agent that has been extensively studied for its bioaccumulating properties in macrophages. However, the accumulation mechanism of CFZ may vary across different tissues and be affected by age and duration of treatment. To determine CFZ distribution patterns, macrophage-rich tissues such as bone marrow and spleen were studied. The innate ability of bone marrow cells to accumulate CFZ, the impact of CFZ on bone density, immune response to CFZ, and cell sequestering patterns were investigated in young (4-weeks-old) male mice with increasing CFZ treatment duration (2-32 weeks). Furthermore, in the spleen, I studied the impact of CFZ on spleen mass, and cell sequestering patterns in young (4-weeks-old) and old mice (61-weeks-old) with different durations of CFZ treatment (8-65 weeks). The findings suggest that CFZ treatment decreases trabecular bone density and alters cytokine levels in the bone marrow, and bone marrow cells increase their CFZ sequestering ability with long-term (32 week) treatment. Whereas in the spleen, the mass increased with CFZ treatment, and the distribution pattern did not differ with either age or duration. These results suggest that the accumulation mechanism of CFZ is tissue dependent, highlighting the importance of understanding drug distribution patterns in different tissues for optimizing drug development and drug dosing.

2.3 Introduction

Clofazimine (CFZ), an FDA-approved oral antibiotic, is used for leprosy, tuberculosis, and has been shown to broadly inhibit coronaviruses [2, 3]. Its mechanism of action involves the drug transitioning from a free base to crystal-like drug inclusions (CLDIs), an insoluble crystalline membrane-bound complex that binds with chloride (CFZ hydrochloride, CFZ-HCL) in macrophage lysosomal compartment [4]. However, factors such as age and long-term treatment

that can affect CFZ distribution in macrophage-rich tissues such as the bone and spleen have not been fully investigated.

Due to CFZ's physiochemical properties, it extensively accumulates in macrophages, which provokes an immune response and causes a mass increase of the spleen, a vital organ for the immune system that has a large population of tissue resident macrophages [4-6]. The spleen has been shown to undergo age-related changes causing alterations in cell population and drug response [7, 8]. However, there has not been a thorough examination of the variation in CFZ distribution in the spleen with respect to age and extent of treatment. Additionally, the drug sequestering abilities of bone marrow, the site of macrophage production and storage, found in the trabecular bone layer (red marrow) at the ends of long bones, has not been explored [9].

To investigate CFZ accumulation in the spleen, young (4-weeks old) and old (61-weeks old) C57BL/6J male mice were treated with CFZ for 8-weeks, as well as young mice treated for 65 weeks, where young mice were treated with CFZ for 2, 4, 8, and 32 weeks to investigate drug distribution in the bone marrow. In addition, I measured bone density, and bone marrow cytokine levels, to better understand the relationship between macrophage-rich tissues and medication exposure. By understanding the mechanisms underlying CFZ accumulation in macrophages, it will help optimize drug safety and therapeutic properties.

2.4 Materials and Methods

2.4.1 Animal Studies

Male C57BL/6J mice (Jackson Laboratory, Bar Harbor, Maine USA) were used, and animal care was provided by the University of Michigan's Unit for Laboratory Animal Medicine (ULAM). Animal use protocols were approved by the University of Michigan's Institutional Committee on Use and Care of Animals (PRO00009404; December 13, 2022).

CFZ (C8895, Sigma-Aldrich) or vehicle (equivalent sesame oil, 720189601668, Kadoya) was added to the feed at a dose of 36 mg/kg/day [4] for 2, 4, 8, and 32 weeks in young mice (4-weeks-old) and for 8 weeks in old mice (61-weeks-old). Mice were randomly assigned to receive either CFZ or vehicle treatment: 2, 4, and 8 week treated mice (n=5/group); 32 week treated mice (n=3/group); 65 week treated mice (n=4/group); 8 week treated young and old mice (n=5-6/group). At the end of the treatment period, the animals were euthanized following AVMA Guidelines through CO2 inhalation and a cardiac puncture. The spleens were immediately isolated, washed with 1X PBS (10010023, Gibco), blotted dry, and weighed.

2.4.2 CLDI Stability Studies in Bone Marrow Derived Macrophage

Bone marrow was derived into macrophages as previously described [10]. Briefly, the femora were isolated from young mice that received CFZ treatment for 32 weeks and cleared of debris using gauze and 1X PBS (10010023, Gibco). Bone marrow cells were collected by snipping the ends of the femora and flushing the cavity with media containing 80% RPMI (11875119, Gibco), 20% certified fetal bovine serum (16000044, Gibco), 1% GlutaMAX (35050061, Gibco), 0.1% penicillin-streptomycin (15140122, Gibco), 0.1% 1:400 β-mercaptoethanol (M3148, Sigma-Aldrich), and 0.05% 1:1000 m-CSF (416-mL-050, R&D Systems). The bone marrow cells were plated and incubated at 37 °C with 5% CO2 for six days to differentiate into macrophages.

Macrophages derived from bone marrow were resuspended in DMEM (11995065, Gibco) with 5% certified fetal bovine serum (16000044, Gibco), and seeded in 6-well plates (500,000 cells/well). After 24 hours, the cells were treated with 1 μM bafilomycin (54645S, Cell Signaling Technology), staurosporine (120056, Abcam), or the equivalent amount of vehicle (DMSO, 4-X, ATCC). Brightfield and fluorescence images were taken at 0, 12, 24, 48, and 72 hours using a 40x magnification on an Eclipse Ti inverted microscope (Nikon Instruments, Melville, NY, USA). The

fluorescence channels with an exposure time of 500 ms were used to detect CLDIs (CY5, red channel) and CFZ-Freebase (FITC, green channel), as previously shown in [1]. After 72 hours, the cells were resuspended in HBSS (14175103, Gibco) and 1:1 trypan blue (15250061, Gibco) to determine cell viability, which was calculated in triplicate for treated and duplicated for control samples (with at least 200 cells measured per sample).

2.4.3 Femora Preparation and Nanocomputed Tomography

The femora from young (4-weeks) and old (61-weeks) mice treated for 8 weeks were dissected free from associated connective tissue, wrapped in gauze soaked with 1X PBS (10010023, Gibco), placed in sealed containers, and frozen at −20 °C until use. Nanocomputed tomography (nanoCT) was performed by the Micro and NanoCT Advanced Imaging Core at the University of Michigan. In brief, specimens were immobilized inside a plastic tube and scanned using a nanotom M nanoCT (phoenix x-ray, Waygate Technologies USA, LP; Skaneateles, New York). The X-ray tube was powered to 80 kV and 400 µA, utilized a diamond coated tungsten target, a 0.381mm Aluminum filter, and was set to a spot size of 0. Imaging was done at 8 µm voxel size using an exposure time of 500 ms; 3 frames averaged and 1 skipped for each rotation. The sample stage rotated through 360 degrees and collected 2000 images per scan. Image acquisition and reconstruction of raw data were performed using Datos|x 2 version 2.6.1 (phoenix x-ray, Waygate Technologies USA, LP; Skaneateles, New York).

2.4.4 Cytokine Analysis of Bone Marrow

Cytokine levels in the bone marrow of young 8-week treated mice were assessed using the proteome profiler array kit (ARY006, R&D Systems) according to the manufacturer's instructions, where a total of 200 μg of femora bone marrow lysate protein was used. After isolating the bone

marrow samples, they were immediately placed in the recommended lysis buffer and vortexed until the cell pellet was disrupted. Lysates where then gently rocked (4 °C, 30 min) and centrifuged (14,000 x g, 5 min, 4 °C). Lysate protein was measured using a bicinchoninic acid (BCA) assay (23225, Pierce) following the manufacturer's guidelines. Samples were simultaneously assayed for cytokines using chemiluminescence (iBright CL15000, Invitrogen/Thermo Fisher Scientific). Pixel density was quantified using the instrument's software. Detected cytokine densities were background subtracted and normalized by the density of the positive controls of the corresponding membrane.

2.4.5 Bone Marrow CFZ Sequestering Studies

Femora were harvested at various time points (2, 4, 8, and 32 weeks) and cleaned with gauze and 1X PBS (10010023, Gibco). The bone marrow was isolated by snipping the ends of the femora and flushing with media consisting of 80% RPMI (11875119, Gibco), 20% certified fetal bovine serum (16000044, Gibco), 1% GlutaMAX (35050061, Gibco), 0.1% penicillin-streptomycin (15140122, Gibco), and 0.1% 1:400 β-mercaptoethanol (M3148, Sigma-Aldrich). The marrow was vortexed until the cell pellet was disrupted and then centrifuged (200 x *g*, 10 min, 4 °C). The supernatant was removed, and the cells were resuspended in 1X PBS (2 million cells/mL). To achieve a final concentration of 1 million cells/mL, 4% paraformaldehyde (15710, Electron Microscopy Sciences) was added to the sample. The cells were incubated (15 min, RT), washed twice with 1X PBS to maintain 1 million cells/mL; the cell pellet was resuspended in 20 μL of 1X PBS. A 2μL aliquot of the cell suspension was added to glass slides, which were then mounted with a drop of ProLong® Gold antifade with DAPI (P36941, Molecular Probes) for nuclear detection. A coverslip was placed and sealed with clear nail polish, and the slides were stored (-80°C) until imaging was conducted.

The slides were imaged at 10x magnification using fluorescent microscopy (Vectra Polaris). Fluorescence imaging was performed using the Cy5 channel (640/670 nm, CLDI) and DAPI channel (340/435 nm, nucleus) with exposure times of 300 ms and 3 ms, respectively. Images were analyzed using QuPath (0.4.2; University of Edinburgh, Edinburgh, Scotland, UK), and the CY5 channel signal area (mm^2) and cells (DAPI+ and DAPI+/CLDI+) were collected as objects. Analyzed field area (mm^2) populated by cells was used to correct signals.

2.4.6 Spleen CFZ Sequestering Studies

Fluorescence immunohistochemistry was performed on spleen sections from mice that received an 8- or 65-weeks of CFZ treatment starting at 4 weeks old, and an 8-week treatment starting at 61-weeks-old, as previously described [11] with slight modifications. Briefly, spleens were washed with 1X PBS (10010023, Gibco), blotted dry, and embedded in Tissue-Plus Optimal Cutting Temperature (OCT) compound (4585, Fisher); specimens were frozen (-80°C). In preparation for analysis, OCT preserved spleens were sectioned (10 μm) using a Leica 3050S cryostat. Sections were stained with anti-F4/80 (ab6640; Abcam), followed by Alexa Fluor 488-conjugated secondary antibody (4416, Signaling Technology), and mounted with a ProLong® Gold antifade reagent with DAPI (P36941, Molecular Probes). Fluorescent microscopy (Nikon Eclipse Ti, Nikon Instruments, Melville, NY, USA) was used to acquire images at 40x magnification, with exposure times of 500 ms, using the CY5 channel (640/670 nm, CLDI), FITC channel (490/510 nm, F4/80 macrophages), and DAPI channel (340/435 nm, nucleus) on three sections per mouse, where three random areas were captured. Image analysis was conducted using Image J (National Institute of Health, Maryland, USA). Analyzed field area was used to correct signals.

2.4.7 Estimation of Spleen CFZ and Macrophage Cargo

Macrophage drug cargo in spleens were calculated in young (4-weeks-old) and old (61-weeks old) mice treated 8-weeks with CFZ and 65-week CFZ-treated mice that began treatment at 4-weeks-old, as previously described in [12]. The total number of macrophages in the CFZ-treated groups was calculated by multiplying a spleen expansion factor (mass) by the F4/80 signal difference of their respective control group and by a reported baseline macrophage population of 5.50E+06 total macrophages [13]. The number of CFZ-sequestering macrophages was determined by visually inspecting the fraction of cells that were positive for CY5 fluorescence and F4/80 staining. The predicted CFZ cargo was determined by using a reported maximum measured CLDI cargo capacity of macrophages (310.5 fmol/cell) and the total number of CFZ-sequestering macrophages [12]. The CFZ concentration (μg/g) was measured by LC-MS. To convert CFZ to mg, concentration values were multiplied by the mass of each sample. The mass of macrophages was determined using a value of 5.37E-07 mg based on the measured amount of lipid (mass and volume) of mice macrophages [14].

2.4.8 Statistical Analysis

A one-way ANOVA was employed to compare data followed by a post-hoc Tukey's test when the ANOVA p-value was significant. An unpaired Student's t-test with equal variance was used to compare two groups. All analyses were performed, and plots were constructed, using PRISM (9.4.1; GraphPad Software, Inc., San Diego, CA USA). Statistical significance was set at a p-value of ≤ 0.05.

2.5 Results

2.5.1 CLDI Stability is Dependent on Macrophage Viability

Treatment with bafilomycin, an ATPase inhibitor that disrupts the pH of the lysosomal compartment, and staurosporine, a kinase inhibitor that induces apoptosis, resulted in the destabilization of CLDIs, as evidenced by a shift from CY5 (CLDI channel) to FITC (CFZ Freebase channel) at 48 h, which was not observed in the control group (**Figure 2-1A, B**). The destabilization of CLDIs was followed by a significant increase in cell death compared to the vehicle controls (**Figure 2-1A, B**).

2.5.2 CFZ Alters Cytokine Levels in Bone Marrow

After 8 weeks of CFZ treatment, young mice showed increased levels of macrophage inflammatory protein-2 (MIP-2), complement C5 (C5), and Interleukin-1 alpha (IL-1a), which are proinflammatory cytokines responsible for macrophage recruitment compared to its control (**Table 2-1**) [15-17]. The increased levels of MIP-2, C5, and IL-1a in the bone marrow indicate an increase in the number of macrophages and an upregulation of bone resorption activity and phagocytosis [18-20].

2.5.3 Trabecular Bone Density Decreased but Spleen Mass Increased with CFZ Treatment

Analysis of femoral bone using nano-CT showed no significant difference in the density of the cortical bone, the outer layer, between young 8-week CFZ-treated mice and their vehicle-treated control (**Figure 2-2A**). However, the density of the trabecular bone, commonly known as the spongy bone, was decreased in young CFZ-treated mice (8+) compared to its control (8-) (**Figure 2-2A**). Spleen-body mass ratio of 8 and 65 (8+, 65+) week CFZ-treated mice, that began at 4-weeks old, increased compared to their negative controls, (8-) and (65-) (**Figure 2-2B**). Old

8-week CFZ-treated mice (old 8+), that began treatment at 61 weeks old, also experienced a decrease in trabecular bone density and an increase in spleen-body ratio mass compared to its control, (old 8-) (**Figure S 2-1**).

2.5.4 Long-Term CFZ Treatment Increases the Cargo Capacity of Bone Marrow Cells

The amount of CLDIs increased as the duration of CFZ treatment increased from 8 to 32 weeks (**Figure 2-3A**). Both the percentage of cells that sequestered CLDIs and the cargo capacity of CLDI signal per cell increased with treatment duration, between 2, 4, 8, and 32 weeks (**Figure 2-3A, Figure S 2-2**). However, there were no differences in CLDI signal, drug-sequestering macrophages, or cargo capacity in young spleens between an 8- and 65-week CFZ treatment (**Figure 2-3B**). Age also did not appear to be a factor in CFZ sequestering macrophages or cargo capacity in the spleen (**Figure S 2-3**).

2.5.5 Spleen Mass Increases with CFZ-Treatment

The predicted total amount of CFZ (mg) did not differ from the measured CFZ cargo in the spleens from each group (young and old mice that received 8-weeks and mice that received 65-weeks of CFZ treatment) (**Table 2-2**). This was used to estimate the mass of recruited macrophages and measured CFZ cargo, which did not fully account for the increase in spleen mass that occurred with CFZ-treatment (**Table 2-2).**

2.6 Discussion

This study provides insights into the mechanisms that contribute to the distribution of CFZ and the impact of long-term treatment on bone and spleen. To understand the relationship between the drug accumulation mechanism of the bone and long-term exposures, we chose the femur (thigh bone) as a representative bone because it contains the tabular bone that houses the red marrow

[21]. We measured bone density, cytokine levels, and sequestering profiles in long-term CFZ treated C57BL/6J mice. We focused on studying the effects of age and long-term treatment in the spleen, as previous studies have looked at the immune response and drug distribution in young 8-week treated mice [4, 22].

Our results indicate that the stability of CLDIs is dependent on macrophage viability, as destabilization of these structures was observed in response to bafilomycin and staurosporine treatment, which disrupt lysosomal pH and induce apoptosis, respectively (**Figure 2-1A**) [23, 24]. These findings suggest that macrophage viability is needed for the maintenance of CFZ sequestration within lysosomal compartments, and that macrophage death or dysfunction could affect the distribution of CFZ.

In addition, the study revelated that CFZ treatment decreases trabecular bone density, which is a hallmark of osteoporosis (**Figure 2-2A**) [25]. This decrease may have been due to CFZ-altered cytokines, which affect bone remodeling and density (**Table 2-1**) [20]. However, the spleen showed an increase in mass (**Figure 2-2B**), known as splenomegaly, that could not be fully explained by the increase in macrophages and CFZ cargo (**Table 2-2**). CFZ treatment has been shown to increase the production of interleukin-1 receptor antagonist (IL-1RA, an anti-inflammatory cytokine) and decrease the levels of regulated upon activation, normal T cells expressed and secreted (RANTES) and chemokine ligand 9(CXCL9) (proinflammatory cytokines) in the spleen, indicating that CFZ has differential effects on cytokine expression in the bone marrow and spleen that may lead to altered tissue structure [4]. Further studies are needed to understand the mechanism underlying this phenomenon.

Long-term CFZ treatment increased the cargo capacity and number of drug-sequestering cells, allowing for accumulation of the drug in bone tissue (**Figure 2-3A**). However, in the spleen, long-

term dosing and age did not impact the percentage of macrophages or cargo capacity (**Figure 2-3B**), relying on the spleen's ability to increase in size to accommodate an increase of drug load (**Figure 2-2B**).

While our study provides insights into the impact of CFZ treatment on bone and spleen structure and immune response, there are limitations to consider when interpreting our findings. We focused specifically on the effects of CFZ on mass and immune response and acknowledge that our findings are unique to this drug. It is likely that other bioaccumulating drugs utilize different accumulation mechanisms. Nonetheless, our findings provide new insight into tissue-dependent drug accumulation and the effects of CFZ in bone marrow and spleen. Further investigation into the mechanisms underlying molecule bioaccumulation in bones and spleen could lead to the optimization of macrophage targeting drugs.

2.7 Acknowledgements and Funding

I would like to express my gratitude to Laura McLellan for providing invaluable technical and analytical support for the cellular assays and Marian Fu for analyzing the spleen images. I would also like to thank the University of Michigan Micro and Nano CT Advanced Imaging Core for their technical and analytical contributions.

This research was funded by grants from the National Institutes of Health, National Institute of General Medical Sciences under award numbers R01GM127787 (Dr. Rosania), P30AR069620 (Dr. Jepsen), and R35GM136312 (Dr. Stringer).

2.8 Figures

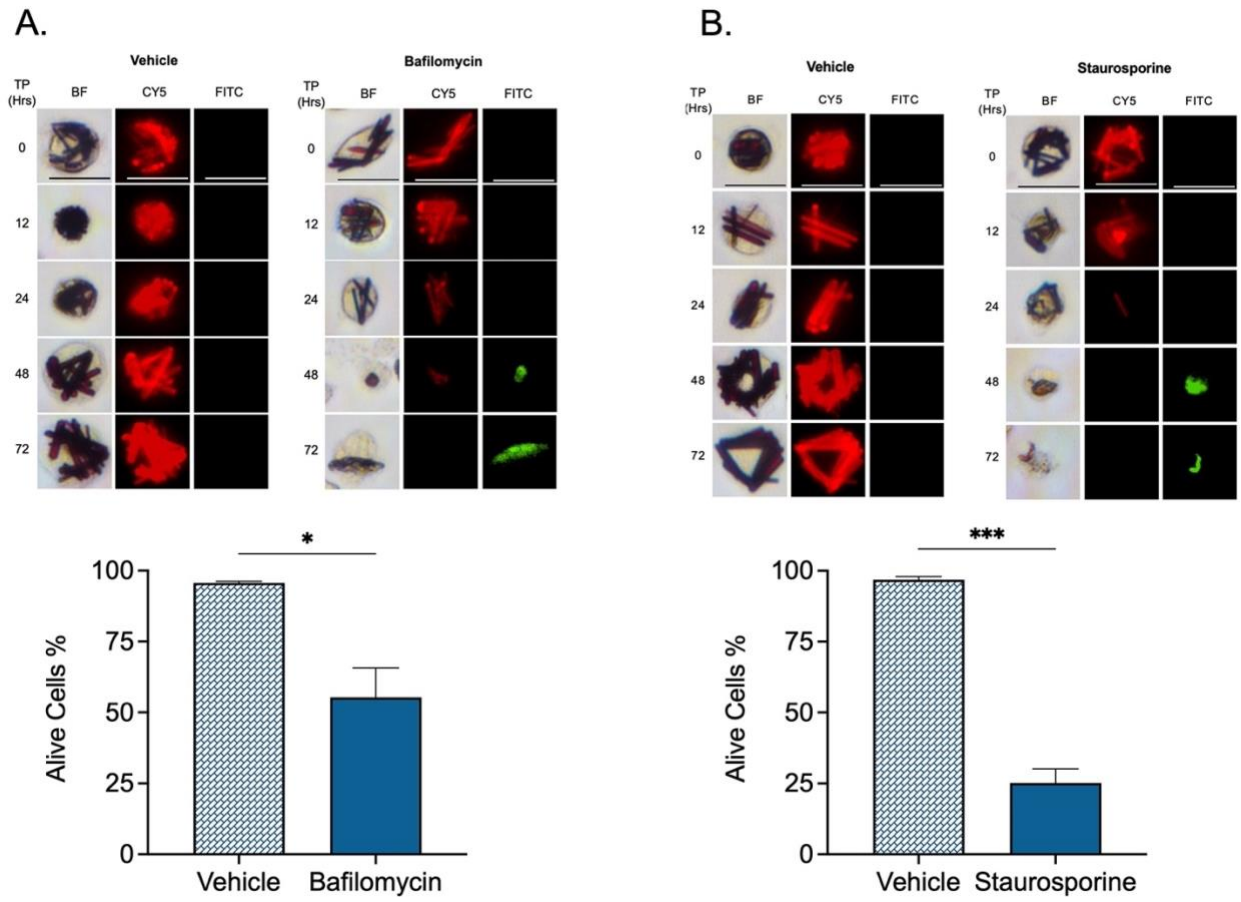

Figure 2-1 CLDI Stability Within Bone Marrow Derived Macrophages

The in vitro stability of CLDIs was evaluated in bone marrow derived macrophages from femora of mice treated with clofazimine for 32 weeks starting at 4-weeks old (scale bar= 20 μm). **A.** The destabilization of CLDIs (shift from CY5 to FITC) occurred at 48 hr after treatment with bafilomycin (n=2-3/group). **B.** Similarly, CLDIs were destabilized in cells treated with staurosporine (n=2-3/group). Viability (mean ± SD) at 72 hr as measured by trypan blue exclusion was 55% in bafilomycin-treated cells and 25% in staurosporine-treated cells, demonstrating increased cell death compared to their controls (bafilomycin, *p=0.01, Student's t-test; staurosporine, ***p=0.0003, Student's t-test).

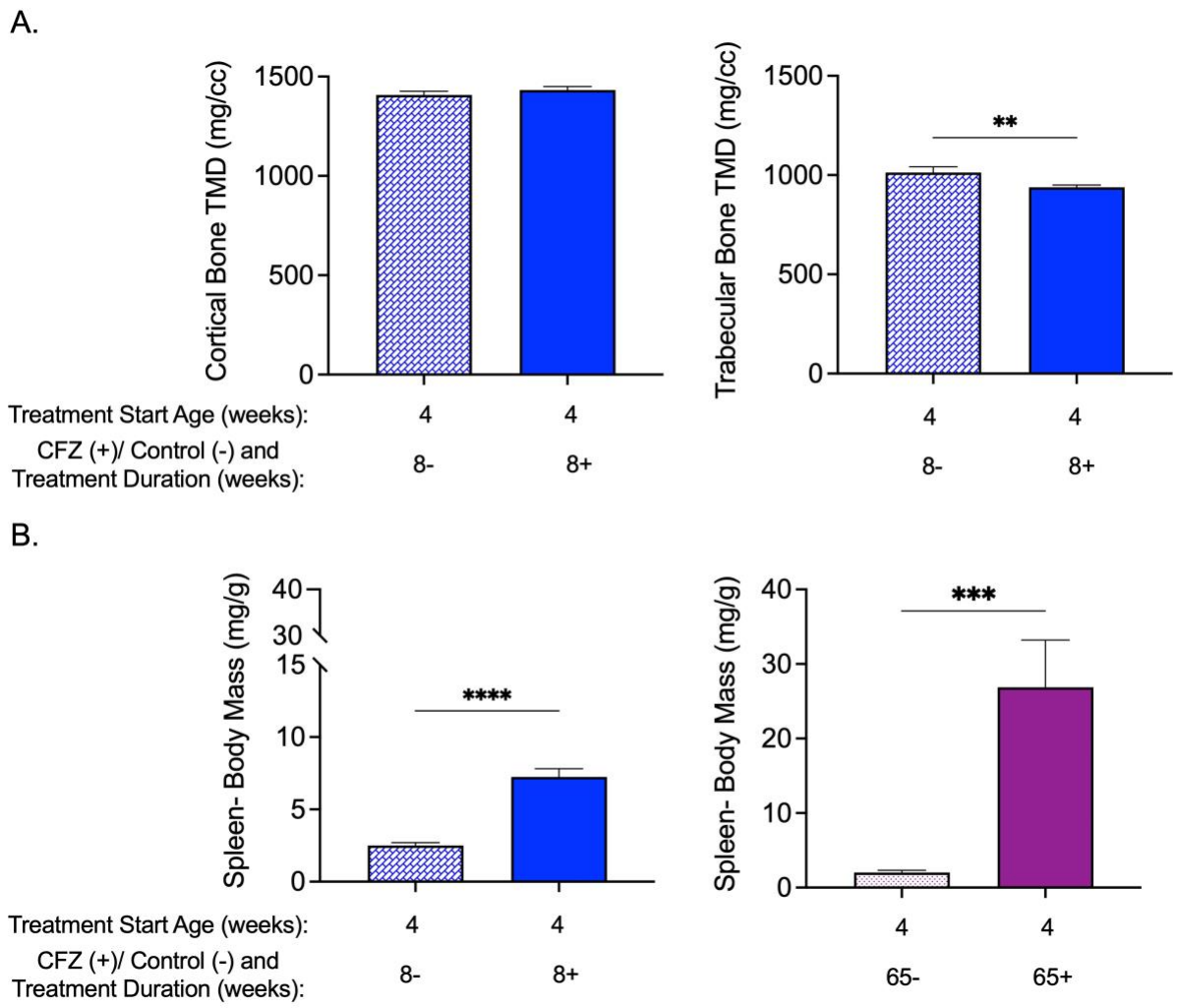

Figure 2-2 Femora Density Measurements and Spleen-Body Mass Ratio

A. The cortical and trabecular tissue mineral density (TMD, mean ± SD) of the femora was measured via Nano-CT in young mice (4-weeks-old) treated with CFZ or vehicle for 8 weeks (n=4/group). There was no difference in the cortical bone density (outer layer) of 8-week CFZ-treated mice (8+) compared to its vehicle control, (8-; p=0.11, Student's t-test). However, CFZ treatment caused a decrease in the trabecular bone (inner layer at the ends) density compared to its control, (8-; **p=0.003, Student's t-test). **B.** Spleen-Body mass ratio (mean ± SD) of 8 week young, treated mice (n=6/group). Unlike the bone, CFZ treatment caused an increase in spleen mass of (8+) mice compared to (8-) mice (****p<0.0001, Student's t-test). The spleen-body ratio (mean ± SD) of 65-week CFZ treated mice (65+) was also higher than its control, (65-; ***p=0.0002, Student's t-test, n=4).

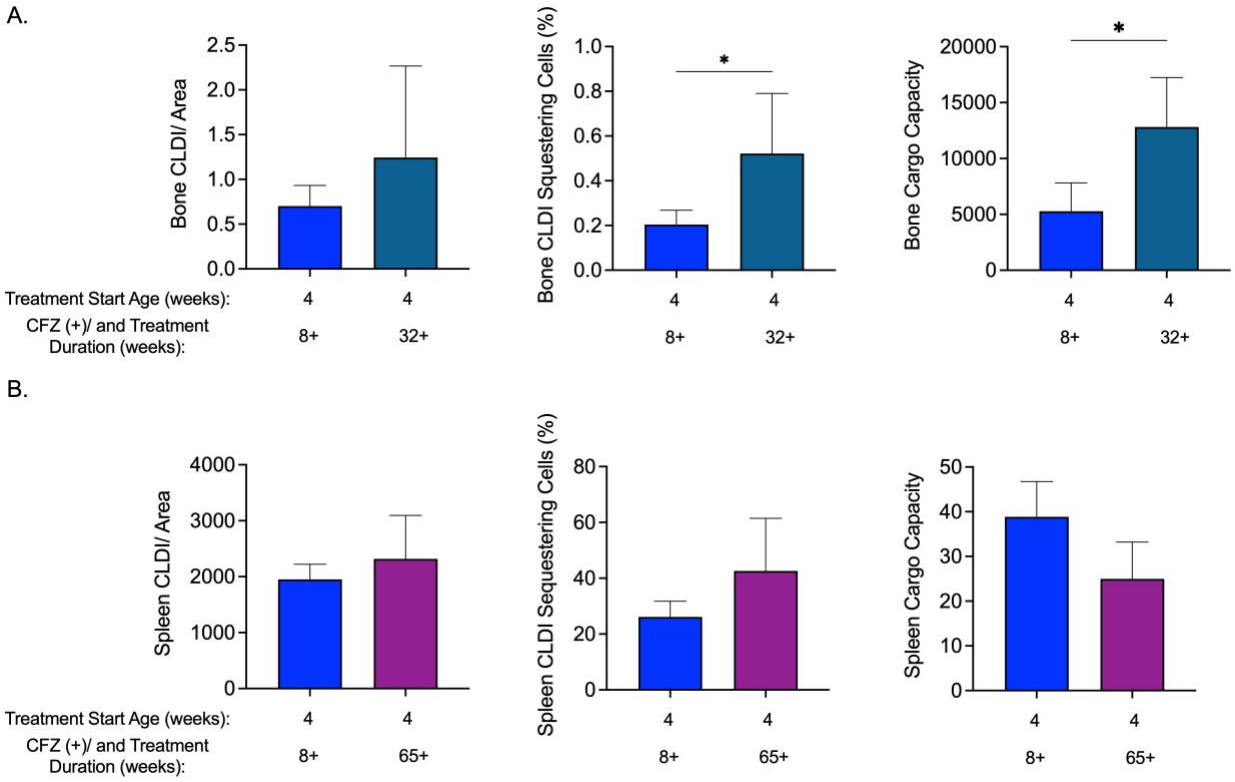

Figure 2-3 Bone Marrow and Spleen CFZ Sequestration During Long-Term Treatment

A. Bone marrow CLDI signal corrected by area, percent of CLDI-sequestering cells determined by objects, and cargo capacity calculated by the total CLDI signal/sequestering cell (mean ± SD, n=3-5/group). The corrected CLDI signal was not different between young (4-week-old) 8-week CFZ-treated mice (8+) and 32-week CFZ-treated (32+) mice (p=0.28, Student's t-test). The 32-week CFZ-treated animals (32+) had a higher percentage of CFZ sequestering cells compared to the 8-week treated group, 8+ (*p=0.04, Student's t-test). The CFZ cargo capacity of bone marrow cells increased with longer treatment regimen (*p=0.02, Student's t-test). **B.** The spleen's CLDI signal corrected by area, reported as the precent of CLDI-sequestering macrophages determined by visual inspection, and cargo capacity calculated by the total CLDI signal/sequestering macrophage (mean ± SD, n=3/group) were not different between the 8 and 65-week treatment groups (p=0.48, p=0.22, p=0.10, respectively, Student's t-test).

2.9 Tables

Table 2-1 CFZ-Induced Changes in Bone Marrow Cytokine Levels

The top 3 out of 40 bone marrow cytokines were measured and the percent (mean) is shown for young 8-week CFZ-treated (8+) and vehicle-treated (8-) mice that started treatment at 4-weeks old. The group densities (mean ± SD) are shown below their respective names (n=5/group). The (8+) group showed a significant increase in MIP-2 (*p=0.02, Student's t-test), C5 (*p=0.02, Student's t-test), and IL-1a (*p=0.03, Student's t-test) levels compared to the (8-) group.

Cytokine	Function	Change (%)	8+	8-	P
MIP-2	Macrophage Recruitment	100	0.069 ± 0.023	0.034 ± 0.013	0.02
C5	Proinflammatory	33	0.462 ± 0.030	0.347 ± 0.083	0.02
IL-1a	Proinflammatory	78	0.352 ± 0.090	0.198 ± 0.095	0.03

Table 2-2 Estimated CFZ and Macrophage Cargo Loads of Spleen

CFZ and macrophage drug cargo was determined in spleens of young (4-weeks-old) and old (61 weeks old) 8-week CFZ-treated mice and 65-week CFZ-treated mice. There was no difference between the percent of sequestering macrophages (mean ± SD) among the groups (p=0.19, one-way ANOVA, n=3/group). No difference was found between the predicted and measured total CFZ mass (mean ± SD) of each group (n=4-5/group). The spleen mass increase (mean ± SD) represents the difference between the CFZ-treated groups and their respective controls (n=4-6/group), where it cannot be explained by the increase in macrophage mass and accumulated CFZ mass.

CFZ Groups		Total Macrophages	CLDI Sequestering Macrophages (%)	Predicted Total CFZ (mg)	Measured Total CFZ (mg)	Macrophage and CFZ Mass (mg)	Spleen Mass Increase (mg)
Treatment Start Age (weeks)	Treatment Duration (weeks)						
4	8	8.25E+07	38.85 ± 7.91	3.41 ± 0.73	2.96 ± 0.53	44.27 ± 0.41	111.60 ± 19.26
61	8	3.88E+07	27.25 ± 3.46	1.51 ± 0.22	1.31 ± 0.49	19.18 ± 0.49	50.65 ± 24.50
4	65	1.90E+08	24.97 ± 8.25	12.83 ± 5.67	9.49 ± 1.42	108.80 ± 1.42	534.2 ± 128.00

2.10 Supporting Information

2.10.1 Figures

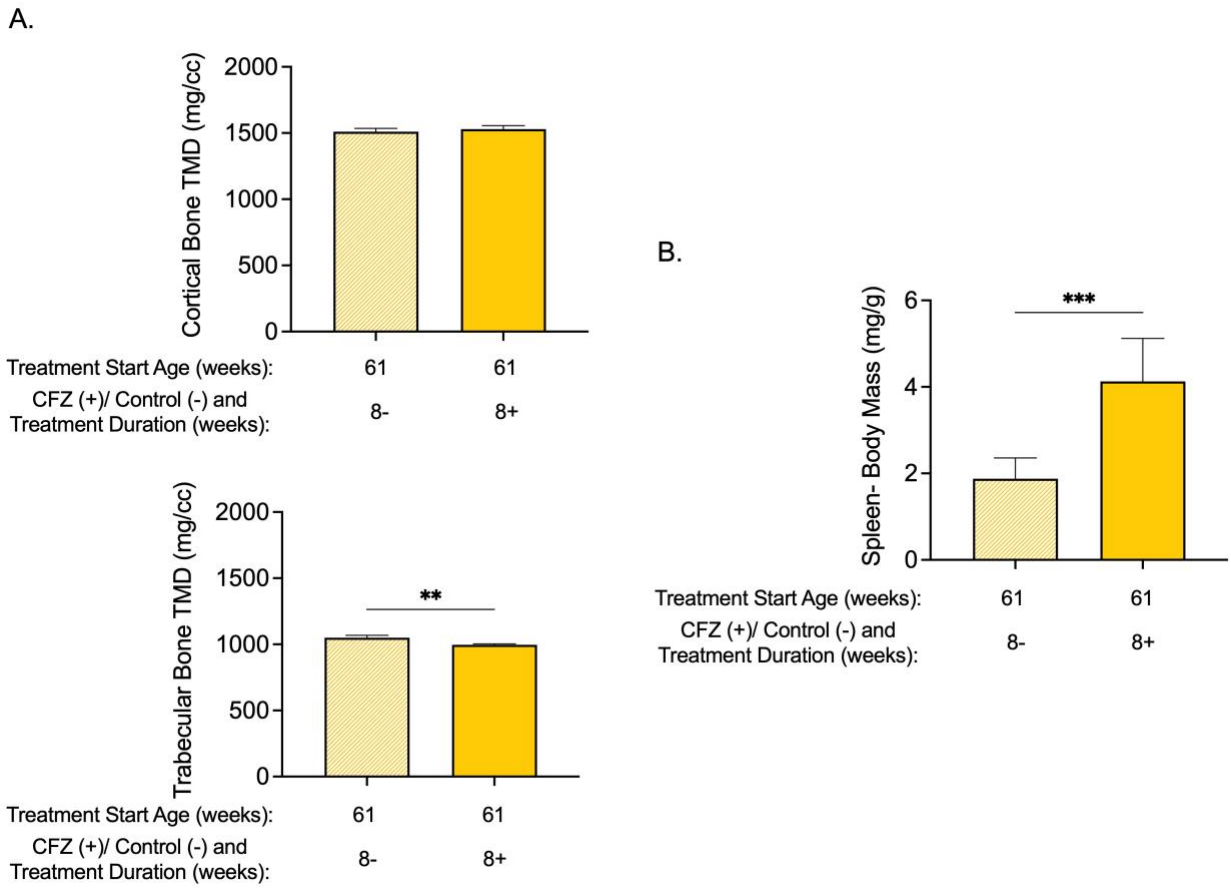

Figure S 2-1 Femora Density Measurements and Spleen-Body Mass Ratio of Old Mice

A. There was no difference in the cortical bone density (mean ± SD) of old (61-weeks-old) 8-week CFZ-treated mice compared to its vehicle control (p=0.33, Student's t-test, n=4). CFZ altered the trabecular bone density (mean ± SD), where CFZ-treated mice (old 8+) displayed a decrease in TMD compared to old 8- (**p=0.001, Student's t-test, n=4). **B.** Spleen-Body ratio (mean ± SD) of old 8 week treated mice (n=5-6/group). CFZ treatment caused an increase in spleen mass of old 8+ mice compared to old 8- mice (***p=0.001, Student's t-test).

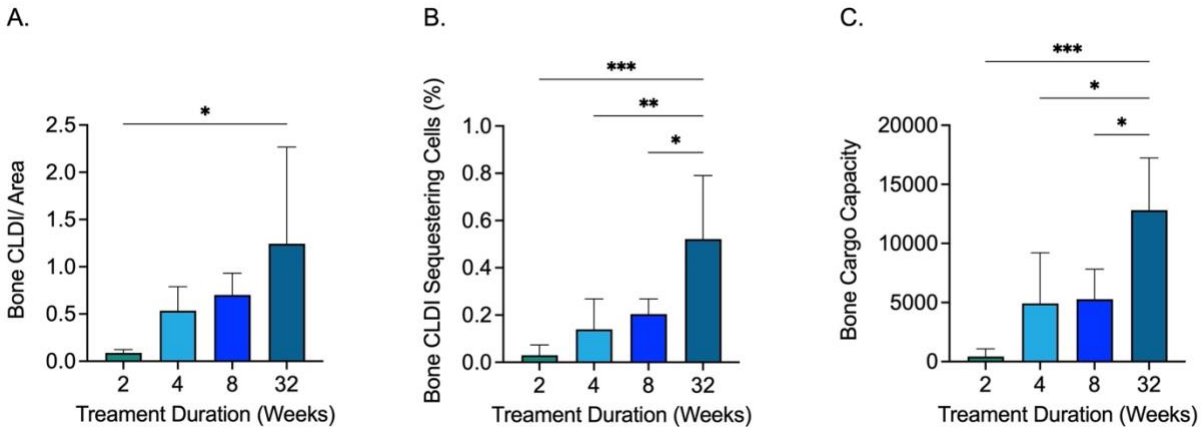

Figure S 2-2 Bone Marrow CFZ Sequestration Throughout Increasing Treatment Durations

CFZ treatment of 2,4,8, and 32 weeks was given to 4-week-old mice. **A.** CLDI signal (mean ± SD) corrected by area (n=3-5/group). The CLDI signal increased with longer treatment duration (2+ vs 32+, p=0.01, Tukey). **B.** Percent of CLDI-sequestering cells (mean ± SD) determined by objects (n=3-5/group). The 32-week CFZ-treated group (32+) had a higher percentage of CFZ sequestering cells compared to 2 (***p=0.0007, Tukey), 4(**p=0.006, Tukey), and 8 (*p=0.02, Tukey) weeks. C. CLDI/sequestering cells (mean ± SD) displayed as the ratio between the CLDI signal and the number of CLDI sequestering macrophages and corrected by area (n=3-5/group). The CFZ cargo capacity of bone marrow cells increases throughout the treatment regimens (2 vs 32, ***p=0.0005; 4 vs 32, *p=0.02; 8 vs 32, *p=0.03; Tukey).

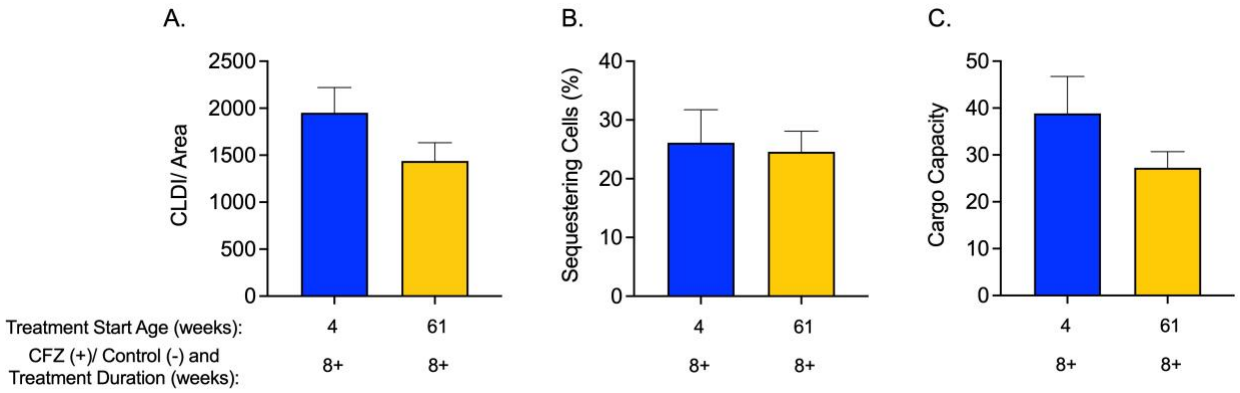

Figure S 2-3 Spleen CFZ Sequestration of Old Mice

CFZ distribution in spleens of 8-week treated mice, that started treatment at 4- (young) and 61- (old) weeks old. **A.** Age did not affect the corrected CLDI signal (mean ± SD, p=0.06, Student's t-test, n=3/group). **B.** Percent of CLDI-sequestering macrophages (mean ± SD) determined by visual inspection was not different between the young 8+ and old 8+ (p=0.71, Student's t-test, n=3/group). **C.** Cargo capacity (mean ± SD) calculated by the total CLDI signal/sequestering macrophage of young and old mice did not differ (p=0.81, student's t-test, n=3/group).

2.11 References

1. Murashov, M.D., et al., *Synthesis and Characterization of a Biomimetic Formulation of Clofazimine Hydrochloride Microcrystals for Parenteral Administration.* Pharmaceutics, 2018. **10**(4).

2. Willmer, A.R., et al., *Molecular design of a pathogen activated, self-assembling mechanopharmaceutical device.* J Control Release, 2022. **347**: p. 620-631.

3. Yuan, S., et al., *Clofazimine broadly inhibits coronaviruses including SARS-CoV-2.* Nature, 2021. **593**(7859): p. 418-423.

4. Baik, J., et al., *Multiscale distribution and bioaccumulation analysis of clofazimine reveals a massive immune system-mediated xenobiotic sequestration response.* Antimicrob Agents Chemother, 2013. **57**(3): p. 1218-30.

5. Swirski, F.K., et al., *Identification of splenic reservoir monocytes and their deployment to inflammatory sites.* Science, 2009. **325**(5940): p. 612-6.

6. Willmer, A.R., et al., *An Adaptive Biosystems Engineering Approach towards Modeling the Soluble-to-Insoluble Phase Transition of Clofazimine.* Pharmaceutics, 2021. **14**(1).

7. Lewis, S.M., A. Williams, and S.C. Eisenbarth, *Structure and function of the immune system in the spleen.* Sci Immunol, 2019. **4**(33).

8. Turner, V.M. and N.A. Mabbott, *Influence of ageing on the microarchitecture of the spleen and lymph nodes.* Biogerontology, 2017. **18**(5): p. 723-738.

9. Oftadeh, R., et al., *Biomechanics and mechanobiology of trabecular bone: a review.* J Biomech Eng, 2015. **137**(1): p. 0108021-01080215.

10. Tsang, A.W., et al., *Altered membrane trafficking in activated bone marrow-derived macrophages.* J Leukoc Biol, 2000. **68**(4): p. 487-94.

11. Trexel, J., et al., *Macrophage-Mediated Clofazimine Sequestration Is Accompanied by a Shift in Host Energy Metabolism.* J Pharm Sci, 2017. **106**(4): p. 1162-1174.

12. Rzeczycki, P., et al., *An Expandable Mechanopharmaceutical Device (1): Measuring the Cargo Capacity of Macrophages in a Living Organism.* Pharm Res, 2018. **36**(1): p. 12.

13. Lee, S.H., P.M. Starkey, and S. Gordon, *Quantitative analysis of total macrophage content in adult mouse tissues. Immunochemical studies with monoclonal antibody F4/80.* J Exp Med, 1985. **161**(3): p. 475-89.

14. LaLone, V., et al., *An Expandable Mechanopharmaceutical Device (3): a Versatile Raman Spectral Cytometry Approach to Study the Drug Cargo Capacity of Individual Macrophages.* Pharm Res, 2018. **36**(1): p. 2.

15. Matzer, S.P., et al., *Constitutive expression of macrophage-inflammatory protein 2 (MIP-2) mRNA in bone marrow gives rise to peripheral neutrophils with preformed MIP-2 protein.* J Immunol, 2001. **167**(8): p. 4635-43.

16. Ehrnthaller, C., et al., *Complement C3 and C5 deficiency affects fracture healing.* PLoS One, 2013. **8**(11): p. e81341.

17. Malik, A. and T.D. Kanneganti, *Function and regulation of IL-1alpha in inflammatory diseases and cancer.* Immunol Rev, 2018. **281**(1): p. 124-137.

18. Corbett, Y., et al., *Phagocytosis and activation of bone marrow-derived macrophages by Plasmodium falciparum gametocytes.* Malar J, 2021. **20**(1): p. 81.

19. Daniel, D.S., et al., *The reduced bactericidal function of complement C5-deficient murine macrophages is associated with defects in the synthesis and delivery of reactive oxygen radicals to mycobacterial phagosomes.* J Immunol, 2006. **177**(7): p. 4688-98.

20. Lee, Y.M., et al., *IL-1 plays an important role in the bone metabolism under physiological conditions.* Int Immunol, 2010. **22**(10): p. 805-16.

21. Ott, S.M., *Cortical or Trabecular Bone: What's the Difference?* Am J Nephrol, 2018. **47**(6): p. 373-375.

22. Yoon, G.S., et al., *Clofazimine Biocrystal Accumulation in Macrophages Upregulates Interleukin 1 Receptor Antagonist Production To Induce a Systemic Anti-Inflammatory State.* Antimicrob Agents Chemother, 2016. **60**(6): p. 3470-9.

23. Mauvezin, C. and T.P. Neufeld, *Bafilomycin A1 disrupts autophagic flux by inhibiting both V-ATPase-dependent acidification and Ca-P60A/SERCA-dependent autophagosome-lysosome fusion.* Autophagy, 2015. **11**(8): p. 1437-8.

24. Belmokhtar, C.A., J. Hillion, and E. Segal-Bendirdjian, *Staurosporine induces apoptosis through both caspase-dependent and caspase-independent mechanisms.* Oncogene, 2001. **20**(26): p. 3354-62.

25. Osterhoff, G., et al., *Bone mechanical properties and changes with osteoporosis.* Injury, 2016. **47 Suppl 2**(Suppl 2): p. S11-20.

Chapter 3 Clofazimine Induces an Age-Related Macrophage-Mediated Alteration in Skeletal Muscle

3.1 Relevance to Thesis

The objective of my thesis research was to examine the accumulation of drugs in young and old mice that were given an 8-week treatment with CFZ or vehicle, and assess its impact on skeletal muscle, which is one of the tissues most affected by aging. To achieve this, I used techniques described in Chapter 2, including the measurement of CFZ fluorescent profiles and analysis of macrophage sequestering behavior and immune response.

The results of this study demonstrated that aged muscle had the highest percent change in drug accumulation compared to other tissues, such as spleen, liver, and kidney. Additionally, I used a modified pharmacokinetic model to computationally demonstrate the decline in muscle mass throughout aging and medication exposure. In addition, I demonstrated the structural and physical effects of long-term treatments and explored the role of macrophages in drug sequestration and cytokine responses. These findings have significant implications as they highlight the susceptibility of aged organisms to drugs.

3.2 Abstract

The aging process is generally characterized by an inevitable loss of muscle mass and function. To study how the skeletal muscle (SM) is impacted by age and environmental exposures, young (4-weeks-old) and old (61-weeks-old) male C57BL/6J mice were given the FDA-approved drug clofazimine (CFZ), a medication that accumulates in macrophages, or vehicle for 8 weeks. Muscle

mass of mice with and without CFZ was modeled from birth to 3 years-old to understand muscle atrophy throughout aging, and mice were strength-tested via grip strength 1 week prior to the end of treatment to evaluate muscle function. At the end of treatment, cytokine arrays, collagen, fiber diameter, and macrophages were analyzed to assess muscle immune response and composition. Mice treated with CFZ experienced a decrease in muscle mass and fiber diameter compared to their respective controls. When exposed to the same CFZ treatment regimen, macrophages were responsible for the higher drug content found in SM of old mice compared to SM of young mice. Quantitative analysis of the differential impact of CFZ on old vs young mice indicate that age enhances the immunological response responsible for chemical bioaccumulation in muscle.

3.3 Introduction

Aging leads to sarcopenia, a condition defined by the decline in strength, and thickness of skeletal muscle (SM) fibers [1]. The lower quantity and cross-sectional area of muscle fibers cause decreased muscle mass, power, speed, and elasticity [2]. Aging SM also exhibits slower regeneration and wound healing, impaired proteolysis, and slower debris clearance [3, 4]. Environmental factors, such as medication exposure that is often sustained throughout a patient's life, have been shown to contribute to muscle decline and poor physical capability [5, 6]. However, the processes involved in SM aging as they relate to daily environmental exposures are not fully understood.

Accumulation of drugs in tissues is a common environmental exposure and an underappreciated potential culprit of clinical myopathy [7]. For example, weakly basic drugs accumulate in the low pH environment of the macrophage lysosomal compartment via ion-trapping [8]. This phenomenon may be particularly important in aging because tissue macrophages

are responsible for organ repair, and macrophage numbers, which are better indicators of biological age than chronological age, are correlated with a predisposition to disease and mortality [9, 10].

The characteristics of clofazimine (CFZ), an FDA–approved oral antibiotic that is used to treat leprosy, multidrug-resistant tuberculosis, and other nontuberculous mycobacterial infections, can be exploited to understand SM macrophages and drug bioaccumulation in aging because it is visually detectable in macrophages [11, 12]. Once CFZ enters the lysosomal compartment of the macrophage, it precipitates as an insoluble, crystalline membrane-bound complex with chloride known as crystal-like drug inclusions (CLDIs) [13]. This results in an immune response that prompts an increase in CFZ sequestration [14].

Since age is associated with muscle mass decline and the elderly often take numerous chronic medications, we aimed to investigate the role of bioaccumulating drug exposure on SM using CFZ as a probe [15]. Given that C57BL/6J mice bioaccumulate CFZ and their SM undergoes major restructuring during aging that is similar to humans, we used young (4-week-old) and old (61-weeks-old) mice to identify the differential impact of changing tissue macrophage content and CFZ bioaccumulation in aging SM [11, 16]. Further understanding of mechanisms that underlie drug bioaccumulation in SM could lead to interventions that prevent or reduce age-related muscle mass and function decline, which would translate to billions of dollars in healthcare savings each year.

3.4 Materials and Methods

3.4.1 Animal Studies

Male C57BL/6J mice (Jackson Laboratory, Bar Harbor, Maine USA) were utilized, and animal care was provided by the University of Michigan's Unit for Laboratory Animal Medicine (ULAM). With accordance with ULAM guidelines, animals did not require acclimation prior to

experimentation. Animal use protocols were approved by the University of Michigan's Institutional Committee on Use and Care of Animals (PRO00007593; May 5, 2017, PRO00009404; December 13, 2022). At the end of their treatment, animals were euthanized via CO2 inhalation following a cardiac puncture for the acquisition of a blood sample, in accordance with AVMA Guidelines. Blood samples were flash-frozen in liquid nitrogen and stored in -80 °C. After euthanasia, tissues were isolated, washed with 1X PBS (10010023, Gibco), blotted dried, weighted, and flash-frozen in liquid nitrogen.

3.4.2 Computational Model

Muscle mass data from untreated mice were collected from 4-, 8-, 12-, 36-, 69-, and 130-week old mice, and CFZ (36 mg/kg/day; C8895, Sigma-Aldrich) treatment was initiated in mice 4-weeks old up until 12-, 36-, and 69-weeks of age. Quadricep (QUAD) and triceps (TRI) muscle pairs were isolated from each mouse and weighed; computational models used the average mass of the muscle pairs. For the total muscle mass computational model, the sum of the QUADs and TRIs for each mouse was calculated. The average sum (SD) for each group of mice was determined and used for the model.

Due to similarities in changes in muscle mass and drug concentration over time, a modified traditional one-compartment pharmacokinetics (PK) model was used to model muscle aging and drug-induced muscle atrophy. Assuming first-order absorption and elimination, a traditional PK model displays the concentration of drug in the plasma.

$$(\boldsymbol{eq\ 1}.\ Drug\ Concentration)\ \boldsymbol{C_P} = \frac{\boldsymbol{D_0 \cdot K_A \cdot F \cdot (e^{-Kt} - e^{-K_A t})}}{\boldsymbol{V_D \cdot (K_A - K)}}$$

In **eq 1**., C_P is the concentration of the drug in the plasma, V_D is the volume of distribution, K_A represents the drug absorption rate constant, K is the drug elimination rate constant, D_0 is the

dosage given, F reflects the fraction of drug absorbed, and t is the time since the start of treatment. Whereas, for our model, we used the following modified equation (**eq 2.**) which combined D_0 and F. D_0 and F traditionally represent drug bioavailability, but we renamed it M_0 to reflect the initial growth potential that is available for the SM compartment.

$$(\textbf{eq 2.}\,\text{Muscle Model})\ \mathbf{M(t)} = \frac{\boldsymbol{K_A \cdot M_0 \cdot (e^{-Kt} - e^{-K_A t})}}{\boldsymbol{(K_A - K)}}$$

Cp·VD (**eq 1.**) represents the total amount of drug given; it was renamed M(t) in **eq 2.**, to represent the total amount of muscle mass with respect to age. In **eq 2.**, KA is the muscle growth potential absorption rate constant, and K represents the muscle atrophy rate constant.

A non-linear mixed-effects model was used to fit the SM mass data using the R package *dplyr*. A gestation time of 18.5 days, the average gestation time for male C57BL/6 mice [17], was used to incorporate the absorption and elimination phase of the muscle growth potentials beginning at the time of egg fertilization. A "slider" for each parameter was created to ensure that the fitted curve had a minimal residual error, and the results were plotted using the R package *ggplot2*.

3.4.3 CFZ Treatment of Young and Old Mice

CFZ (C8895, Sigma-Aldrich) or vehicle (equivalent sesame oil, 720189601668, Kadoya) was added to chow for 8 weeks as previously described [18]. The CFZ dose equated to 36 mg/kg/day. Mice were randomized to receive treatment: young mice (4-weeks-old), CFZ (n=16) or vehicle (n=10); old mice (61-weeks-old), CFZ (n=18) or vehicle (n=19). At the end of the treatment, mice were placed in specialized metabolic cages (3700M022, Tecniplast) for 18 hours to measure food consumption. CFZ dose was calculated using the food intake data and terminal body mass.

3.4.4 Quantification of CFZ in Tissues and Whole Blood

Quantification of CFZ in whole blood and tissues was performed by the Pharmacokinetic and Mass Spectrometry Core (University of Michigan). Detailed information for each assay is given in the supplemental information section. In brief, harvested tissue was homogenized using n-dimethylformamide-PBS solution. Acetonitrile was added to whole blood samples and tissue homogenate to extract CFZ. Concentrations of CFZ were determined by LC-MS/MS and data were processed using Analyst (1.6, SCIEX, Framingham, MA, USA).

3.4.5 Isolation of CFZ-Freebase and CLDIs from Skeletal Muscle

CFZ freebase (CFZ-FB) and CLDIs were isolated and quantified from SM as previously described [19-21] with some modification. The QUADs were homogenized using a liquid nitrogen-cooled mini mortar and pestle (H37260-0100, Bel-Art). Homogenized samples were placed in an Eppendorf tube with a solution that contained 1:100 diluted protease inhibitor cocktail (78410, Thermo Scientific) and EDTA in an established buffer (pH 4.5) that mimics the lysosomal compartment [22]. Samples were vortexed (1hr, 4 ℃) and then sonicated on ice (10s). The samples were then centrifuged (21,000 x *g*, 1 min). The CLDI pellet was purified using a 3-layer discontinuous sucrose gradient as previously described in [19], and then resuspended in 10% sucrose. CFZ in the supernatant and pallet was isolated using xylenes (1330-20-7/100-41-4, Fisher Chemical) and 9M sulfuric acid (A3000-212, Fisher Chemical). The CFZ concentration (μM) of the samples was determined using a plate reader (Infinite M1000 PRO, Tecan) at wavelength 450 nm and with 9 M sulfuric acid CFZ standards.

3.4.6 Chemical Imaging of CFZ Chemical Form in Skeletal Muscle

Raman microscopy (alpha300R, WiTec) was performed on QUAD sections (10 μm thick) mounted on glass slides that were generated from frozen tissue blocks, as previous described [22]. Large area scans (50 μm by 50 μm) were acquired with a step size of 50 μm and an integration time of 0.1 ms per pixel. Analysis was done using a Zeiss EC EPIPLAN 50x objective (N.A. = 0.75) and a 532 nm laser. Cosmic rays were removed from all spectra using the WiTec Project FOUR software. A MATLAB® processing algorithm developed in-house was used to baseline-subtract, normalize, and assess the collected muscle sample spectra by comparing them to the references of pure CFZ-FB and CFZ-hydrochloride (CFZ-HCL), the chemical composition of CLDIs, to identify the protonation state of CFZ.

3.4.7 Grip Strength Measurements

Strength testing was conducted with the help of the University of Michigan's Physiology Phenotyping Core 1 week before the end of experimentation. Forelimb muscle strength was measured using a grip strength meter (1027SM, Columbus Instruments, Columbus, OH) set on T-Peak mode [23]. Mice were held by the base of the tail and encouraged to grab the gauge bar with only their forelimbs. Five measurements were taken per mouse with a 1min break between each, and the average measurement was reported.

3.4.8 Trichrome Staining and Immunohistochemistry

Muscles (QUADs) were isolated, washed with 1X PBS (10010023, Gibco), blotted dry, embedded in Tissue-Plus Optimal Cutting Temperature (OCT) compound (4585, Fisher), and frozen on dry ice. The blocks were stored (-80 °C) until they were cryosectioned (10 μm; Leica 3050S cryostat). Sections were trichrome stained by the In Vivo Animal Core (IVAC) core at the

University of Michigan. Macrophage identification was conduct as previously described [18]. In brief, sections were fixed in 4% paraformaldehyde (15710, Electron Microscopy Sciences) for 10 min, and blocked with 1% bovine serum albumin (BSA) (810033, MP Biomedicals), 5% goat serum (G9023, Sigma-Aldrich), and 0.3 M glycine (G8898, Sigma-Aldrich) in 1X PBS (10010023, Gibco) for 2 h. The samples were then incubated with primary antibody, anti-F4-80 (ab6640, Abcam) or purified rat IgG2a isotype control antibody (400502, Biolegend), overnight (4°C) in humidity chambers (NC0370987, Electron Microscopy Sciences), followed by three washes with 1X PBS (10010023, Gibco) for 5 min on a rocker. The slides were then incubation with anti-rat IgG (H + L) Alexa Fluor® 488 conjugate secondary antibody (4416, Cell Signaling Technology) for 1 h (RT), followed by three washes (1X PBS for 5 min on a rocker). After staining was complete, sections were mounted with a drop of ProLong® Gold antifade reagent with DAPI (P36941, Molecular Probes) for nuclear detection. A cover slip was immediately placed and sealed with nail polish. The slides were left to dry overnight in the dark and stored (-80 °C). The QUAD macrophage images were acquired by fluorescent microscopy (Apotome, Zeiss). Fluorescence imaging was done using the Cy5 channel (640/670 nm, CLDIs), FITC channel (490/510 nm, F4-80 macrophages), and DAPI channel (340/435 nm, nuclei) with exposure times of 6s, 3s, and 165ms, respectively. The trichrome stains were digitized by the IVAC core using 20x magnification. Images were analyzed using images using QuPath (0.4.2; University of Edinburgh, Edinburgh, Scotland, UK). The area (mm^2) for the CY5 and FITC channels was measured, and objects such as DAPI+ cells, DAPI+/F4-80+ cells, and DAPI/F4-80+/CLDI+ cells were identified.

3.4.9 Cytokine Analysis

Cytokines were measured using the proteome profiler array kit (ARY006, R&D Systems) following the manufacturer's protocol and using 300 μg of TRI lysate protein. Briefly, TRI samples were minced and placed in 1X PBS (10010023, Gibco) with the recommended protease inhibitors and then placed in a homogenizer (BeadBug 6, Benchmark Scientific) for three cycles (20 s each, at speed 4350 x *g*). Samples were then vortexed (1h, 4°C) and sonicated on ice (10s). After homogenization, Triton X-100 was added to achieve a final concentration of 1%, and samples were centrifuged (10,000 x *g*, 5min, 4°C). Lysate protein was measured by bicinchoninic acid (BCA) assay (23225, Pierce) following the manufacturer's instructions. Samples from each group were simultaneously assayed and imaged via chemiluminescence (iBright CL15000, Invitrogen). The pixel density was quantified using the iBright Analysis Software (iBright Analysis Software, Thermo Fisher Scientific). Detected cytokine densities were background subtracted and normalized by the density of the positive controls of the corresponding membrane. The cytokine densities of the treated groups were normalized by their respective control group.

3.4.10 Statistics

A one-way ANOVA was employed to compare data across groups. It was followed by post-hoc Tukey's test when the ANOVA p-value was significant. An unpaired Student's t-test with equal variance was used to compare two groups. Statistical analysis was conducted using PRISM (9.4.1; GraphPad Software, Inc., San Diego, CA USA). Statistical significance was set at a p-value of ≤ 0.05.

3.5 Results

3.5.1 Long-term Treatment with CFZ Affects Skeletal Muscle Mass during Aging

A one-compartment pharmacokinetic (PK) model was used to describe muscle aging and drug-induced muscle atrophy over time (**Figure 3-1A**). CFZ-treated mice exhibited muscle maturation around 6 months, while untreated mice matured around 8 months (**Figure 3-1B, C, D**). Maximum muscle mass, half-life of the curve, area under the curve (AUC), and M_0 values of CFZ-treated mice curves trended lower than those of untreated mice, indicating decreased muscle mass overtime (**Figure 3-1E**). Overall, CFZ-treated mice at the end of their lifespan (69-week-old) demonstrated a larger muscle lost than body mass decrease compared to their untreated control (**Figure 3-1E**). The K values of non-treated and CFZ-treated groups were greater than their respective KA values, which is indicative of flip-flop pharmacokinetics (**Figure 3-1E**). This PK phenomenon describes the underlying kinetics of muscle aging, whereby the rate constant of muscle atrophy is limited by the rate constant of muscle development.

3.5.2 CFZ-treatment Decreases Body and Muscle Mass in Old Mice

Following 8-weeks of CFZ treatment, old mice were 20% lighter than their negative controls (**Figure 3-2A**), while no weight difference was observed between young untreated and CFZ-treated mice. The difference in weight between old CFZ and control mice was not attributed to the differences in chow consumption (**Figure 3-2B**). Both groups of CFZ-treated mice received the same average CFZ dose (36 mg/kg/day), equivalent to a human dose (**Figure 4-2C**). In addition, the measured whole blood CFZ concentration was not different in old and young mice (**Figure 3-2D**). Nevertheless, both young and old CFZ-treated mice exhibited a decrease (~14%)

in isolated QUAD and TRI muscle masses compared to their respective negative controls (**Figure 3-2E**).

3.5.3 CFZ Treatment Accelerates Changes Typically Associated with Aging

In addition to the CFZ-induced loss in total isolated muscle mass (**Figure 3-2E**), old CFZ-treated mice displayed a decrease in absolute grip strength compared to old negative control mice (**Figure 3-3A**). Even though young CFZ-treated mice had a decrease in absolute muscle mass after the 8-week CFZ treatment, they did not experience a loss in strength. To explain this discrepancy, we microscopically accessed muscle fiber size and collagen content. The skeletal muscle of old, CFZ-treated mice had 24% more collagen than their control (**Figure 3-3B**), where muscle collagen content increases with age and is present in fibric tissue [24]. Not only did the muscle structure change in the old CFZ-treated mice, but the fibers also decreased in size compared to old control mice (**Figure 3-3C**). Even though the young CFZ-treated mice had no change in grip strength, they had a fiber size decrease of 16% compared to their control (**Figure 3-3C**). These data suggest that CFZ-induced muscle atrophy (**Figure 3-2E**) is associated with a decrease in fiber size (**Figure 3-3C**), which is a relationship commonly seen in aging [25].

3.5.4 CFZ Distribution Differences Between Old and Young Mice

Since aging may alter organ drug distribution, we assessed CFZ distribution in the major drug sequestering organs of young and old mice, where the old mice had more cells with CLDIs available in the peritoneal layer compared to young mice (**Figure S 3-1)**. CFZ-treated animals displayed age-dependent differences in organ distribution in muscle, kidney, brain, lung, spleen and liver (**Figure 3-4**). Of these, CFZ distribution into skeletal muscle was the greatest with a 142% increase in old CFZ-treated versus young CFZ-treated mice, where old CFZ-treated

experienced a negative percent change in CFZ amount in the spleen (**Figure 3-4**), even though it experienced an increase in mass (**Figure S 3-2**). In addition, this increase CFZ amount in the muscle of old mice (O+) compared to young mice (Y+) remained significant even after correcting for total amount of CFZ consumed during treatment (**Figure S 3-3**).

3.5.5 CFZ Accumulation in the Skeletal Muscle is Age-Dependent

To further test age-related drug sequestering capability of SM in mice, we measured CFZ in young and old mice. Even though there was no difference in the CFZ dose of the treated mice, CFZ per gram of muscle was lower in young CFZ-treated mice (27 ± SD µg) than in old CFZ-treated (58 ±S D μg) mice. This was due to a uniform increase in SM CFZ in old mice compared with young mice (**Figure 3-5A**), where the muscle continued to accumulate CFZ throughout extended treatment (65-week treatment, **Figure S 3-4**). To further analyze the factors impacting the increased accumulation of CFZ in the SM of older mice, CFZ distribution was compared by chemically isolating CFZ and using chemical imaging techniques on frozen cryosections, and stoichiometric mixtures were analyzed to determine CFZ signals of the different forms (**Figure S 3-4**). Based on the analysis of the chemically isolated drug, the protonated form of the drug, CFZ-hydrochloride (CFZ-HCL), in both CFZ-treated groups, was three-times higher than the freebase (CFZ-FB) form (**Figure 3-5B**). Also, the spectral signals from the CFZ-treated groups indicated changes in the CFZ-FB to CFZ-HCL ratio, where a higher signal characteristic of CLDIs was detected by Raman microspectroscopy (**Figure 3-5C**). Even though two samples from the old CFZ-treated group showed spectral characteristics of freebase, the spectra more often resembled CFZ-HCL (**Figure 3-5C**). Taken together, the difference in accumulation and distribution of the freebase form of CFZ, which is associated with body fat, and the distribution of the insoluble,

precipitated hydrochloride form CFZ, which is associated with CLDIs, implicates macrophages as drivers of CFZ accumulation in SM.

3.5.6 Macrophage Drug Collection in Old Mice Drives High Amounts of Drug Accumulation

Macrophage population in the aging SM was identified using anti-F4-80, an established macrophage marker with the addition of DAPI, a nuclei marker (**Figure 3-6A**). No differences in the percent of F4-80 + cells among the groups were found, as has been previously reported [26] (**Figure 3-6B**). The old CFZ-treated mice had a higher CLDI (CY5) signal per cross-sectional area (CSA, mm^2) compared to the young CFZ-treated mice (**Figure 3-6C**), as was seen via Raman microscopy (**Figure 3-5C**). The percent of drug sequestering macrophages (F4-80+, DAPI+, and CY5+) and number of drug sequestering macrophages per CSA (mm^2) was lower in the old (O+) compared to young (Y+) mice (**Figure 3-6A**, **C**). However, the old CFZ-treated mice experienced a larger cargo capacity compared to the young CFZ-treated mice, signifying that the macrophages in the old mice (O+) sequestered higher amounts of CFZ (CY5 signal) per sequestering cell (**Figure 3-6C**).

3.5.7 CFZ Alters Cytokine Levels in Skeletal Muscle

CFZ treatment and age altered cytokine levels in skeletal muscle (**Table. 3-1**). Old CFZ-treated mice demonstrated a decrease in keratinocyte chemoattractant (KC), and a trending decrease in interleukin 6 (IL-6) and granulocyte-macrophage colony-stimulating factor (GM-CSF), cytokines that are responsible for neutrophil macrophage recruitment and proinflammatory response compared to young CFZ-treated mice [27-29]. A decrease in KC, IL-6, and GM-CSF in the SM may contribute to lower muscle efficiency, such as a decrease in metabolism, muscle regeneration, and decrease in macrophage M1 recruitment [30-32]. Also, old (O+) mice displayed a positive

percent change in the regulated upon activation, normal T cells expressed and secreted (RANTES) cytokine, that has been linked to diseased muscle and is a negative regulator of macrophage apoptotic processes. This finding suggests that age predisposes for a more pronounced CFZ-induced SM injury [33, 34]. In addition, old (O+) mice displayed more downregulated cytokine responses which may indicate that CFZ has a profound effect on old muscle compared to young SM.

3.6 Discussion

This study aimed to investigate the impact of common environmental exposures on SM in young and old mice. Given that macrophages are responsible for phagocytosing foreign material [35], aging is a crucial factor in the bioaccumulation of chemicals in tissues, particularly in the SM, which experiences low turnover as it ages [36]. To determine bioaccumulation patterns in SM, we selected two muscles: the hindlimb QUAD and the forelimb TRI. CFZ was chosen as a probe because it accumulates in macrophages as insoluble, solid rigid bodies known as CLDIs [13]. This property makes it possible to measure and manipulate lysosomal occupancy in a controlled, quantitative manner.

Our results shed light on the impact of age on SM immune cells. Interestingly, we found that macrophages were responsible for higher levels of CFZ in the SM of old mice compared to young mice (**Figure 3-6C**), challenging the general assumption that cellular membranes and adipose tissue are primarily responsible for lipophilic drug accumulation [37]. Specifically, macrophages from old mice had a larger drug sequestering capacity than those from young mice. This age-related phenomenon has also been observed in macrophages and intercellular ROS production and lipofuscin [38]. Notably, the increased cargo capacity may have been caused by less macrophage recruitment to SM that is evidenced by cytokine data (**Table 3-1**). These findings suggest that in

muscle from old mice, the macrophage cargo capacity is an immunological expanding compartment that appears to increase with age.

As seen in the computational muscle model, human relevant long-term treatment of CFZ, results in a significant decrease in muscle mass (**Figure 3-1**). However, the model displayed that CFZ disrupts the muscle atrophy rate, suggesting that CFZ exposure from a young age isn't required to see changes in muscle mass. These effects were evident in both young and old, 8-week CFZ-treated mice, and were associated with reduced size in fiber diameter (**Figure 3-2E, Figure 3-3C**). Old mice also experienced a decrease in body mass, altered muscle function, and an increase in collagen compared to young mice. These findings along with the aforementioned macrophage and cytokine data, suggest that macrophages may play a key role in regulating age-related changes in muscle mass and function, which highlights the importance of understanding the complex interplay between the immune system and muscle tissue during the aging process.

Our assessment of muscle immune response, composition, and function provides a promising understanding into the role of bioaccumulating molecules on the muscle. However, there are some limitations. Our assessment was done using CFZ, a macrophage accumulating drug; thus, future studies of additional common environmental exposures should be conducted to identify potential additional mechanisms for increased accumulation in old skeletal muscle.

Overall, our findings add to the complexities of understanding age-related bioaccumulation of drugs in SM. This process does not only occur via receptor-mediated pathways but can also occur via a macrophage-mediated process that varies with age. A better understanding of the mechanisms underlying drug bioaccumulation in SM could lead to interventions potential interventions to prevent or reduce drug-acerated muscle atrophy in older adults, such as drug dosing adjustments or the use of alternative medications.

3.7 Acknowledgements and Funding

I would like to thank Winnie Wen and Andrew Willmer for their invaluable contribution to the muscle mass computational model. I would also like to extend my appreciation to the Physiology Phenotyping Core at the University of Michigan for their technical assistance with the strength testing, and to the Pharmacokinetic and Mass Spectrometry Core at the University of Michigan for their technical assistance in measuring CFZ via LC-MS/MS.

This research was funded by grants from the National Institutes of Health, National Institute of General Medical Sciences under award numbers R01GM127787 (Dr. Rosania), P30AR069620 (Dr. Jepsen), and R35GM136312 (Dr. Stringer).

3.8 Figures

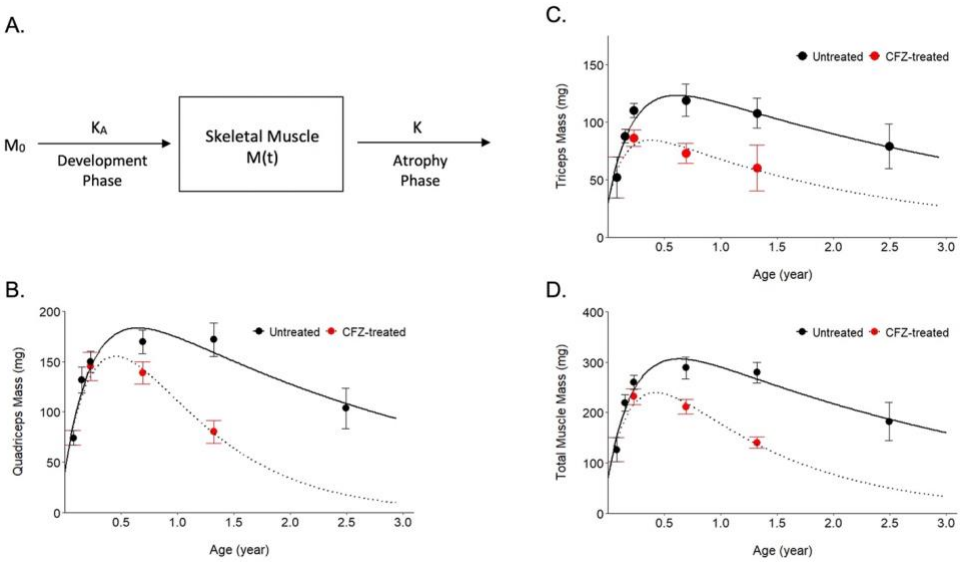

E.

Muscle Type	Treatment	Maximum Muscle Mass (mg)	Curve's $T^{1/2}$ (Years)	Area Under the Curve (AUC) (Mass*Years)	Mass at 69- Weeks (mg)	Normalized Mass at 69-Weeks (mg/g)	M_0	K_A	K
Quadriceps	Untreated	183.2	2.1	318.0	171.7 ± 16.8	5.3 ± 0.5	1659.1	0.3	3.8
	CFZ	155.3	0.5	161.1	80.3 ± 11.4 ****p<0.0001	3.6 ± 0.4 ***p=0.0002	620.4	1.4	2.8
Triceps	Untreated	123.1	2.6	224.5	107.7 ± 13.0	3.3 ± 0.5	2422.3	0.3	4.5
	CFZ	84.2	1.5	134.2	60.1 ± 19.7 ***p=0.001	2.7 ± 1.0 p=0.179 n.s.	1449.6	0.5	6.6
Total Muscle	Untreated	306.1	2.2	542.8	279.4 ± 20.4	8.6 ± 0.6	5062.6	0.3	4.1
	CFZ	239.4	0.8	294.8	140.5 ± 11.4 ****p<0.0001	6.3 ± 0.6 ***p=0.0002	1748.1	0.9	4.2

M_0: Initial muscle growth potential
K_A: Muscle development rate constant
K: Muscle atrophy rate
Data represent the mean or mean ± SD

Figure 3-1 Computational Model and Parameters of Muscle Aging and Drug-Induced Muscle Atrophy

A. Schematic diagram of the first-order one-compartment model. **B.** Averaged quadricep muscle pair mass (mean ± SD) **C.** Averaged triceps muscle pair mass (mean ± SD) **D.** Total muscle mass (mean ± SD), which represents the sum of B and C. **B-D.** CFZ (red data points and dotted line curve) and untreated (black data points and solid line curve) muscle mass change throughout the lifespan of mice (0-3 years). Untreated muscle masses were collected at 4, 8, 12, 36, 69, and 130 weeks (n= 8, 4, 6, 5, 7, and 6, respectively). CFZ-treated muscle mass data were collected from mice that started treatment at 4-weeks-old until 4, 12, 36, and 69 weeks old (n= 8, 16, 8, and 4, respectively). **E.** Parameter table of curves from B-D. 65-week-treated CFZ mice (69-week-old, n=4) demonstrated a decrease in muscle mass compared to untreated 69-week-old mice (n=7) which was sustained when muscle mass was corrected for body mass (normalized mass).

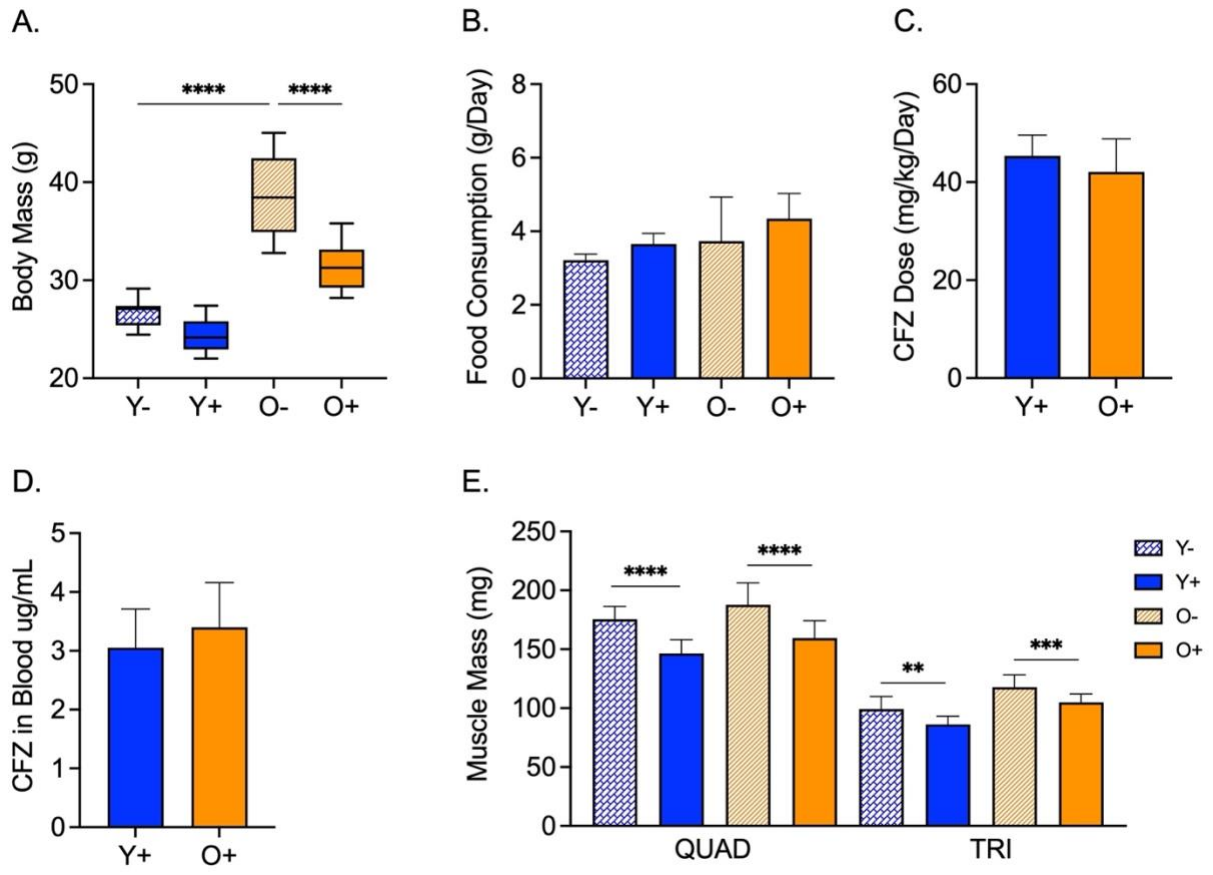

Figure 3-2 CFZ Dose and Concentration in Whole Blood, Food Consumption, and Body and Muscle Mass

A. Terminal body mass (mean ± SD, n=10-19/group). Old CFZ-treated mice (O+) displayed a decrease in body mass compared their vehicle-treated control, O- (****p<0.0001, Tukey). An age-related difference in body mass was observed between the young (Y-) and old (O-) control groups, with (O-) having a larger body mass (****P<0.000, Tukey). **B.** Food consumption (mean ± SD) was determined from an 18-hour metabolic study conducted immediately before euthanasia (n=10-12/group). **C.** CFZ dose (mean ± SD) was calculated using data from the terminal body mass and food consumption study (n=16-18/group). No difference in CFZ dose was found between Y+ and O+ (p=0.104, Student's t-test). **D.** Whole blood CFZ concentration (mean ± SD) was determined by LC-MS (n=10-15/group). No difference was found in CFZ levels between Y+ and O+ (p=0.254, Student's t-test). **E.** Average (± SD) mass of paired quadricep (QUAD) and triceps (TRI) muscles (n=10-19). CFZ-treated groups (Y+ and O+) had smaller muscle mass compared to their respective controls, Y- and O- (QUADs, ****p<0.0001, Tukey; TRI of Y+ vs Y-, **p=0.003, Tukey; TRI O+ vs O-, ***p=0.0002, Tukey).

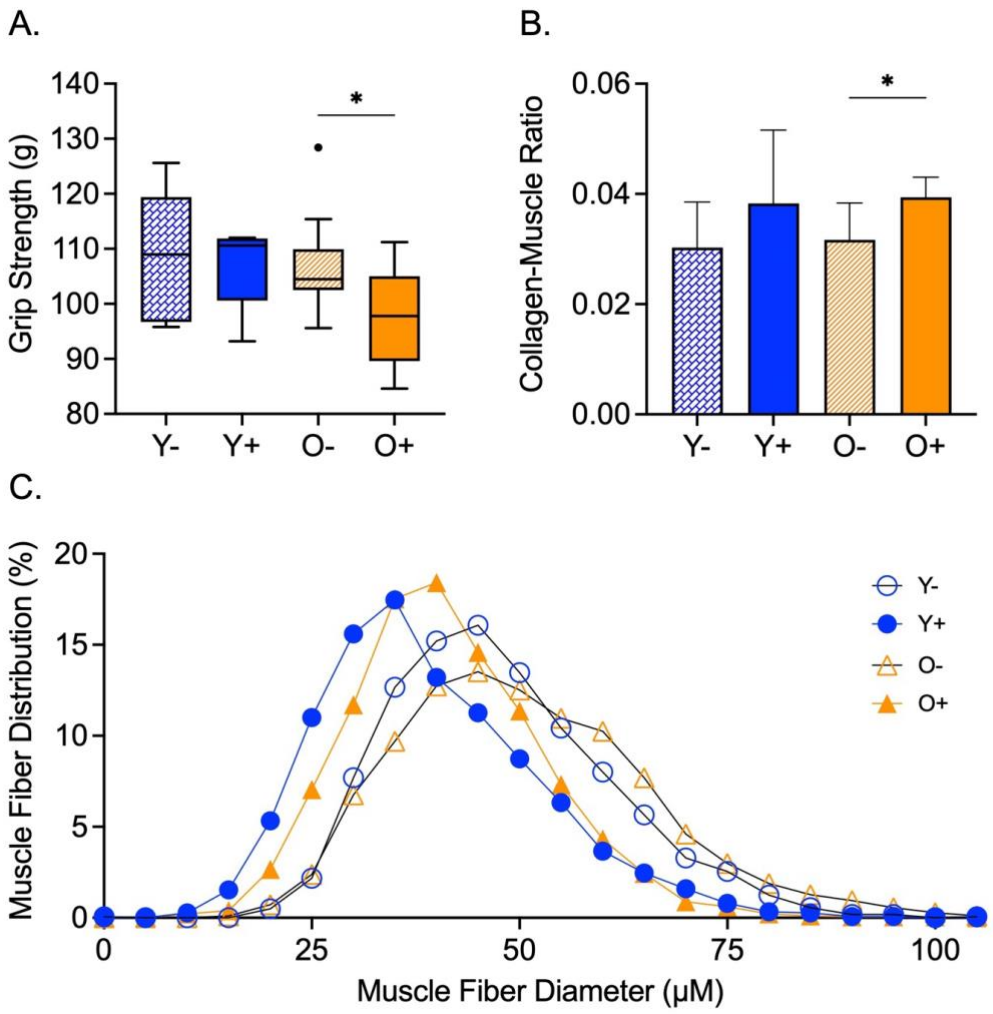

Figure 3-3 CFZ Treatment Changes Muscle Composition and Strength

A. Absolute forelimb strength (mean ± SD) measured by a grip strength meter (n=5-14/group). Old CFZ-treated mice (O+) had decreased strength compared to old vehicle-treated mice, (O-) (*p=0.042, Tukey). **B.** Collagen-muscle ratio (mean ± SD) derived from trichrome stained sections (n=5-6/group). O+ displayed an increase in collagen levels compared to O- (*p=0.03, Tukey). **C**. SM fiber diameter (mean ± SD) displays the frequency of each fiber measurement between 0 μM to 100 μM of trichrome stained sections (n=5-6/group). Young (Y+) and old (O+) CFZ-treated mice had decreased fiber diameter compared to their respective control, Y- (*p=0.04, Tukey) and O- (**p=0.01, Tukey).

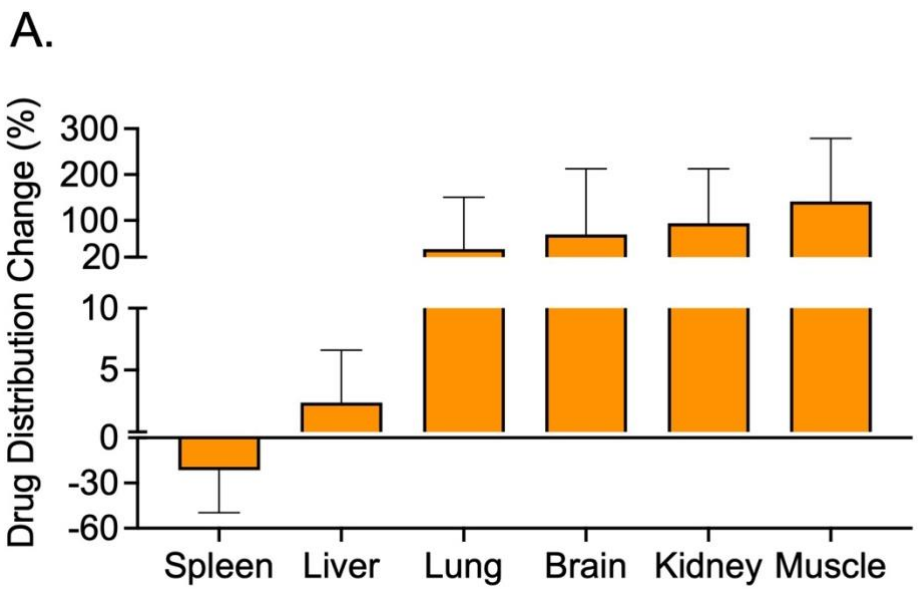

Figure 3-4 CFZ Distribution Differences Between Old and Young Mice

The percentage difference (mean ± SD) in CFZ distribution between old and young mice demonstrates the age-relatedness of organ specific amounts of CFZ (n=16-18/group). The skeletal muscle had the greatest difference in CFZ levels between old and young CFZ-treated mice, with old mice experiencing a 142% increase in CFZ. The liver was the least impacted by age, with old CFZ-treated mice having only a 2% rise in drug content. This was not attributable to greater CFZ consumption (see **Figure 4-2B**).

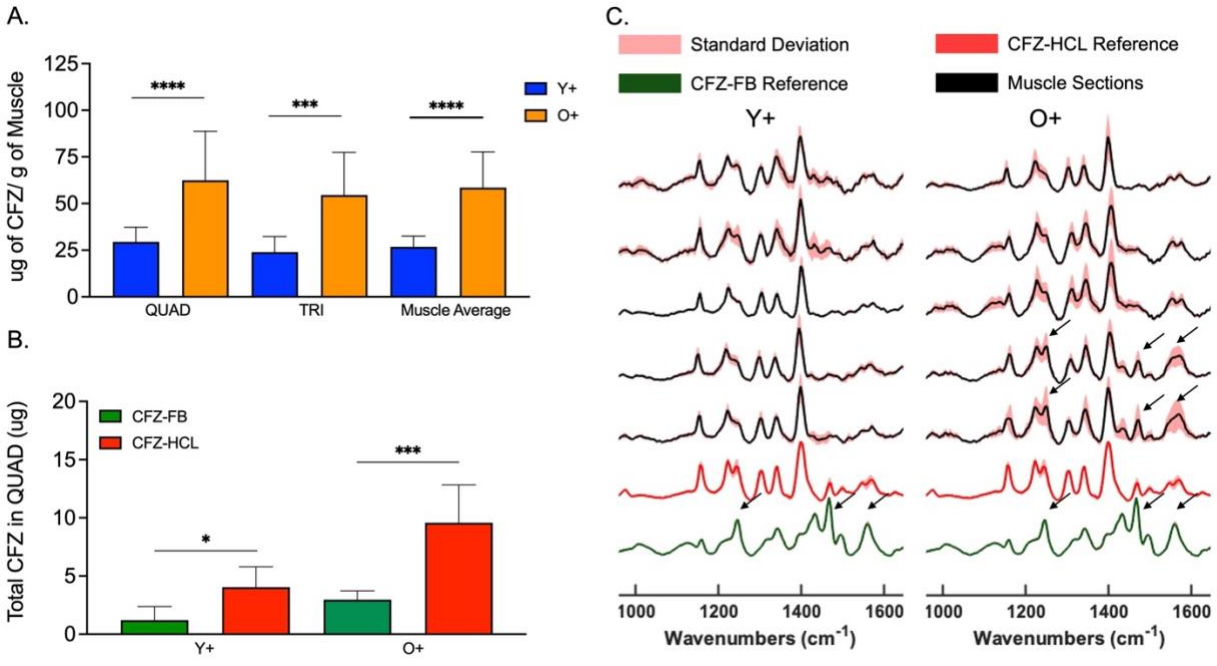

Figure 3-5 CFZ Concentration and Chemical Form in Skeletal Muscle

A. CFZ concentration in skeletal muscle (mean ± SD) was determined by LC-MS (n=10-18 /group). Old mice (O+) had higher CFZ concentrations in all muscle types, compared to young CFZ-treated mice (Y+) (QUAD, ****p<0.0001, Student's t-test; TRI, ***P=0.001, Student's t-test; averaged muscle, ****p<0.0001, Student's t-test). **B.** CFZ form (mean ± SD) measured by UV-Vis (n=5-6/group). Based on the CFZ form isolation study, the CFZ-HCL in both CFZ-treated groups was three-times higher than the freebase form (Y+, *p=0.02, Student's t-test; O+, ***p=0.001, Student's t-test). **C.** CFZ form (mean ± SD) detected by Raman microscopy on cryosection (n=5). The spectral signals from the CFZ-treated groups (black spectrum) indicated a change in the CFZ-FB (green spectrum) to -HCL (red spectrum) ratio, where a higher signal characteristic of HCL was detected. CFZ-HCL is the form of CFZ created via ion-trapping in the lysosome of macrophages known as CLDIs.

A.

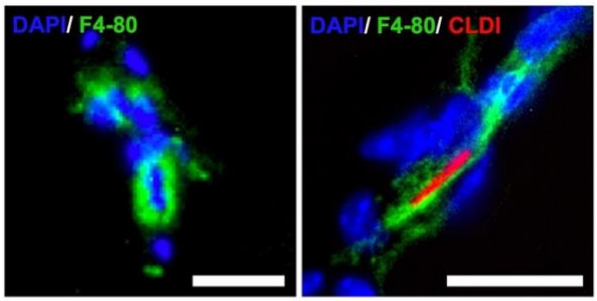

B.

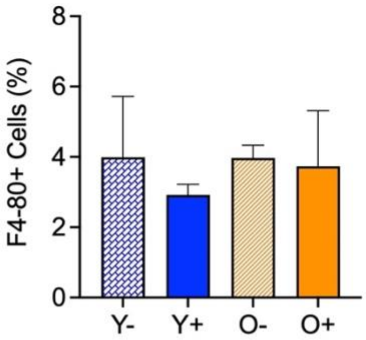

C.

Group	CLDI/ CSA[1]	CLDI Sequestering Macrophages %	CLDI Sequestering Macrophages/ CSA	CLDI/Sequestering Macrophage[2]
Y+	0.005 ± 0.001	7.3 ± 2.4	3.4E-4 ± 1.3E-4	9.1 ± 3.2
O+	0.007 ± 0.001	2.6 ± 1.3	5.8E-4 ± 1.9E-4	15.0 ± 3.2
	***p=0.01**	****p=0.005**	**n.s. p=0.05**	***p=0.0218**

[1]: Determined by CY5 Area
[2]: Corrected by CSA

Figure 3-6 Macrophage Population and CFZ-Sequestering Ability in Skeletal Muscle

A. Skeletal muscle macrophages were identified by DAPI+ (blue, nuclei) and F4-80 (green, macrophage) staining; CFZ sequestering macrophage were identified by DAPI+ (blue), F4-80+ (green), and CLDI+ (red). **B.** The percent of F4-80+ cells (mean ± SD) in skeletal muscle was not different among the groups (n=4-5/group, p=0.50, one-way ANOVA). **C.** Corrected CLDI signal (mean ± SD) was higher in old mice than in young mice (n=4-5/group, *p=0.01, Student's t-test). Percent of CLDI sequestering macrophages (mean ± SD) was higher in young mice compared to old (n=4-5/group, **p=0.005, Student's t-test). The corrected CLDI sequestering signal were not different between the CFZ groups (Y+ and O+, n=4-5/group, p=0.051, Student's t-test), however, the CLDI/sequestering Macrophage (mean ± SD) calculated taking the ratio between the corrected CLDI and CLDI sequestering macrophages values was larger in the old mice compared to young (n=4-5/group, *p=0.022, Student's t-test).

3.9 Tables

Table 3-1 CFZ and Age-Induced Cytokine Levels in SM

Percent change (mean) of the top 4 of 40 measured cytokines between old CFZ-treated mice (O+) and young CFZ-treated (Y+) mice are shown, where the density of they cytokine pixels (mean ± SD) of treated groups were normalized by their controls (n=5/group). O+ experienced a decrease in KC levels compared to Y+ ($p=0.02$, Student's t-test) and displayed a trending decrease in immune cell recruitment; however, O+ had a slight increase in RANTES, a negative regular of the macrophage apoptotic process.

Cytokine	Function	Change (%)	O+	Y+	P
KC	Neutrophil Recruitment	-60	0.630 ± 0.214	1.560 ± 0.671	**0.02**
IL-6	Proinflammatory	-43	0.894 ± 0.316	1.567 ± 0.578	0.05
RANTES	Proinflammatory	45	1.438 ± 0.260	0.994 ± 0.385	0.07
GM-CSF	Macrophage recruitment	-40	0.784 ± 0.517	1.317 ± 0.517	0.08

3.10 Supporting Information

3.10.1 Sample Preparation and CFZ LC-MS/MS Analysis

To measure CFZ in blood, 160 μL of verapamil (30 ng/mL) in acetonitrile (internal standard solution) and 20 μL of acetonitrile were added to 20 μL of heparinized whole blood. The mixture was vortexed for 10 min and centrifuged (3500 rpm for 10 min). Then, the supernatant was transferred to autosampler vials for LC–MS/MS analysis.

Tissue samples were homogenized (Precellys tissue homogenizer, Bertin Technologies, Montigny-le-Bretonneux, France) with 80% N-Dimethylformamide (DMF)-PBS solution using a ratio of 5:1 volume (mL) to weight of muscle (g). For protein precipitation, 160 μL of internal standard solution and 20 μL of acetonitrile were added into 20 μL of homogenized tissue. The mixture was vortexed for 10 min and centrifuged (3500 rpm for 10 min). The supernatant was transferred to autosampler vials for LC–MS/MS analysis.

A Shimadzu LC-20AD HPLC system (Kyoto, Japan) was used to measure CFZ concentration. Chromatographic separation of the tested compound was achieved using a Waters XBridage reverse phase C18 column (5 cm × 2.1 mm I.D., packed with 3.5 μm) at 25 °C. Five μL of the supernatant was injected per sample. The flow rate of gradient elution was 0.4 ml/min with mobile phase A (0.1% formic acid in purified deionized water) and mobile phase B (0.1% formic acid in acetonitrile). An AB Sciex QTrap 4500 mass spectrometer equipped with an electrospray ionization source (ABI-Sciex, Toronto, Canada) in the positive-ion multiple reaction monitoring (MRM) mode was used for detection. Protonated molecular ions and the respective ion products were monitored at the transitions of m/z 473.0 > 431.1 for clofazimine and 455.2 > 303.2 for the internal standard. We adjusted the instrument settings to maximize analytical sensitivity and

specificity of detection, and quality control samples were run before, in the middle, and after the samples to evaluate the accuracy and intra-batch precision of the developed method.

3.10.2 Peritoneal Cavity Cells (PCC) Isolation and Slide Preparation

PCCs (n=5) were isolated by making a small incision in the abdomen's peritoneal layer and flushing the cavity with cold 5% FBS (10ml; 16000044, Gibco) in 1X PBS (10010023, Gibco). The return lavage fluid was mixed with ACK lysing buffer (A1049201, Gibco) to remove red blood cells following the manufacturer's protocol. Isolated PCCs were cryopreserved in 10% DMSO (4-X, ATCC) and 10% FBS in DMEM (11995-065, Gibco) and stored in liquid nitrogen (vapor phase). For assay, PCCs were fixed on glass slides for analysis, cells were thawed at 37 ° and centrifuged (200 x g for 10 min at 4 °C). The supernatant was removed, and cells were diluted in 1X PBS (2 million cells/mL). An equal volume of 4% paraformaldehyde (15710, Electron Microscopy Sciences) was added to achieve a final sample dilution of 1 million cells/mL. Samples were incubated (15 min, RT) and then centrifuged (200 x g for 10 min at 4 °C). The supernatant was removed, and the cell pellet was washed twice with 1X PBS. After the washes, PMs were resuspended in 1X PBS, pipetted onto slides, and a drop of ProLong® Gold antifade reagent with DAPI (P36941, Molecular Probes) was added before placing the coverslip and sealing it with nail polish. The slides were left to dry overnight in the dark and stored until the time of assay (-80 °C.) For the PCC analysis counts (100 cells/slide), a Nikon Eclipse Ti inverted microscope (Nikon Instruments, Melville, NY) with a magnification of 40x was used to capture brightfield images (Nikon DS-3 camera, Nikon Instruments). The fluorescence imaging was done using the Cy5 channel (640/670 nm, far-red, CLDIs) and DAPI channel (340/435 nm, blue, nuclei) with a Photometrics CoolSnap MYO camera system with an exposure time of 500 ms and analyzed with ImageJ.

3.10.3 CFZ-FB & CFZ-HCL Stoichiometric Calibration Methodology

To create the CFZ calibration standards mixtures, jet-milled CFZ-HCL and CFZ-FB were mixed with methanol. The pure components used as references were dissolved in methanol solution at a concentration of 1mg of jet-milled drug per milliliter of methanol, and then mixed according to stoichiometric ratios. Next, 500 uL of each calibration solution was deposited onto separate glass slides and allowed to dry, leaving a thin film of mixed material on the slide surface. Large area scans were used to acquire the calibration spectra, which were processed in the same manner as the samples.

3.10.4 Figures

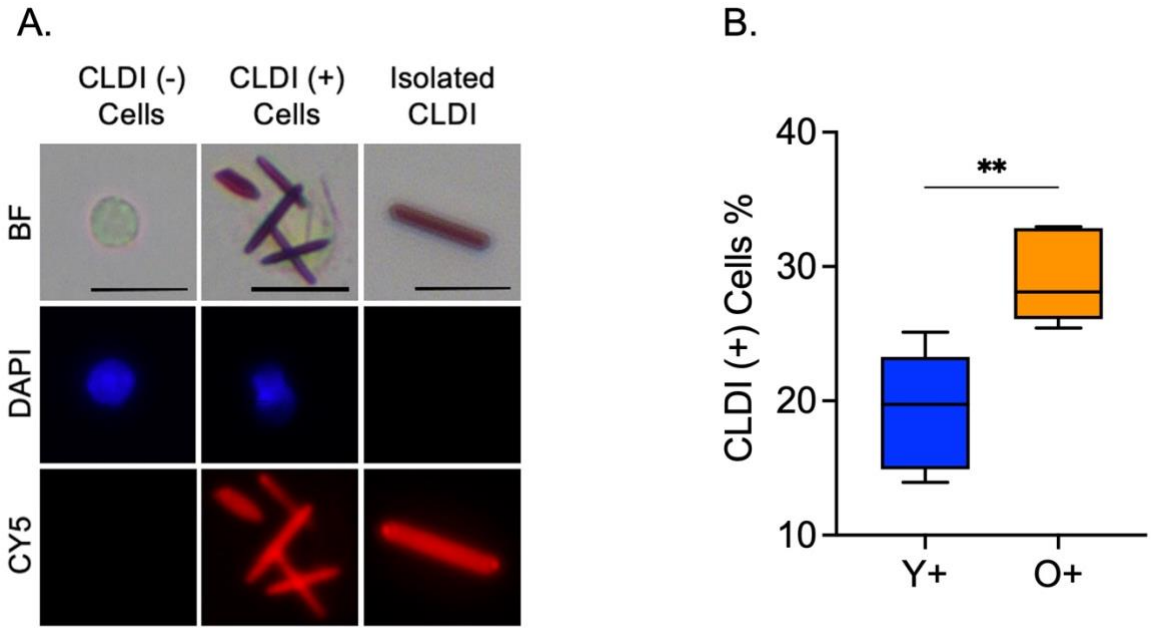

Figure S 3-1 Age-Related Drug Distribution in the Peritoneal Cavity

A. Fluorescent profiles of drug sequestering cells from the peritoneal cavity, which surrounds major drug sequestering organs. **B.** Percent CLDI positive cells (mean ± SD). Old CFZ-treated mice (O+) had a higher amount of drug sequestering peritoneal cells compared to young CFZ-treated mice (Y+) (n=5, **p=0.004, Student's t-test).

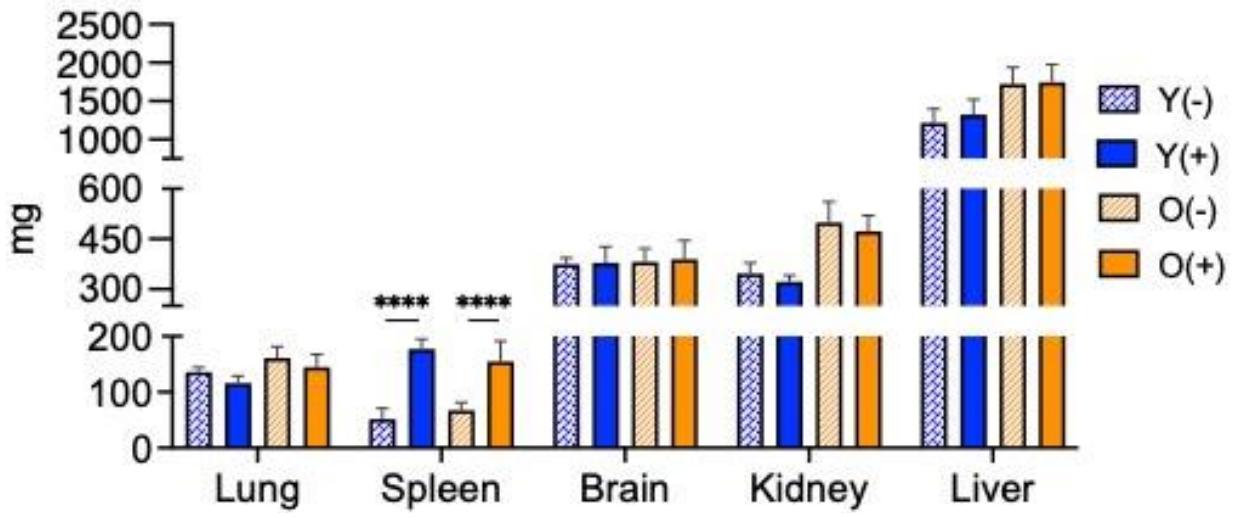

Figure S 3-2 Tissue Mass Response to CFZ Accumulation

Spleen mass (mean ± SD) of young (Y+) and old (O+) CFZ-treated mice was larger than their controls, Y- and O- (****p<0.0001, Tukey, n=5-19/group).

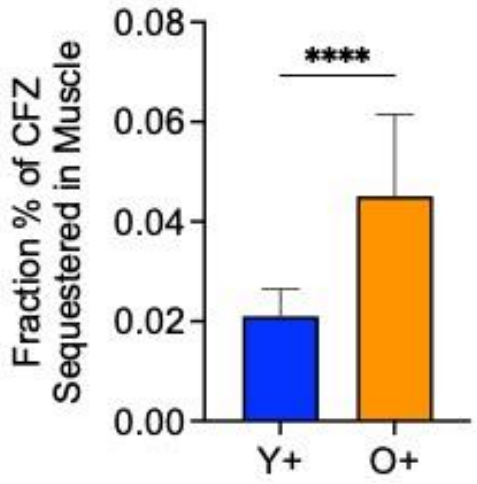

Figure S 3-3 Fraction % of CFZ Sequestered in Muscle

Percent fraction of CFZ sequestered in the QUAD and TRI muscles (mean ± SD) of young (Y+) and old (O+) CFZ-treated mice (n=16-18/group) was calculated by taking the ratio of CFZ (mg) found in the muscles and the total CFZ (mg) consumed throughout the 8-week treatment. O+ mice displayed an increased fraction % of CFZ in the muscle compared to Y+ mice (****$p<0.0001$, Student's t-test).

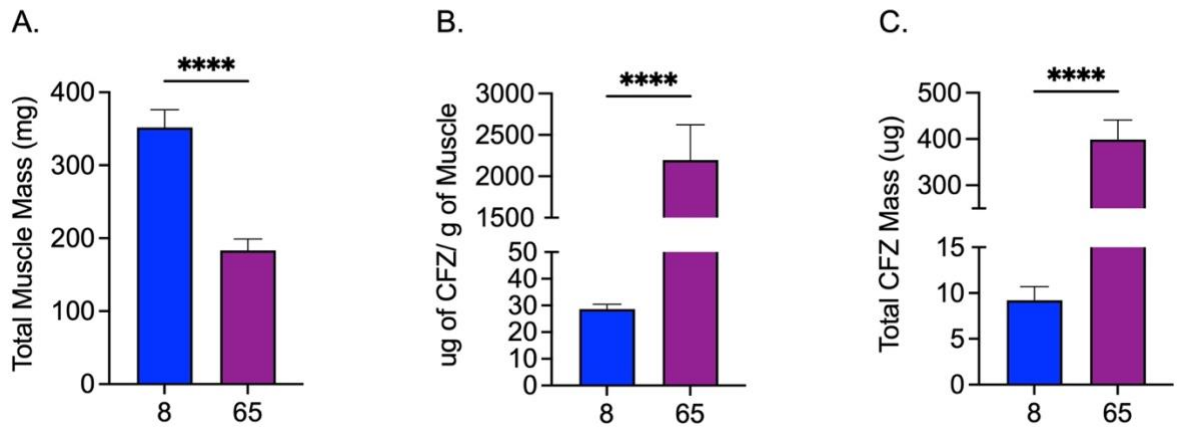

Figure S 3-4 CFZ Accumulation in the Skeletal Muscle of 8 and 65-Week Treated Mice

A. Total mass (mean ± SD) of isolated muscle pairs (QUAD, TRI, gastrocnemius). **B.** LC-MS measured CFZ concentration (mean ± SD) of the muscle pairs. **C.** Total CFZ mass (mean ± SD) in the muscle (calculated by multiplying A and B) (****$p<0.0001$, Student's t-test, n=3-11/group).

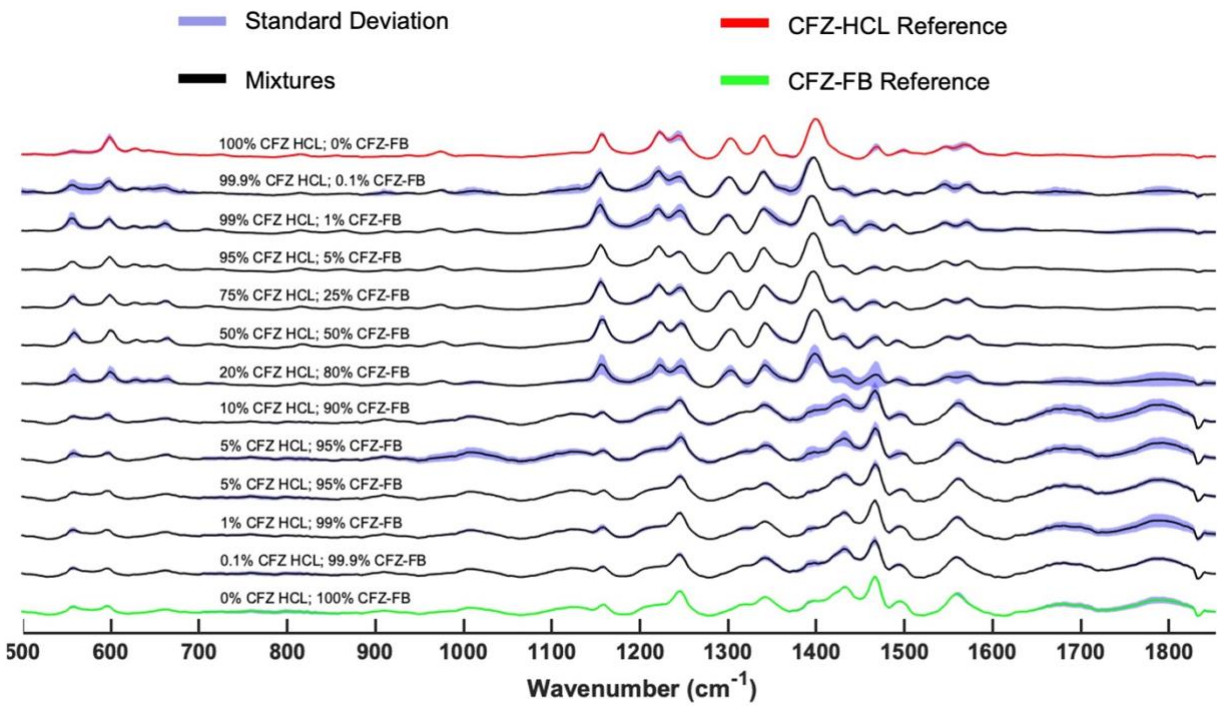

Figure S 3-5 CFZ Stoichiometric Mixtures

The stoichiometric mixtures (black spectra) of CFZ freebase (CFZ-FB; green spectra) and CFZ hydrochloride (CFZ-HCL; red spectra) allow for the determination of the relative mass ratio of the different CFZ forms within samples (spectra=mean, purple shadow= standard deviation).

3.11 References

1. Larsson, L., et al., *Sarcopenia: Aging-Related Loss of Muscle Mass and Function.* Physiol Rev, 2019. **99**(1): p. 427-511.

2. Nilwik, R., et al., *The decline in skeletal muscle mass with aging is mainly attributed to a reduction in type II muscle fiber size.* Exp Gerontol, 2013. **48**(5): p. 492-8.

3. Rahman, F.A., et al., *Impaired ECM Remodeling and Macrophage Activity Define Necrosis and Regeneration Following Damage in Aged Skeletal Muscle.* Int J Mol Sci, 2020. **21**(13).

4. Zacks, S.I. and M.F. Sheff, *Age-related impeded regeneration of mouse minced anterior tibial muscle.* Muscle Nerve, 1982. **5**(2): p. 152-61.

5. Yrjana, K.R., et al., *Anticholinergic medication exposure predicts poor physical capability: Findings from a large prospective cohort study in England.* Maturitas, 2020. **142**: p. 55-63.

6. Bozzetti, F., *Chemotherapy-Induced Sarcopenia.* Curr Treat Options Oncol, 2020. **21**(1): p. 7.

7. Casado, E., et al., *Antimalarial myopathy: an underdiagnosed complication? Prospective longitudinal study of 119 patients.* Ann Rheum Dis, 2006. **65**(3): p. 385-90.

8. Derendorf, H., *Excessive lysosomal ion-trapping of hydroxychloroquine and azithromycin.* Int J Antimicrob Agents, 2020. **55**(6): p. 106007.

9. Tidball, J.G., *Mechanisms of muscle injury, repair, and regeneration.* Compr Physiol, 2011. **1**(4): p. 2029-62.

10. Sayed, N., et al., *An inflammatory aging clock (iAge) based on deep learning tracks multimorbidity, immunosenescence, frailty and cardiovascular aging.* Nat Aging, 2021. **1**: p. 598-615.

11. Willmer, A.R., et al., *Molecular design of a pathogen activated, self-assembling mechanopharmaceutical device.* J Control Release, 2022. **347**: p. 620-631.

12. Rzeczycki, P., et al., *An Expandable Mechanopharmaceutical Device (1): Measuring the Cargo Capacity of Macrophages in a Living Organism.* Pharm Res, 2018. **36**(1): p. 12.

13. Baik, J. and G.R. Rosania, *Molecular imaging of intracellular drug-membrane aggregate formation.* Mol Pharm, 2011. **8**(5): p. 1742-9.

14. Baik, J., et al., *Multiscale distribution and bioaccumulation analysis of clofazimine reveals a massive immune system-mediated xenobiotic sequestration response.* Antimicrob Agents Chemother, 2013. **57**(3): p. 1218-30.

15. Pazan, F. and M. Wehling, *Polypharmacy in older adults: a narrative review of definitions, epidemiology and consequences.* Eur Geriatr Med, 2021. **12**(3): p. 443-452.

16. van Dijk, M., et al., *Sarcopenia in older mice is characterized by a decreased anabolic response to a protein meal.* Arch Gerontol Geriatr, 2017. **69**: p. 134-143.

17. Murray, S.A., et al., *Mouse gestation length is genetically determined.* PLoS One, 2010. **5**(8): p. e12418.

18. Trexel, J., et al., *Macrophage-Mediated Clofazimine Sequestration Is Accompanied by a Shift in Host Energy Metabolism.* J Pharm Sci, 2017. **106**(4): p. 1162-1174.

19. Rzeczycki, P., et al., *Detecting ordered small molecule drug aggregates in live macrophages: a multi-parameter microscope image data acquisition and analysis strategy.* Biomed Opt Express, 2017. **8**(2): p. 860-872.

20. Woldemichael, T., et al., *Reverse Engineering the Intracellular Self-Assembly of a Functional Mechanopharmaceutical Device.* Sci Rep, 2018. **8**(1): p. 2934.

21. Tan, J.W.Y., et al., *Photoacoustic imaging of clofazimine hydrochloride nanoparticle accumulation in cancerous vs normal prostates.* PLoS One, 2019. **14**(7): p. e0219655.

22. Murashov, M.D., et al., *Synthesis and Characterization of a Biomimetic Formulation of Clofazimine Hydrochloride Microcrystals for Parenteral Administration.* Pharmaceutics, 2018. **10**(4).

23. Rodgers, B.D., et al., *Micro-dystrophin Gene Therapy Partially Enhances Exercise Capacity in Older Adult mdx Mice.* Mol Ther Methods Clin Dev, 2020. **17**: p. 122-132.

24. Brashear, S.E., et al., *Passive stiffness of fibrotic skeletal muscle in mdx mice relates to collagen architecture.* J Physiol, 2021. **599**(3): p. 943-962.

25. Narici, M.V. and N. Maffulli, *Sarcopenia: characteristics, mechanisms and functional significance.* Br Med Bull, 2010. **95**: p. 139-59.

26. Kawanishi, N. and S. Machida, *Alterations of macrophage and neutrophil content in skeletal muscle of aged versus young mice.* Muscle Nerve, 2021. **63**(4): p. 600-607.

27. Hogan, K.A., et al., *Tumor-derived cytokines impair myogenesis and alter the skeletal muscle immune microenvironment.* Cytokine, 2018. **107**: p. 9-17.

28. Bivona, J.J., 3rd, et al., *Macrophages augment the skeletal muscle proinflammatory response through TNFalpha following LPS-induced acute lung injury.* FASEB J, 2021. **35**(4): p. e21462.

29. Martins, L., et al., *Skeletal muscle healing by M1-like macrophages produced by transient expression of exogenous GM-CSF.* Stem Cell Res Ther, 2020. **11**(1): p. 473.

30. Korbecki, J., et al., *The Importance of CXCL1 in Physiology and Noncancerous Diseases of Bone, Bone Marrow, Muscle and the Nervous System.* Int J Mol Sci, 2022. **23**(8).

31. Munoz-Canoves, P., et al., *Interleukin-6 myokine signaling in skeletal muscle: a double-edged sword?* FEBS J, 2013. **280**(17): p. 4131-48.

32. Jaguin, M., et al., *Polarization profiles of human M-CSF-generated macrophages and comparison of M1-markers in classically activated macrophages from GM-CSF and M-CSF origin.* Cell Immunol, 2013. **281**(1): p. 51-61.

33. *Ccl5 chemokine (C-C motif) ligand 5 [Mus musculus (house mouse)]*. Gene 2023 [cited 2021 02-21]; Gene ID: 20304]. Available from: https://www.ncbi.nlm.nih.gov/gene/20304.

34. Kohno, S., et al., *Rantes secreted from macrophages disturbs skeletal muscle regeneration after cardiotoxin injection in Cbl-b-deficient mice.* Muscle Nerve, 2011. **43**(2): p. 223-9.

35. Hirayama, D., T. Iida, and H. Nakase, *The Phagocytic Function of Macrophage-Enforcing Innate Immunity and Tissue Homeostasis.* Int J Mol Sci, 2017. **19**(1).

36. Thorley, M., et al., *Changes in Communication between Muscle Stem Cells and their Environment with Aging.* J Neuromuscul Dis, 2015. **2**(3): p. 205-217.

37. Bruno, C.D., et al., *Effect of lipophilicity on drug distribution and elimination: Influence of obesity.* Br J Clin Pharmacol, 2021. **87**(8): p. 3197-3205.

38. Vida, C., et al., *Role of macrophages in age-related oxidative stress and lipofuscin accumulation in mice.* Redox Biol, 2017. **12**: p. 423-437.

Chapter 4 Clofazimine-Mediated, Age-Related Changes in Skeletal Muscle Mitochondrial Metabolites

4.1 Relevance to Thesis

Specific aim 3 was to compare the accumulation of CFZ in muscle and explore any associated differences. Thus, in this chapter, I examined young (4-week-old) old (61-week-old) mice, as the work presented in Chapter 3 demonstrated that old mice had higher levels of CFZ in skeletal muscle compared with young mice. Given the risk for age-related adverse drug reactions (ADRs) and that CFZ has been shown to interact with the mitochondrial membrane, an investigation into these mechanisms were warranted. To accomplish this, I used the CFZ Raman imaging technique from Chapters 3.

The results revealed that the skeletal muscle of old CFZ-treated mice had disrupted mitochondrial metabolism, greater changes in body weight and muscle function compared to controls, but altered mitochondrial metabolism was not detected in the blood. Old mice were also more susceptible to CFZ-induced catabolism, which indicates overall altered metabolism. Based on these data, routine assessment of body weight and caloric intake may be useful for identifying mitochondrial-related ADRs in elderly patients. These findings also highlight the need to identify blood markers to capture ADRs in individuals that may be high risk including elderly patients.

4.2 Abstract

Mitochondrial health declines with age, and older patients can demonstrate dysfunction in mitochondrial-rich tissues, such as cardiac and skeletal muscle. Aged mitochondria may make

older adults more susceptible to adverse drug reactions (ADRs). We assessed mitochondrial metabolic function by measuring two metabolites, l-carnitine and acetylcarnitine, to determine their effectiveness as candidate clinical biomarkers for age-related, drug-induced alterations in mitochondrial metabolism. To study age and medication-related changes in mitochondrial metabolism, we administered the FDA-approved mitochondriotropic drug, clofazimine (CFZ), or vehicle for 8-weeks to young (4-weeks-old) and old (61-weeks-old) male C57BL/6J mice. At the end of treatment, whole blood and cardiac and skeletal muscle were analyzed for l-carnitine, acetylcarnitine, and CFZ levels; muscle function was measured via a treadmill test. No differences were found in blood or cardiac carnitine levels of CFZ-treated mice but CFZ-treated mice lost displayed lost body mass and alterations in endurance and levels of skeletal muscle mitochondrial metabolites. These findings demonstrate age-related susceptibility of the skeletal muscle to mitochondria drug toxicity. Since drug-induced alterations in mitochondrial metabolism in skeletal muscle were not reflected in the blood by l-carnitine or acetylcarnitine levels, drug-induced catabolism and changes in muscle function appear more relevant to stratify individuals at increased risk for ADRs.

4.3 Introduction

Mitochondrial dysfunction is a hallmark of aging, which leads to changes in metabolism and manifests as structural and functional impairments in various organ systems including muscle, which has a high energy demand [1-3]. Many medications that accumulate in mitochondria can also cause disruptions in mitochondrial function [4, 5]. The combination of age-related declines in mitochondrial function could enhance the susceptibility to adverse drug reactions (ADRs) of mitochondriotropic drugs, particularly those with known effects on cardiac and skeletal muscle function [6, 7]. In these cases, elderly patients may be at higher risk for drug toxicity affecting

muscle function resulting from mitochondrial drugs compared to the younger population [8]. Hence, there is a need to identify biomarkers for monitoring drug mitochondriotoxicity in elderly patients.

Many FDA-approved medications are cell membrane permeant small molecules that concentrate in organelles such as lysosomes and mitochondria via physicochemical mechanisms involving pH and ion gradients across the membranes bounding these organelles [9, 10]. Lysosomes and mitochondria are both important organelles for lipid metabolism and energy production [11]. Mitochondria are involved in lipid biosynthesis and synthesize large amounts of ATP through fatty acid beta-oxidation that is dependent on the carnitine shuttle, where l-carnitine gets converted to acetylcarnitine [12]. Lysosomes are important organelles for phospholipid uptake into cells via endocytosis of low-density lipoprotein particles and lipid degradation by lysosomal lipases [13].

To study age-related differences in medication-induced alterations in mitochondrial-related metabolism, we used the mitochondriotropic and lysosomotropic drug, clofazimine (CFZ), an FDA–approved antibiotic that accumulates in both lysosomes and mitochondria, with effects on both lysosomal and mitochondrial structure and function [14, 15]. As an easily accessible, systemic biomarker of mitochondrial and lysosomal changes induced by drugs that accumulate in these organelles, l-carnitine and its acetylated metabolite, acetylcarnitine, have been proposed as clinically relevant biomarkers to detect patients at increased risk of serious ADRs, especially among the elderly [5, 16]. While there are numerous mitochondrial metabolites, these attributes make l-carnitine and acetylcarnitine viable candidate biomarkers for ADRs [5]. Therefore, to further understand the relationship between age and medication exposure and mitochondrial

metabolic function, we used measurements of l-carnitine and acetylcarnitine, and accompanying changes in total body mass, food intake, muscle mass and endurance.

Metabolite measurements were made in blood, skeletal and cardiac muscle of young and old C57BL/6J mice treated with either CFZ or vehicle.

4.4 Materials and Methods

4.4.1 Animal Studies

Animal use protocols were approved by the University of Michigan's Institutional Committee (PRO00007593; May 5, 2017, PRO00009404; December 13, 2022), and animal care was provided by the University of Michigan's Unit for Laboratory Animal Medicine (ULAM), where animals were maintained at 22 ± 2 ℃ and relative humidity of 55 ± 5%, a standard 12-h dark-light cycle, and had unconstrained access to water and food. In accordance with ULAM guidelines, young (4 weeks) and old (61 weeks) male C57BL/6J mice from Jackson Laboratory, USA, did not require acclimation prior to experimentation. These mice were randomized to receive either CFZ (C8895, Sigma-Aldrich) to achieve a dose of 36mg/kg/day or equal amounts of vehicle sesame oil (720189601668, Kadoya) for 8 weeks. At the end of treatment, food consumption was monitored via specialized cages (3700M022, Tecniplas) for 18 hours, after which animals were euthanized by CO_2 inhalation following a cardiac puncture for blood sample acquisition in compliance with American Veterinary Medical Association Guidelines. Immediately after euthanasia, the heart and gastrocnemius (GAS) muscle were isolated, washed with 1X phosphate buffered saline (PBS), blotted dry, and flash-frozen in liquid nitrogen. While experiments were conducted in compliance with the Animal Research: Reporting of In Vivo Experiments guidelines [17], it should be noted that true blinding of the experiments was not feasible due to the red pigmentation in the skin induced by CFZ. This is readily apparent at the time of experiment

termination. In addition, CFZ induces readily apparent changes at the molecular level of the organ tissue (e.g., CFZ crystals) that do not permit sustained blinding.

4.4.2 Quantification of Carnitine, Acetylcarnitine and CFZ

Quantification of l-carnitine, acetylcarnitine, and CFZ in whole blood, GAS, and heart, with randomization of the samples prior to assay, was performed by the Pharmacokinetic and Mass Spectrometry Core (University of Michigan). Detailed information for each assay is given in the Supplemental Text. In brief, muscle was homogenized in n-dimethylformamide-PBS solution. Acetonitrile was added to whole blood and muscle homogenate for protein precipitation and CFZ extraction. For both assays, concentrations (***μ***g/mL) were derived from an internal standard as measured by liquid chromatography (LC)-mass spectroscopy (MS)/MS. Resulting data were processed using Analyst (1.6, SCIEX, Framingham, MA, USA) for CFZ and SCIEX OS (2.1.6, SCIEX, Framingham, MA, USA) for l-carnitine and acetylcarnitine and blinded analysis of acetylcarnitine and carnitine data was conducted. To convert CFZ muscle data from ***μ***g/mL to ***μ***g, concentration values were multiplied by the mass (g) of each sample. Blood concentration data were converted from µg/ml to µM by dividing concentration (µg/ml) by molecular weight (l-carnitine, 161.2; acetylcarnitine, 203.2; clofazimine, 473.4) and multiplying by 1000.

4.4.3 Endurance Testing

Treadmill testing is a reproducible, non-invasive method to assess skeletal muscle function and endurance [18, 19]. Mice were randomized for testing and at the time of testing each mouse was placed in its own lane on a treadmill (1050-RM, Columbus Instruments). Up to four mice were tested simultaneously and each one ran to exhaustion [20]. Each mouse had a two-minute warm-up session before the endurance treadmill study. The mice ran eight meters per minute with

no pulse shocks during the first minute of the warm-up session. For the remaining minute of the warm-up session, pulse shocks were initiated (200-millisecond pulses with a repetition rate of 4 pulses per second and a shock intensity at 3.4 milliamps). The endurance test started immediately after the warm-up session (with the pulse shocks on) and the treadmill speed was set to eight meters per minute. The treadmill speed was increased by one meter every minute. The mice were deemed exhausted if they were on the shock grids for greater than three consecutive seconds without attempting to reengage the treadmill, spent greater than 50% of their time on the shock grid, or at the third time the animal was willing to sustain 2 seconds or more on the shock grid rather than returning to the treadmill.

4.4.4 Chemical Imaging of CFZ Accumulation in Muscles

Confocal Raman microscopy analysis, as previously described [21], was used to assess the protonation state (freebase or hydrochloride salt) of CFZ that accumulated in the heart and GAS from cryosections (10 μm thick on glass slides). Briefly, a Raman microscope (alpha300R, WiTec) coupled to a 532 nm laser and a Zeiss EC EPIPLAN 50x objective (N.A. = 0.75) was used to acquire large area scans (50 μm by 50 μm) with a step size of 50 μm and an integration time of 0.1 ms per pixel throughout the sections. The WiTec Project FOUR software was utilized to remove cosmic rays, and a MATLAB® processing algorithm developed in-house was used to baseline-subtract, normalize, and generate the differences between spectra. Muscle spectral references were gathered from CFZ-crystal negative regions and true muscle reference spectra were gathered from vehicle-treated sections. Sample spectra were compared to the reference spectra of pure CFZ-freebase (CFZ-FB) and CFZ-hydrochloride (CFZ-HCL) to assess the protonation state of the drug present in association with the tissue samples.

4.4.5 Statistics

Data were compared using either a one-way ANOVA followed by post-hoc Tukey's test when the ANOVA p value was significant or an unpaired Student's t-test with equal variance, when comparisons between two groups were made; no data were excluded. Statistical analyses and associated graphics were done using PRISM (9.4.1; GraphPad Software, Inc., San Diego, CA USA), where a p-value of ≤ 0.05 was considered significant. Based on prior work using a standard deviation range of 10-15 [22], an $\boldsymbol{\alpha}$ of 0.05, and a power of 80%, we calculated a sample size between 10-17 mice per group.

4.5 Results

4.5.1 Age and CFZ-related Changes in Muscle Mitochondrial Metabolites are not Reflected in the Blood

Chemical analysis of whole blood samples revealed age-related differences in acetylcarnitine levels that were not altered by CFZ treatment (**Figure 4-1A**). Neither age nor CFZ treatment altered the whole blood l-carnitine or acetylcarnitine/carnitine ratios (**Figure 4-1A**).

Cardiac levels of l-carnitine in old vehicle-treated (O-) mice were lower than levels in young vehicle-treated (Y-) mice; however, acetylcarnitine levels remained unchanged (**Figure 4-1B**). CFZ treatment resulted in higher l-carnitine and acetylcarnitine levels in old mice (O+) compared with its negative control (O-) (**Figure 4-1B**). The acetylcarnitine to l-carnitine ratios of the cardiac muscle did not differ by age or CFZ treatment (**Figure 4-1B**).

Skeletal muscle carnitine levels were not affected by age (**Figure 4-1C**). However, CFZ treatment resulted in a greater change in skeletal muscle l-carnitine in old, (O+) than in, young, (Y+), mice (**Figure 4-1C**). There was no change in acetylcarnitine among the groups **(Figure 4-**

1C). Old, CFZ-treated mice (O+) had a lower acetylcarnitine to l-carnitine ratio compared to young, CFZ-treated mice (Y+) and old, vehicle control mice (O-), demonstrating a more profound CFZ-induced alteration in mitochondrial-related metabolism in old mice (**Figure 4-1C**).

4.5.2 Both Young and Old CFZ-treated Mice Exhibited a Pronounced, Catabolic Phenotype Compared with Control, Vehicle-treated Mice

CFZ treatment was initiated in mice at 4 weeks of age (young) or at 61 weeks of age (old). Both groups of mice received the same average CFZ dose in their feed for 8 weeks. The mean whole blood CFZ concentration was not different between the two groups (**Figure 4-2A**). Body mass change from the start to the end of treatment was larger in young control mice (Y-) than in young CFZ-treated mice (Y+) and old control mice (O-) (**Figure 4-2B**). Old CFZ-treated mice (O+) lost body mass and their absolute change was larger than in young, CFZ-treated (Y+) and old-vehicle-treated (O-) mice (**Figure 4-2B**). Even though the CFZ-treated groups (Y+ and O+) had smaller body masses at the end of treatment compared to their controls (Y- and O-), the CFZ-treated mice consumed more food than their vehicle controls (**Figure 4-2B, C**).

4.5.3 CFZ Treatment Decreased Endurance in Old Mice

Cardiac mass corrected by body mass was not different among the groups (**Figure 4-3A**). The normalized skeletal mass by body mass showed an age-related change between Y- and O-, and Y+ and O+, where old mice had lower skeletal-to-body ratios than the young mice (**Figure 4-3B**). In old CFZ-treated mice (O+), this translated to a reduction in endurance compared to its negative control, O- (**Figure 4-3C**).

4.5.4 Greater CFZ Accumulation Occurred in Skeletal and Cardiac Muscle of Old Mice

CFZ accumulation in cardiac and skeletal muscle was influenced by age, where CFZ per gram of tissue was 2.0X higher in the cardiac muscle and 2.7X higher in the skeletal muscle of old mice compared to young mice (**Figure 4A, B**). Not surprisingly, this translated to a higher total amount of CFZ in cardiac (Y+= 18.5 $\pm$ 10.7, O+= 50.8 $\pm$ 10.1; ****p< 0.0001, Tukey) and skeletal (Y+= 2.5 $\pm$ 0.6, O+= 7.8 $\pm$ 1.8; ****p< 0.0001, Tukey) muscle of old mice compared to young mice. Given this finding and since CFZ is known to accumulate in the macrophages, we were prompted to assess macrophage numbers in residual skeletal muscle specimens (**see Supplemental Text**). We found that there was no difference in macrophage number between CFZ-treated young and old mice (**Figure S1A-C**). The CFZ concentration quantified in the muscle of the control mice, Y- and O-, was negligible.

4.5.5 Chemical Analysis of Skeletal and Cardiac Muscle Reveals CFZ is Present in Discrete, Microscopic Crystalline Inclusions as the Protonated Salt Form of the Drug

Brightfield (BF) images of CFZ-treated cardiac and skeletal muscles revealed crystal-like structures, smaller than 20 μM within the sections, which can fit inside cells (**Figure 5A, B**) [14]. The crystals resembled the protonated form of CFZ, CFZ-hydrochloride (CFZ-HCL). By analyzing muscle tissue sections with a Raman confocal microscope, the Raman generated heat maps, using the 1400 cm^{-1} signature peak of CFZ-HCL, revealed CFZ was present as the protonated salt form, within microcrystalline structures in the muscle tissue (**Figure 5A, B**); this is consistent with our previous findings [21]. Based on the size and Raman spectra of the CFZ in the cardiac and skeletal muscles, the spectral evidence indicated that the drug was in the protonated, charged form which is associated with intracellular (mitochondrial and lysosomal) drug distribution. There were no peaks associated with the presence of the neutral, freebase form

of the drug (CFZ-FB), which is the form that typically partitions into body fat and adipose tissue (**Figure 5C**) [15, 23]. To determine whether the muscle reference spectra from crystal-free regions did not contain CFZ-FB, the reference spectra of muscle from the vehicle control mice were subtracted (**Figure S2A, B**), demonstrating that the freebase signal was absent from CFZ-treated muscle spectra.

4.6 Discussion

To understand medication-induced alterations in mitochondrial-related metabolism, we used a mitochondriotropic drug, CFZ, in young and old mice to assess the utility of the mitochondrial metabolites, l-carnitine and acetylcarnitine, as biomarkers of drug-induced changes in mitochondrial function [24]; the choice of these metabolites was influenced by our prior work that identified a CFZ-induced alteration in blood levels of l-carnitine [22]. Since the musculature is highly affected by age-related energy metabolism decline [5, 25, 26], we studied cardiac and skeletal muscle. We chose the gastrocnemius as a representative skeletal muscle because it has been shown to demonstrate the same age-related changes in structure and metabolism as other skeletal muscle types [27] while also being important for mobility and endurance [28]. We measured the function of the gastrocnemius and heart simultaneously via a treadmill test in both untreated and CFZ-treated mice.

Unlike the cardiac muscle, skeletal muscle sustained a drug-induced disruption in l-carnitine homeostasis as measured by the acetylcarnitine/l-carnitine ratio [29], and loss of body-mass adjusted mass. This occurred despite a lower per gram tissue accumulation of CFZ compared with the cardiac muscle. Notably, the lack of a detectable difference in blood levels of l-carnitine or acetylcarnitine in CFZ-treated mice was unexpected, given that muscle is a primary site of mitochondrial metabolism and there were drug induced changes in endurance and total body mass.

Collectively, these findings suggest that in old individuals, skeletal muscle may be more vulnerable to mitochondria drug-toxicity, a problem that does not appear to be readily identified by measurements of blood levels of high abundant mitochondrial-related metabolites but is better reflected by a decrease in total body mass in the presence of an increase in caloric intake (catabolism).

Age-related changes in muscle mass give insight into the metabolic vulnerability of skeletal muscle and the metabolic flexibility of cardiac muscle. We have previously shown that 8 weeks of CFZ treatment induces a catabolic state [22]. This was evident in our current study and was more pronounced in old mice (**Figure 2B**). Catabolism is known to target fat and skeletal muscle mass [30] and spare vital organs like the heart. Specifically, the heart can use a range of substrates to maintain adenosine triphosphate (ATP**)** production [31] whereas skeletal muscle serves as an important source of amino acids during times of metabolic stress [32]. Our findings suggest that skeletal muscle is more vulnerable to CFZ-induced catabolism in old mice so much so that it resulted in an organ-level disruption in l-carnitine homeostasis (**Figure 1C**), loss of mass (**Figure 3B**), and a reduction in physical endurance (**Figure 3C**). Again, this did not translate to a detectable change in blood levels of either l-carnitine or acetylcarnitine (**Figure 1A**).

The bioaccumulation of CFZ in both cardiac and skeletal muscle also provides some clues about our reported age-related differences. Old mice accumulated much more CFZ in both skeletal and cardiac muscle compared with young mice. We have previously shown that CFZ progressively bioaccumulates in the lysosomes of resident macrophages [23, 33]. The CFZ form present in both cardiac and skeletal muscle was predominantly the protonated form. This is the form of CFZ that is present inside acidic organelles like lysosomes, gets trapped in macrophages and only clears after macrophages undergo apoptosis or when treatment is discontinued [15]. Although we did not

specifically measure CFZ in skeletal or cardiac muscle macrophages, differences in age-related accumulation may stem from slower macrophage turnover and/or changes in macrophage phenotypes that occur with increased age [34-36]. This phenomenon could permit greater CFZ accumulation in old mice compared with young mice. Alternative, macrophages of old mice may have a greater cargo capacity than those of young mice, since there was no age-related change in macrophage numbers groups in skeletal muscle (**Figure S1C**). Similarly, the higher accumulation of CFZ in cardiac muscle compared with skeletal muscle could be due to fundamental differences in the function of resident macrophages in these tissues as described in the previous paragraph [37, 38].

While our findings were unexpected and provocative, we acknowledge there are limitations. We recognize that the measurement of l-carnitine and acetylcarnitine does not represent a comprehensive assessment of mitochondrial metabolic function. However, these metabolites are abundant and readily detectable in the blood. They are also upstream of numerous metabolic processes in the mitochondria [29, 39]. As such, disruption in carnitine homeostasis was hypothesized as a reasonable gauge of mitochondrial metabolic perturbations. The duration of treatment and/or ages studied may not have generated a significant alteration in host mitochondrial metabolic function for detection in whole blood. In previous research, CFZ altered carnitine levels in whole blood, but this study used a smaller sample and a different analytical technique (nuclear magnetic resonance spectroscopy) to quantify l-carnitine [22]. While we did not find differences in l-carnitine levels in whole blood with CFZ treatment that would have sufficiently altered the ratio of mitochondrial-related metabolites, we were able to detect an age- and tissue-dependent alteration in mitochondrial metabolism accompanied by CFZ-induced catabolism. However, the specific mechanism(s) that drive these differences require more detailed, physiological studies.

Finally, to understand the extent to which these findings could bear relevance in humans will require clinical studies.

In conclusion, age is associated with an increased risk of ADRs and disturbed energy metabolism, which results in altered organ function; this is most often evident in tissues that require and/or use large amounts of energy [40]. While it has been proposed that blood levels of two abundant mitochondrial metabolites could serve as surrogate biomarkers for assessing changes in mitochondrial metabolism and potentially identify occult ADRs, we did not find measurable changes in either l-carnitine or acetylcarnitine blood levels following the administration of a known mitochondriotropic and lysosomotropic drug [5]. Nevertheless, there were clear changes in total body weight, food consumption, and exercise endurance that could be useful as functional biomarkers, which in humans could translate to routine assessment of body weight, estimation of calorie consumption, and exercise tolerance/endurance, for stratifying patients at increased risk for ADRs. Future studies will be aimed at deciphering the organ specific mechanisms that contribute to weight loss and decreased endurance. These future directions could also consist of cellular-based studies of carnitine shuttle enzymes and skeletal muscle composition that could aid in pinpointing specific mechanisms. Importantly, in addition to CFZ, there are other drugs (e.g., doxorubicin, carbamazepine, haloperidol, chlorpromazine, and amiodarone) that are known mitochondrial toxicants which accumulate in the lysosome, illustrating the value of detecting individuals at increased ADR risk [5, 41]. Doxorubicin has been shown to elicit age-related ADRs such as cardiotoxicity and muscle atrophy [42-44]. Thus, establishing clinically actionable biomarkers of mitochondrial toxicity that could identify patients at greatest ADR risk would be an advancement in patient care, particularly in the elderly who are most vulnerable to ADRs.

4.7 Acknowledgements and Funding

We would like to thank the University of Michigan Pharmacokinetic Core research group (in particular, Drs. Manjunath (Amit) Pai, Bo Wen, and Lu Wang) for their technical and analytical contributions. Furthermore, we would like to acknowledge the University of Michigan Laboratory Animal Medicine- In Vivo Animal Core for their technical and analytical contributions with the histology and immunohistochemistry, specifically Dr. Ingrid L. Bergin, Pavlina Zafirovska, and Wendy Rosebury-Smith. Additionally, we thank Jae Hyun Kim for technical assistance with the Raman analysis and the Physiology Phenotyping Core at the University of Michigan for their assistance with the treadmill study.

This research was funded by grants from the National Institutes of Health, National Institute of General Medical Sciences under award numbers R01GM127787 (Dr. Rosania), P30AR069620 (Dr. Jepsen), and R35GM136312 (Dr. Stringer).

4.8 Figures

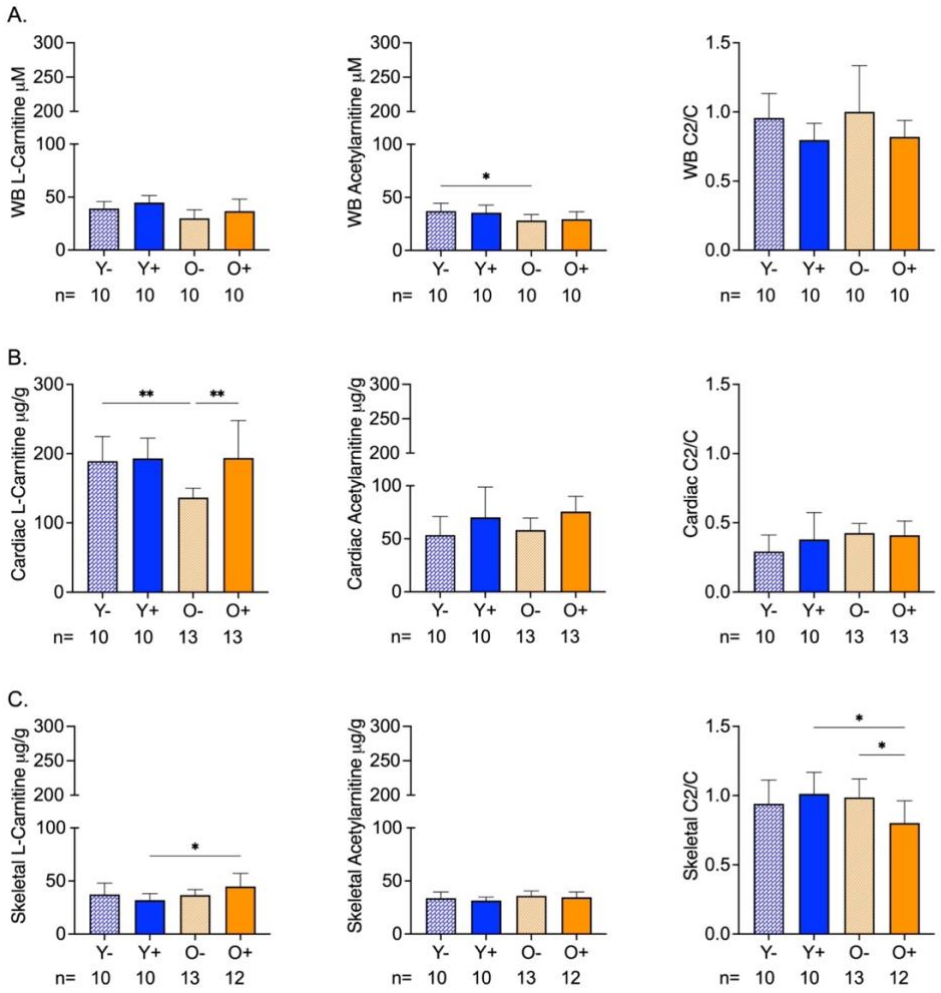

Figure 4-1 Carnitine (C) and Acetylcarnitine (C2) Levels in Whole Blood and Cardiac and Skeletal Muscles of Aged and CFZ-Treated Mice

A. Whole blood C and C2 levels and C2/C ratios (mean ± SD). Old vehicle-treated (O-) mice had lower C2 levels than young vehicle-treated (Y-) mice (*p= 0.03, Tukey). The C2/C ratios of aged and CFZ-treated were not different across groups. **B.** Cardiac muscle C and C2 levels and C2/C ratios (mean ± SD). C decreased in O- mice compared to Y- (**p= 0.01, Tukey), where C was higher in old CFZ-treated mice (O+) than in its negative control, O- (**p= 0.001, Tukey). CFZ-treatment and age did not change the C2/C ratios. **C.** Skeletal muscle C and C2 levels and C2/C ratios (mean ± SD). CFZ-treatment increased C levels in old mice (O+) compared with young mice, Y+ (*p= 0.01, Tukey) but neither were different from its respective negative control. CFZ-treatment decreased the C2/C ratio in old (O+) mice compared to young (Y+) mice (*p=0.01, Tukey) and vehicle-treated old, O-, mice (*p= 0.02, Tukey). The number of mice per group is shown below the x-axis of each plot.

A.

Age	Group	Age Treatment Started/Ended (Weeks)	Calculated CFZ Dose (mg/kg/day)	Measured CFZ in WB (μM)
Young	CFZ	4/12	46.9 ± 4.3	6.45 ± 1.39
	Vehicle		0	0
Old	CFZ	61/69	42.6 ± 7.6	7.18 ± 1.61
	Vehicle		0	0

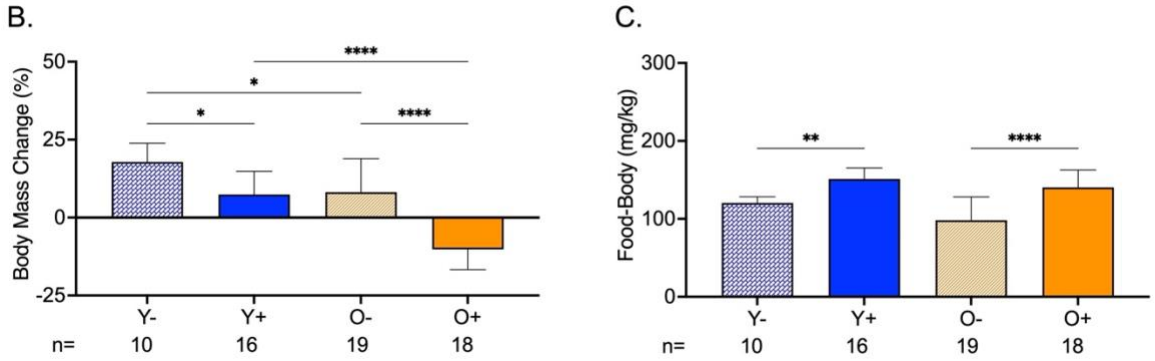

Figure 4-2 Treatment Groups, Body Mass Changes, and Food Consumption During CFZ-Treatment

A. Treatment groups, CFZ dose (mean ± SD), and CFZ in whole blood (mean ± SD). CFZ treatment did not result in different drug doses (p=0.25, Student's t-test) or drug concentrations in whole blood (p=0.10, Student's t-test) in young (Y+) and old (O+) mice. Drug dose was calculated using the terminal body mass and amount of drug-laced food consumed during an 18-hour food consumption study conducted prior to euthanasia (n=16-18/group). Whole blood (WB) CFZ concentration was determined by LC-MS (n=10-15/group**). B.** Body mass change (mean ± SD) from the start to the end of treatment. Old mice (O-) gained less weight than young mice (Y-) (*p= 0.02, Tukey). Of the CFZ-treated mice, old mice (O+) showed a greater change in percent body mass than young (Y+) mice (****p< 0.0001, Tukey). Young, CFZ-treated mice (Y+) had a smaller mass change than their negative control, Y- (*p= 0.01, Tukey), and old, CFZ treated mice (O+) had a decline in percent body mass change compared to its negative control, O- (**** p< 0.0001, Tukey). **C.** Food-to-body ratio (mean ± SD), food consumption (mg) corrected for body weight (kg), was calculated using food consumption measurements made before euthanasia and the terminal body mass. Both young (Y+) and old (O+) CFZ-treated mice consumed more food than their respective controls, Y- (**p= 0.005, Tukey) and O- (****p< 0.0001, Tukey). The number of mice per group is shown below the x-axis of each plot.

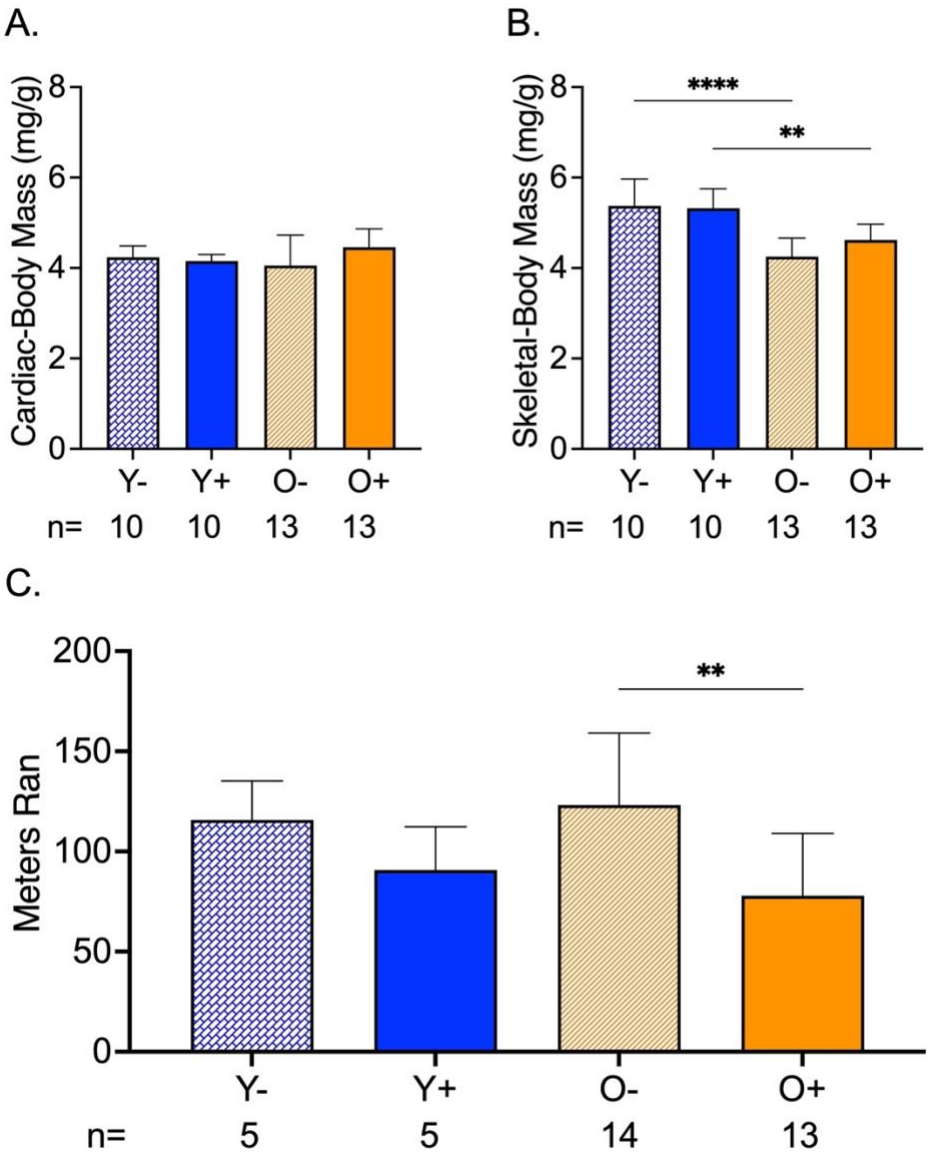

Figure 4-3 CFZ and Age Induced-Changes in Cardiac and Skeletal Muscle Mass and Endurance

A. Cardiac mass (mean ± SD) corrected for body mass was not different across treatment groups. **B.** When accounting for body mass, old vehicle-treated (O-) mice had smaller skeletal muscle mass compared to, young, vehicle treated, Y-, mice (****$p < 0.0001$, Tukey). This finding was sustained in mice treated with CFZ (**$p < 0.003$, Tukey). **C.** Endurance (mean ± SD), as measured by distance ran in a forced treadmill running study, was reduced by CFZ-treatment in old (O+) compared with their negative control, O- (**$p = 0.003$; Tukey). The number of mice per group is shown below the x-axis of each plot.

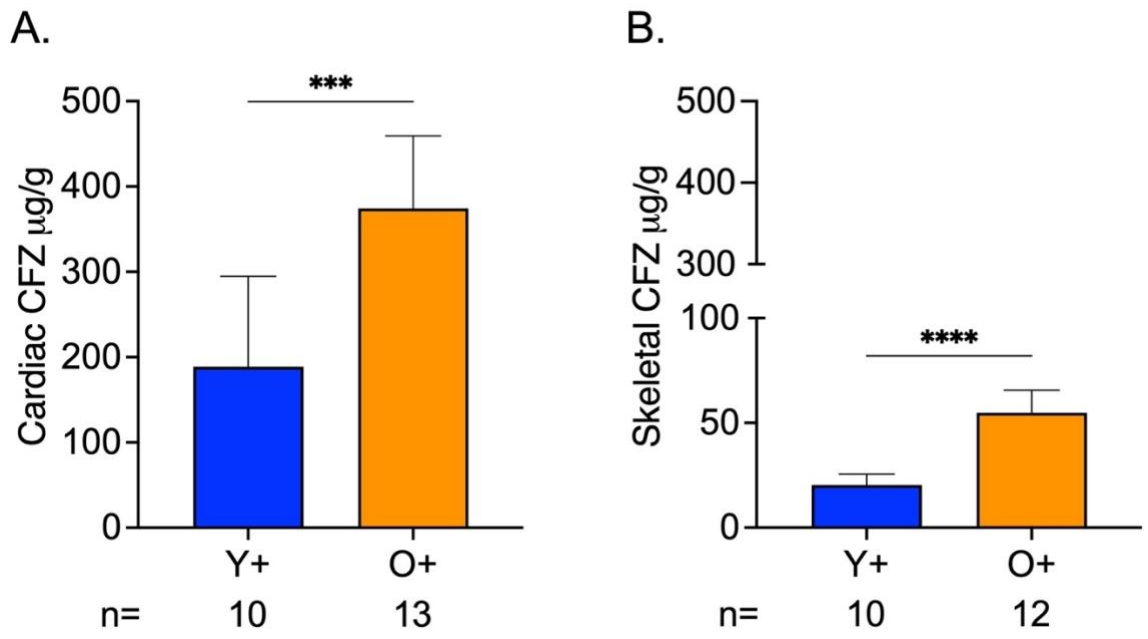

Figure 4-4 CFZ Accumulation is Greater in the Skeletal and Cardiac Muscle of Old Versus Young Mice

A. CFZ concentration in cardiac muscle per gram of tissue. **B.** CFZ concentration in skeletal muscle per gram of tissue. Based on LC-MS analysis, CFZ concentration (mean $\pm$ SD) in the cardiac and skeletal muscle revealed that old mice had a significantly higher CFZ concentration in the cardiac (***p= 0.0001, Student's t-test) and skeletal (****p< 0.0001, Student's t-test) muscles. The number of mice per group is shown below the x-axis of each plot.

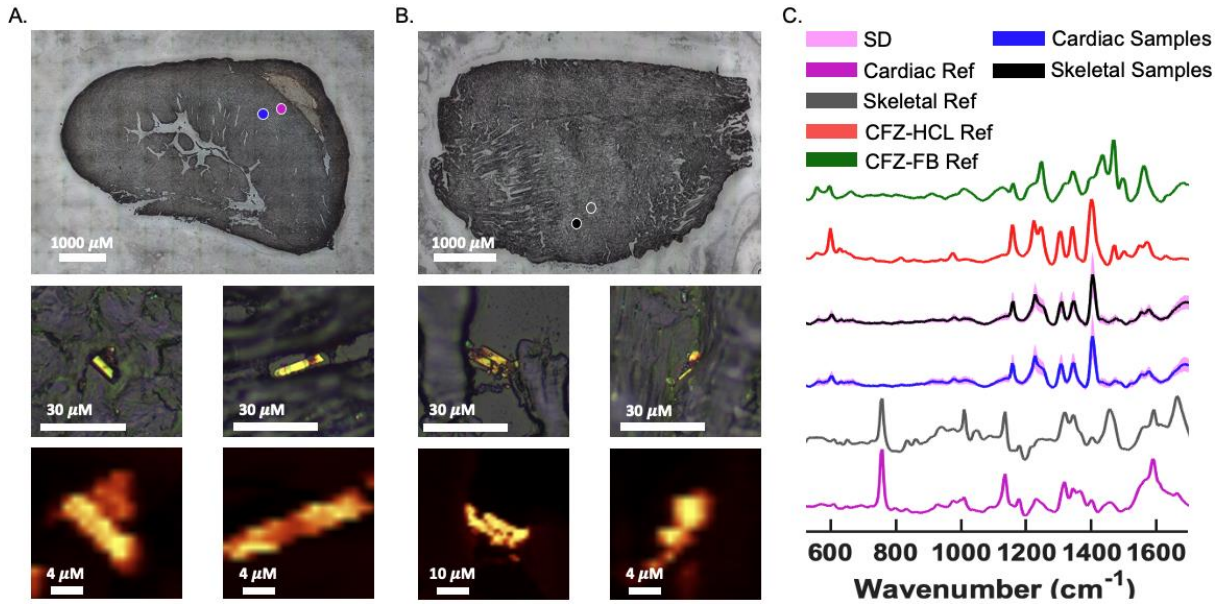

Figure 4-5 CFZ is Predominantly in the Protonated Form in Skeletal and Cardiac Muscle

Raman bright field (BF) images of a cryo-section of (**A**) cardiac and (**B**) skeletal muscle from a CFZ-treated mouse that show positive CFZ-crystal area (blue dot) in relation to a negative CFZ-crystal area (purple dot). Negative CFZ-crystal areas were scanned to generate (**C**) cardiac muscle reference (purple) (n=5) and skeletal reference spectra (gray) (n=5). Raman heat maps (1400 cm^{-1}) of CFZ-positive areas in the cardiac and skeletal muscle are shown under their corresponding positive CFZ-crystal BF image. C. CFZ-treated mice spectral signals (mean ± SD, SD=pink outline) from CFZ-positive areas of cardiac (blue spectrum) and skeletal (black spectrum) muscles reveal no indication of the neutral form of CFZ (CFZ-FB, green spectrum), but rather it is present entirely as the protonated salt form (CFZ-HCL, red spectrum) (n=5/group). This protonated salt form was exclusively detected in both muscle types.

4.9 Supporting Information

4.9.1 Sample Preparation and L-Carnitine and Acetylcarnitine LC-MS/MS Analysis

Blood samples were diluted 1:50 (10 µL of WB in 490 µL water). Five µL of internal standard solution (l-carnitine-13C, D3 and acetylcarnitine-D3, 5 µg/mL in acetonitrile) were added into the diluted samples and mixed for 30 min at room temperature. For protein precipitation, 150 µL of acetonitrile was added to 50 µL of the sample. The mixture was vortexed for 10 min and centrifuged (3500 rpm for 10 min); the supernatant was transferred to autosampler vials for LC–MS/MS analysis.

Muscle samples were homogenized (Precellys tissue homogenizer, Bertin Technologies, Montigny-le-Bretonneux, France) with 80% N-Dimethylformamide (DMF)-PBS solution using a ratio of 5:1 volume (mL) to weight of muscle (g). Then, the muscle homogenate was diluted 50 times with water and treated using the same procedure as that for the blood samples to extract the compounds for LC–MS/MS analysis.

A Shimadzu LC-20AD HPLC system (Kyoto, Japan), and chromatographic separation of l-carnitine and acetylcarnitine was achieved using an Agilent Poroshell 120 EC-C18 column (3.0 x 100 mm, 2.7 µm at 25 °C). Five µL of the supernatant were injected per sample. The flow rate of gradient elution was 0.35 ml/min with mobile phase A (10 mM ammonium formate and 0.1% formic acid in purified deionized water) and mobile phase B (0.1% formic acid in acetonitrile). A Sciex QTOF X500R mass spectrometer equipped with an electrospray ionization source (ABI-Sciex, Toronto, Canada) in the positive-ion high resolution multiple reaction monitoring (HRMRM) mode was used for detection. Protonated molecular ions and the respective ion products were monitored at the transitions of m/z 162.11 > 103.0364 for L-Carnitine, 204.12 > 85.0250 for Acetyl-L-Carnitine, 166.14 > 103.0380 for L-Carnitine-13C, D3 and 207.14 > 85.0255

for Acetyl-L-carnitine-D3. We adjusted the instrument settings to maximize analytical sensitivity and specificity of detection, and quality control samples were run before, in the middle, and after the samples to evaluate the accuracy and intra-batch precision of the developed method.

4.9.2 Sample Preparation and CFZ LC-MS/MS Analysis

To measure CFZ in blood, 160 μL of verapamil (30 ng/mL) in acetonitrile (internal standard solution) and 20 μL of acetonitrile were added to 20 μL of heparinized whole blood. The mixture was vortexed for 10 min and centrifuged (3500 rpm for 10 min). Then, the supernatant was transferred to autosampler vials for LC–MS/MS analysis.

Muscle samples were homogenized (Precellys tissue homogenizer, Bertin Technologies, Montigny-le-Bretonneux, France) with 80% N-Dimethylformamide (DMF)-PBS solution using a ratio of 5:1 volume (mL) to weight of muscle (g). For protein precipitation, 160 μL of internal standard solution and 20 μL of acetonitrile were added into 20 μL of homogenized tissue. The mixture was vortexed for 10 min and centrifuged (3500 rpm for 10 min). The supernatant was transferred to autosampler vials for LC–MS/MS analysis.

A Shimadzu LC-20AD HPLC system (Kyoto, Japan) was used to measure CFZ concentration. Chromatographic separation of the tested compound was achieved using a Waters XBridage reverse phase C18 column (5 cm × 2.1 mm I.D., packed with 3.5 μm) at 25 °C. Five μL of the supernatant was injected per sample. The flow rate of gradient elution was 0.4 ml/min with mobile phase A (0.1% formic acid in purified deionized water) and mobile phase B (0.1% formic acid in acetonitrile). An AB Sciex QTrap 4500 mass spectrometer equipped with an electrospray ionization source (ABI-Sciex, Toronto, Canada) in the positive-ion multiple reaction monitoring (MRM) mode was used for detection. Protonated molecular ions and the respective ion products were monitored at the transitions of m/z 473.0 > 431.1 for clofazimine and 455.2 > 303.2 for the

internal standard. We adjusted the instrument settings to maximize analytical sensitivity and specificity of detection, and quality control samples were run before, in the middle, and after the samples to evaluate the accuracy and intra-batch precision of the developed method.

4.9.3 Preparation and Analysis of Skeletal Muscle Macrophage Population

Gastrocnemius (GAS) muscle specimens were isolated, washed with 1X PBS, blotted dry, embedded in Tissue-Plus Optimal Cutting Temperature (OCT) compound (4585, ThermoFisher, Waltham, MA, USA), and frozen on dry ice. To obtain transverse sections, the OCT blocks were thawed (room temperature), fixed in 10% neutral buffered formalin (24 h), and cryoprotected in 20% sucrose (24 h). Sections were then rinsed in water and embedded transversely in a (24x24x5mm) cryomold (Fisher Healthcare, Waltham, MA, USA) using a glycol-resin media (OCT, 4585, ThermoFisher). The cryoblocks were then immediately frozen in the vapor phase of a liquid nitrogen bath suspended in a metal bowl within an outer bath of chilled isopentane. Sections were obtained using a cryostat (10 μm, CM3050 S, Leica BioSystems, Nussloch GmbH 2022).

Sections were fixed in 10% neutral buffered formalin (10 min) and stained using a rat monoclonal antibody (anti-F480, clone Cl:A3-1, MCA497RT, Bio-Rad, Hercules, CA, USA) (dilution of 1:400, 60 min, room temperature) on an automated immunohistochemical stainer (Biocare Intellipath, Biocare Medical, Pacheco, CA, USA) with prior blocking steps for endogenous peroxidases and non-specific binding. Negative control slides utilizing a ready-to-use normal rat serum (Rat Negative Control Sera, Innovex Biosciences, Richmond, CA, USA) in place of the primary antibody and positive control slides using mouse lymph node were concurrently assessed. Detection was performed with a commercial polymer-based, biotin-free reagent (Biocare

Rat Probe and Rat-on-Mouse HRP, Biocare Medical). Hematoxylin was used as a nuclear counterstain. Cover slips were applied to slides using an aqueous mounting media.

Immunostained slides were digitized on a Leica Aperio AT2 digital slide scanner (Leica Biosystems) at resolution up to 0.5 µm/pixel at 20x magnification. Digital slide files were analyzed for F480 stained cells using the positive cell detection algorithm within the open-source program QuPath (0.4.3; University of Edinburgh, Edinburgh, Scotland, UK). Slides were positively annotated to select muscle tissues only for analysis and visible artifacts or confounding areas (folds, debris, bubble, nerve, adjacent non-muscle connective tissue) were excluded by negative annotation. RGB values for DAB and hematoxylin staining were set directly from singly-stained areas in the slides and the algorithm was optimized to detect F480 stained cells. Digital image overlays were visually checked for accuracy by a board-certified veterinary pathologist. The number of F480-stained cells was reported as number of positive cells/mm^2 tissue area. The mean (S.D.) number of F480 positive macrophages was calculated for each group of mice.

4.9.4 Figures

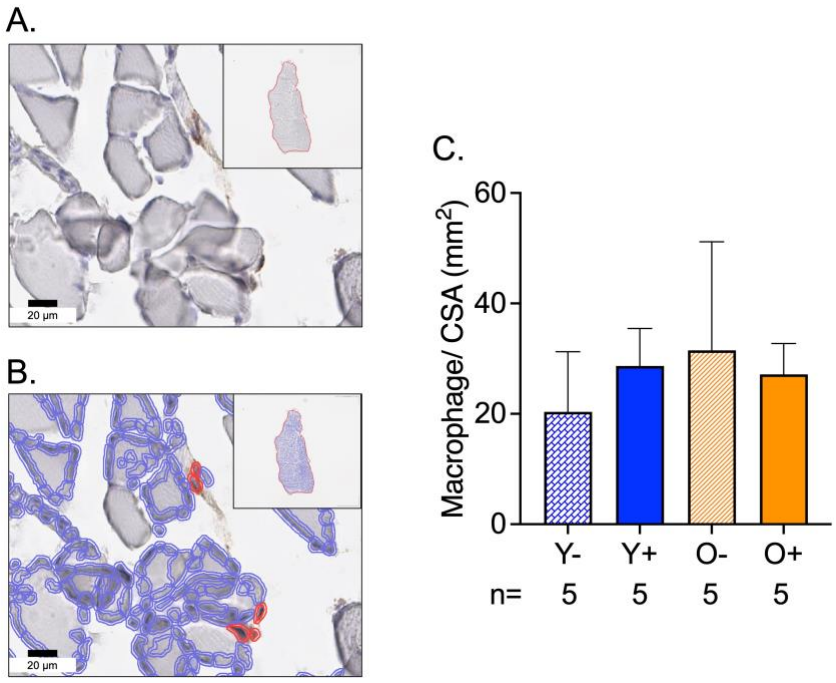

Figure S 4-1 The Number of Macrophages in Skeletal Muscle Remained Unchanged by Age or CFZ Treatment

Macrophage population in skeletal muscle **A**. F480 positive macrophages (brown areas) and nuclei (dark circular spots) in a representative immunostained gastrocnemius (GAS) muscle section (purple areas). **B**. F480 and nuclei immunostained annotated GAS section with false-color digital overlay. Red outline = macrophage positive cells, purple outline = macrophage negative cells. Both **A.** and **B.** contain total tissue overview insets for the same section. **C**. Number of F480 positive macrophages/mm^2 (mean $\pm$ SD) was not different among the groups (p=0.53, one-way ANOVA, n=5/group). The number of mice per group is shown below the x-axis of the plot. CSA= cross-sectional area

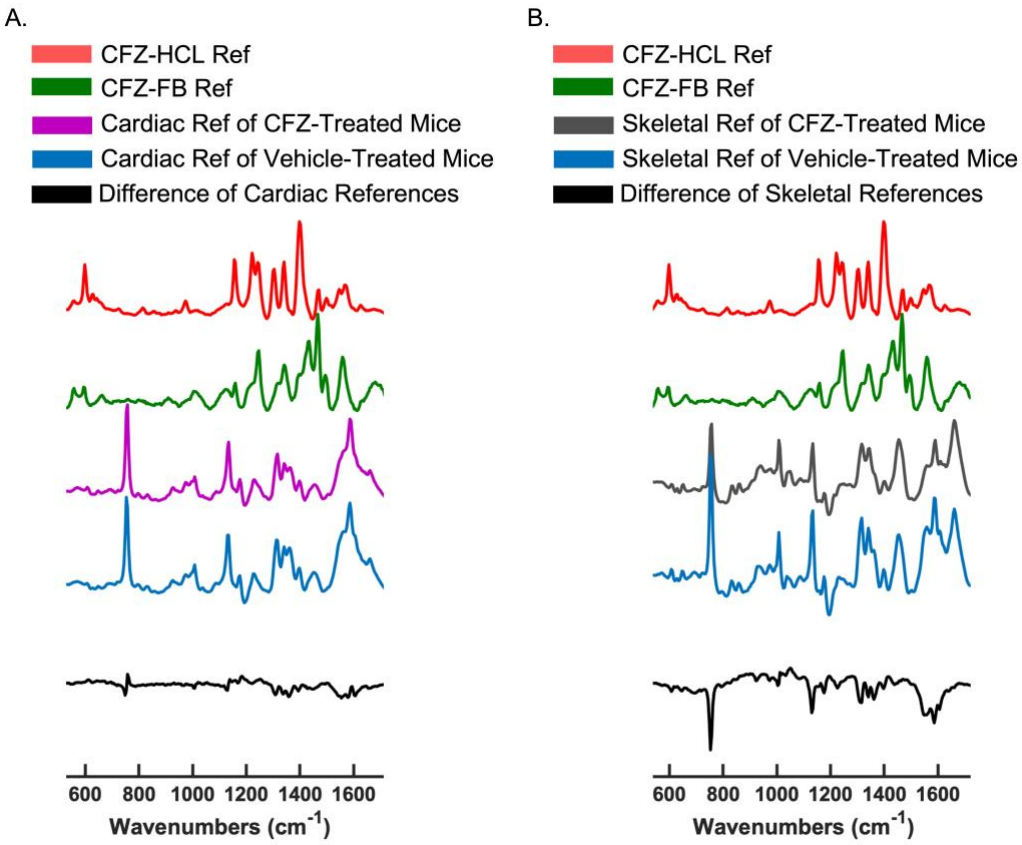

Figure S 4-2 Difference Between Spectral Muscle Raman References of CFZ- and Vehicle-Treated Mice

A. Cardiac muscle spectra (CFZ-treated mice CFZ-HCL (-) areas= purple, vehicle-treated mice =blue, difference between CFZ and vehicle treated mice sections= black). The difference spectrum shows no peaks from CFZ-HCL (red) or CFZ-FB (green) B. Skeletal muscle spectra CFZ-treated mice CFZ-HCL (-) areas= grey, vehicle-treated mice =blue, difference between CFZ and vehicle treated mice sections= black). The difference spectra show no peaks of CFZ-HCL (red) or CFZ-FB (green).

4.10 **References**

1. Heden, T.D., et al., *Mitochondrial PE potentiates respiratory enzymes to amplify skeletal muscle aerobic capacity.* Sci Adv, 2019. **5**(9): p. eaax8352.

2. Kudryavtseva, A.V., et al., *Mitochondrial dysfunction and oxidative stress in aging and cancer.* Oncotarget, 2016. **7**(29): p. 44879-44905.

3. Zhou, B. and R. Tian, *Mitochondrial dysfunction in pathophysiology of heart failure.* J Clin Invest, 2018. **128**(9): p. 3716-3726.

4. Begriche, K., et al., *Drug-induced toxicity on mitochondria and lipid metabolism: mechanistic diversity and deleterious consequences for the liver.* J Hepatol, 2011. **54**(4): p. 773-94.

5. McCann, M.R., et al., *L-Carnitine and Acylcarnitines: Mitochondrial Biomarkers for Precision Medicine.* Metabolites, 2021. **11**(1).

6. Boengler, K., et al., *Mitochondria and ageing: role in heart, skeletal muscle and adipose tissue.* J Cachexia Sarcopenia Muscle, 2017. **8**(3): p. 349-369.

7. Will, Y., J.E. Shields, and K.B. Wallace, *Drug-Induced Mitochondrial Toxicity in the Geriatric Population: Challenges and Future Directions.* Biology (Basel), 2019. **8**(2).

8. Mangoni, A.A. and S.H. Jackson, *Age-related changes in pharmacokinetics and pharmacodynamics: basic principles and practical applications.* Br J Clin Pharmacol, 2004. **57**(1): p. 6-14.

9. Manallack, D.T., *The pK(a) Distribution of Drugs: Application to Drug Discovery.* Perspect Medicin Chem, 2007. **1**: p. 25-38.

10. Zhitomirsky, B. and Y.G. Assaraf, *Lysosomal sequestration of hydrophobic weak base chemotherapeutics triggers lysosomal biogenesis and lysosome-dependent cancer multidrug resistance.* Oncotarget, 2015. **6**(2): p. 1143-56.

11. Bartel, K., et al., *Connecting lysosomes and mitochondria - a novel role for lipid metabolism in cancer cell death.* Cell Commun Signal, 2019. **17**(1): p. 87.

12. Flanagan, J.L., et al., *Role of carnitine in disease.* Nutr Metab (Lond), 2010. **7**: p. 30.

13. Nsiah-Sefaa, A. and M. McKenzie, *Combined defects in oxidative phosphorylation and fatty acid beta-oxidation in mitochondrial disease.* Biosci Rep, 2016. **36**(2).

14. Baik, J. and G.R. Rosania, *Molecular imaging of intracellular drug-membrane aggregate formation.* Mol Pharm, 2011. **8**(5): p. 1742-9.

15. Baik, J., et al., *Multiscale distribution and bioaccumulation analysis of clofazimine reveals a massive immune system-mediated xenobiotic sequestration response.* Antimicrob Agents Chemother, 2013. **57**(3): p. 1218-30.

16. Virmani, M.A. and M. Cirulli, *The Role of l-Carnitine in Mitochondria, Prevention of Metabolic Inflexibility and Disease Initiation.* Int J Mol Sci, 2022. **23**(5).

17. Percie du Sert, N., et al., *The ARRIVE guidelines 2.0: Updated guidelines for reporting animal research.* PLoS Biol, 2020. **18**(7): p. e3000410.

18. Castro, B. and S. Kuang, *Evaluation of Muscle Performance in Mice by Treadmill Exhaustion Test and Whole-limb Grip Strength Assay.* Bio Protoc, 2017. **7**(8).

19. Dougherty, J.P., D.A. Springer, and M.C. Gershengorn, *The Treadmill Fatigue Test: A Simple, High-throughput Assay of Fatigue-like Behavior for the Mouse.* J Vis Exp, 2016(111).

20. Hintze, T.H. and E.G. Shesely, *Is a mouse like any other mouse?* J Mol Cell Cardiol, 2002. **34**(10): p. 1283-6.

21. Murashov, M.D., et al., *Synthesis and Characterization of a Biomimetic Formulation of Clofazimine Hydrochloride Microcrystals for Parenteral Administration.* Pharmaceutics, 2018. **10**(4).

22. Trexel, J., et al., *Macrophage-Mediated Clofazimine Sequestration Is Accompanied by a Shift in Host Energy Metabolism.* J Pharm Sci, 2017. **106**(4): p. 1162-1174.

23. Baik, J. and G.R. Rosania, *Macrophages sequester clofazimine in an intracellular liquid crystal-like supramolecular organization.* PLoS One, 2012. **7**(10): p. e47494.

24. Chung, K.W., *Advances in Understanding of the Role of Lipid Metabolism in Aging.* Cells, 2021. **10**(4).

25. Lesnefsky, E.J., Q. Chen, and C.L. Hoppel, *Mitochondrial Metabolism in Aging Heart.* Circ Res, 2016. **118**(10): p. 1593-611.

26. Al Saedi, A., et al., *Lipid metabolism in sarcopenia.* Bone, 2022. **164**: p. 116539.

27. Ham, D.J., et al., *Distinct and additive effects of calorie restriction and rapamycin in aging skeletal muscle.* Nat Commun, 2022. **13**(1): p. 2025.

28. Bordoni, B. and M. Varacallo, *Anatomy, Bony Pelvis and Lower Limb, Gastrocnemius Muscle*, in *StatPearls*. 2022: Treasure Island (FL).

29. Sharma, S. and S.M. Black, *Carnitine Homeostasis, Mitochondrial Function, and Cardiovascular Disease.* Drug Discov Today Dis Mech, 2009. **6**(1-4): p. e31-e39.

30. van Gassel, R.J.J., M.R. Baggerman, and M.C.G. van de Poll, *Metabolic aspects of muscle wasting during critical illness.* Curr Opin Clin Nutr Metab Care, 2020. **23**(2): p. 96-101.

31. Kolwicz, S.C., Jr., S. Purohit, and R. Tian, *Cardiac metabolism and its interactions with contraction, growth, and survival of cardiomyocytes.* Circ Res, 2013. **113**(5): p. 603-16.

32. Wolfe, R.R., *Regulation of skeletal muscle protein metabolism in catabolic states.* Curr Opin Clin Nutr Metab Care, 2005. **8**(1): p. 61-5.

33. Keswani, R.K., et al., *Chemical Analysis of Drug Biocrystals: A Role for Counterion Transport Pathways in Intracellular Drug Disposition.* Mol Pharm, 2015. **12**(7): p. 2528-36.

34. Baumann, L., *Skin ageing and its treatment.* J Pathol, 2007. **211**(2): p. 241-51.

35. Cui, C.Y. and L. Ferrucci, *Macrophages in skeletal muscle aging.* Aging (Albany NY), 2020. **12**(1): p. 3-4.

36. Cui, C.Y., et al., *Skewed macrophage polarization in aging skeletal muscle.* Aging Cell, 2019. **18**(6): p. e13032.

37. Wang, X., et al., *Heterogeneous origins and functions of mouse skeletal muscle-resident macrophages.* Proc Natl Acad Sci U S A, 2020. **117**(34): p. 20729-20740.

38. Wang, X. and L. Zhou, *The Many Roles of Macrophages in Skeletal Muscle Injury and Repair.* Front Cell Dev Biol, 2022. **10**: p. 952249.

39. Dambrova, M., et al., *Acylcarnitines: Nomenclature, Biomarkers, Therapeutic Potential, Drug Targets, and Clinical Trials.* Pharmacol Rev, 2022. **74**(3): p. 506-551.

40. Cavagna, G.A., *Storage and utilization of elastic energy in skeletal muscle.* Exerc Sport Sci Rev, 1977. **5**: p. 89-129.

41. Wallace, K.B., V.A. Sardao, and P.J. Oliveira, *Mitochondrial Determinants of Doxorubicin-Induced Cardiomyopathy.* Circ Res, 2020. **126**(7): p. 926-941.

42. Bashiri Dezfouli, A., et al., *Evaluation of age effects on doxorubicin-induced toxicity in mesenchymal stem cells.* Med J Islam Repub Iran, 2017. **31**: p. 98.

43. Chatterjee, K., et al., *Doxorubicin cardiomyopathy.* Cardiology, 2010. **115**(2): p. 155-62.

44. Hiensch, A.E., et al., *Doxorubicin-induced skeletal muscle atrophy: Elucidating the underlying molecular pathways.* Acta Physiol (Oxf), 2020. **229**(2): p. e13400.

Chapter 5 Conclusions

5.1 General Conclusions

The pharmacokinetics and pharmacodynamics of lysosomal trapped drugs, like clofazimine (CFZ), can be affected by resident tissue macrophages, organs, and age (**Figure 2-3A, and B**, **Figure 3-6C**). This thesis highlights the importance of considering exposure duration and age when dosing drugs that are known to bioaccumulate in macrophages. The aging process can alter the body's drug metabolism and elimination processes, leaving the elderly more vulnerable to adverse drug reactions (ADRs) [1]. While drug development does not usually consider single-cell pharmacokinetics, it is important for lipophilic weakly basic drugs that can accumulate in the lysosomal compartment of macrophages such as amiodarone, chloroquine, azithromycin, nilotinib, and imatinib, that behave similarly to CFZ [2-5]. Ultimately, understanding the risks and benefits of drug accumulation in various tissues can enhance drug therapy safety, especially for vulnerable patients such as the elderly.

To better understand the drug distribution concerning treatment duration, age, and tissues, CFZ was used as a probe, and C57BL6 mice were used as a model. This mouse strain is often used in aging and toxicity research, and others have previously shown that they accumulate CFZ in similar manner to humans [6, 7]. To establish distribution patterns, macrophage-rich matrices like bone marrow and spleen were used (**Chapter 2**), and skeletal muscle (**Chapter 3**), one of the tissues that changes the most during aging, was utilized to examine age-dependent distribution. I also assessed the utility of whole blood and skeletal measurements of the mitochondrial metabolites, l-carnitine and acetylcarnitine, to detect possible drug adverse effects (ADRs) to prevent fatalities

(**Chapter 4**). My work highlighted that despite profound changes at the tissue/organ level, these were not detected by changes in the blood levels of either l-carnitine or acetylcarnitine (**Figure 4-1**). However, other non-invasive test such as decrease in total body mass and increase in caloric intake (catabolism) and decrease in physical performance can help detect ADRs (**Chapter 3 and 4**).

5.1.1 Tissue-Dependent Drug Accumulation Provides Foundation for Drug Development

Drug distribution in bone and spleen, macrophage-rich tissues, of long-term CFZ-treated mice was studied to gain insights into drug accumulation, macrophage sequestration population, and drug amount per sequestering cell (cargo capacity). The results showed that drug distribution mechanisms are tissue-dependent (**Chapter 2 and 3**). Specifically, CFZ exposure led to an increase in the percentage of drug-sequestering cells and drug capacity in bone marrow (**Figure 2-3A**), while the spleen relied on its ability to increase in size to accumulate a long-term drug treatment (**Table 2-2**). In addition, the tissues displayed different cytokine responses. The bone marrow mounted a proinflammatory response whereas the spleen, as has been previously reported [8], increased its expression of anti-inflammatory cytokines with an associated decrease in proinflammatory cytokines (**Figure 2-1**). The accumulation mechanism of CFZ in different tissues highlights the importance of comprehending drug distribution patterns in various tissues and how they may provide an explanation of the ability of and the response to the accumulation of large amounts of drug.

5.1.2 Age-Dependent Drug Accumulation Demonstrates an Increase in Off-Target Side Effects

Drug distribution was analyzed in young and old mice that were given the same CFZ treatment for 8-weeks. Despite having similar blood drug levels, there was an age-related difference in drug distribution following treatment (**Chapter 3 and 4**). Furthermore, old mice showed the largest positive percent change in drug amount in muscle compared to young mice (**Figure 3-4**). Skeletal muscle from old CFZ-treated mice also exhibited increased collagen (**Figure 3-3B**), changes in cytokines (**Table 3-1**), and a decrease in fiber diameter (**Figure 3-3C**), like what is seen in injured and old muscle [9-13]. These findings suggest that age enhances the immunological and structural response to CFZ in skeletal muscle that may contribute to an increased risk of ADRs in elderly patients.

5.1.3 Detecting ADRs in Vulnerable Populations

This thesis also aimed to identify a blood biomarker for detecting ADRs resulting from age-related bioaccumulation of CFZ in skeletal muscle (**Chapter 4**). To achieve this goal, mitochondrial metabolites, l-carnitine, and acetylcarnitine, were measured in the muscle and blood of young and old mice treated with CFZ (**Figure 4-1**). The study found that old CFZ-treated mice showed the largest catabolic effect during treatment, suggesting an overall metabolism alteration (**Figure 4-2B and C**). They also demonstrated an alteration in skeletal muscle mitochondrial metabolism, which was not observed in young mice (**Figure 4-1C**). However, while muscle from old mice underwent drug-related changes (**Figure 4-4**), this did not result in a detectable change in the blood levels of two mitochondrial-related metabolites (**Figure 4-1A**). Due to the absence of alterations in mitochondrial metabolism in the blood, drug-induced catabolism may be a relevant functional biomarker to identify individuals at increased risk for mitochondrial ADRs.

5.2 Implications and Significance

Previous in vitro research on macrophage capacity for phagocytosis [14] demonstrated that the phagocytic capacity was limited by the amount of available membrane. More recent in vitro studies have demonstrated that sequestering macrophages have a unique phenotype in which they can increase in size to hold increasing amounts of cargo [2]. My findings derived from living organisms are significant as they shed light on the adaptability of macrophages to the increasing loads of accumulating drug cargo during long-term treatments. These data suggest that the total macrophage capacity may adapt to the increasing cargo loads by differentiating into more efficient xenobiotic sequestering cells, leading to changes in organ mass-to-total body mass ratios, muscle structure and function, and the metabolic balance of the organism.

The findings suggest that the capacity of the cargo compartment responds to drug bioaccumulation by increasing the size of the compartment, the fraction of loaded cells, and the fraction of macrophage cells in organs that typically do not contain many macrophages (e.g., skeletal and cardiac muscle). These data also found that as mice age, their macrophages become more adept at taking up cargo, and bone marrow becomes filled with cargo sequestering cells with prolonged treatment.

Overall, these findings have significant implications for understanding the mechanisms of macrophage sequestration of lipophilic drugs. My studies suggest that the total cargo sequestering capacity of the macrophages present in an organism increases with age, rather than being a constant capacity that gets maxed out over time or decreases with age. By understanding how macrophages adapt to increasing cargo loads and enhance their capacity for cargo sequestration with age, we may gain insights into novel approaches for mitigating ADRs caused by drug accumulation.

5.3 Future Outlook

5.3.1 Interplay of the Immune System and Metabolism During Drug Accumulation

The immune system and metabolism of mice were highly affected by CFZ (**Chapter 2 and 4**). Previous studies have shown that cytokines play a role in regulating the immune system and maintaining metabolic homeostasis [15]. Additionally, several metabolic pathways can regulate cytokine production and function [16]. The cytokine array data presented herein represent a significant advancement in understanding the mechanisms of lysosomal drug accumulation and macrophage response to xenobiotics (**Chapter 2**). My findings demonstrated an overall disruption in metabolism (catabolism) and a disruption in mitochondrial metabolism in the skeletal muscle (**Chapter 4**). I also observed a trend in tissues (bone and skeletal muscle) with altered pro-inflammatory cytokines resulting in a decrease in density/mass and tissue (spleen) with altered anti-inflammatory cytokines resulting in increase in mass with 8-weeks of CFZ treatment (**Chapter 2 and 3**).

These results highlight the complex interplay between cytokines and metabolism. However, there is still much to be learned about the underlying mechanisms and how these interactions can be used in therapeutics. Future research directions could include investigating the specific cytokines and metabolic pathways in blood that get altered with drug treatment to detect ADRs. In addition, studies could focus on developing personalized interventions based on an individual's unique cytokine and metabolic profile to optimize the response to treatment.

5.3.2 Potential Application for Muscle Mass Model

The results of the muscle mass modeling demonstrated that CFZ treatment resulted in a decrease in muscle mass and altered muscle kinetics compared to untreated mice, which was collaborated with histological analysis of muscle fiber diameter (**Figure 3-1, Figure 3-3C**). While using a modified pharmacokinetic model (**Equation 2**) to demonstrate mass decrease with age and CFZ-treatment worked well, it can be used to model other important functional parameters, such as strength, that has been shown to follow similar behaviors to muscle mass throughout the lifespan (increasing in younger years and decreasing with age) [17].

The results of the muscle model suggest that CFZ can have a significant impact on skeletal muscle, which is an important consideration in the clinical use of this drug. Further improvement of the model could be used in clinical settings to monitor changes in muscle mass and strength over time in patients undergoing treatment with drugs known to impact muscle function. This could help identify patients who are at risk of developing muscle atrophy and guide interventions to prevent or mitigate this effect.

Collectively, the findings highlight the importance of understanding tissue and age-dependent drug distribution and their role in the development of ADRs. The tissue-dependent accumulation mechanism of CFZ also has implications for drug efficacy and toxicity, and these findings could be used to guide drug regimens that target specific tissues while minimizing ADRs. Future research should focus on developing clinical biomarkers for the early detection of ADRs, which can lead to earlier intervention and prevention of ADRs. In addition, further investigation into the role of the immune response in chemical bioaccumulation can guide the development of more effective drugs that target age-related diseases.

5.4 References

1. Cooke, S.C. and M.L. Tucker, *Geriatric Depression.* Journal of Pharmacy Practice, 2001. **14**(6): p. 498-510.

2. Rzeczycki, P., et al., *An Expandable Mechanopharmaceutical Device (1): Measuring the Cargo Capacity of Macrophages in a Living Organism.* Pharm Res, 2018. **36**(1): p. 12.

3. Morissette, G., et al., *Intracellular sequestration of amiodarone: role of vacuolar ATPase and macroautophagic transition of the resulting vacuolar cytopathology.* Br J Pharmacol, 2009. **157**(8): p. 1531-40.

4. Derendorf, H., *Excessive lysosomal ion-trapping of hydroxychloroquine and azithromycin.* Int J Antimicrob Agents, 2020. **55**(6): p. 106007.

5. Fu, D., et al., *Imaging the intracellular distribution of tyrosine kinase inhibitors in living cells with quantitative hyperspectral stimulated Raman scattering.* Nat Chem, 2014. **6**(7): p. 614-22.

6. Willmer, A.R., et al., *Molecular design of a pathogen activated, self-assembling mechanopharmaceutical device.* J Control Release, 2022. **347**: p. 620-631.

7. van Dijk, M., et al., *Sarcopenia in older mice is characterized by a decreased anabolic response to a protein meal.* Arch Gerontol Geriatr, 2017. **69**: p. 134-143.

8. Baik, J., et al., *Multiscale distribution and bioaccumulation analysis of clofazimine reveals a massive immune system-mediated xenobiotic sequestration response.* Antimicrob Agents Chemother, 2013. **57**(3): p. 1218-30.

9. Larsson, L., et al., *Sarcopenia: Aging-Related Loss of Muscle Mass and Function.* Physiol Rev, 2019. **99**(1): p. 427-511.

10. Nilwik, R., et al., *The decline in skeletal muscle mass with aging is mainly attributed to a reduction in type II muscle fiber size.* Exp Gerontol, 2013. **48**(5): p. 492-8.

11. Korbecki, J., et al., *The Importance of CXCL1 in Physiology and Noncancerous Diseases of Bone, Bone Marrow, Muscle and the Nervous System.* Int J Mol Sci, 2022. **23**(8).

12. Munoz-Canoves, P., et al., *Interleukin-6 myokine signaling in skeletal muscle: a double-edged sword?* FEBS J, 2013. **280**(17): p. 4131-48.

13. Jaguin, M., et al., *Polarization profiles of human M-CSF-generated macrophages and comparison of M1-markers in classically activated macrophages from GM-CSF and M-CSF origin.* Cell Immunol, 2013. **281**(1): p. 51-61.

14. Cannon, G.J. and J.A. Swanson, *The macrophage capacity for phagocytosis.* J Cell Sci, 1992. **101 (Pt 4)**: p. 907-13.

15. Kierdorf, K., et al., *Muscle function and homeostasis require cytokine inhibition of AKT activity in Drosophila.* Elife, 2020. **9**.

16. Hu, C., et al., *Immune cell metabolism and metabolic reprogramming.* Mol Biol Rep, 2022. **49**(10): p. 9783-9795.

17. Cruz-Jentoft, A.J., et al., *Sarcopenia: revised European consensus on definition and diagnosis.* Age Ageing, 2019. **48**(1): p. 16-31.